School of Biosciences

CHLORIDE INTRACELLULAR CHANNEL 4 AS A THERAPEUTIC TARGET IN THE DEVELOPMENT OF PULMONARY ARTERIAL HYPERTENSION

Pulmonary Arterial Hypertension (PAH) is a high-mortality disease centred on the progressive dysfunction of the right ventricle, as a result of pulmonary artery lumen narrowing and increased pulmonary vascular resistance. Chloride intracellular channel (CLIC) 4 has been recently suspected to play a role in the development of PAH pathogenesis via the propagation of vascular remodelling, a hallmark of PAH. CLIC4's involvement is linked to a newly-hypothesised CLIC4/Arf6 pathway, involving the protein Arf GTPase-activating protein (GIT) 1. This thesis shows the investigation into CLIC4 interactions with inhibitor Digoxin, and GIT1, which was modelled by assigning CLIC4 residues to a 2D Heteronuclear Single Quantum Coherence (HSQC) NMR spectrum. The results allowed a binding site on CLIC4 to be predicted manually and computationally, and CLIC4-GIT1 interactions were determined which strongly suggests CLIC4:GIT1 interactions in vivo. Overall, this thesis provides evidence of CLIC4's involvement in vascular remodelling pathways, and its viability as a therapeutic target and supports the novel Arf6/CLIC4 pathway believed to propagate PAH development. With this, the study provides new ideas into combatting PAH development, in a bid to reduce PAH-related mortality.

Thomas Jamieson

MSc-R: 2022/2023

148 Pages

Declaration

No part of this thesis has been submitted in support of an application for any degree or other qualification of the University of Kent, or any other University or institution of learning.

Acknowledgements

Firstly, thank you to Dr. Jose Ortega Roldan for guidance and encouragement through this project, providing support and advice on difficult concepts, especially NMR, alongside Dr. Gary Thompson for assistance on the theory and running of NMR samples. I would like to thank Angela Serrano Sanchez for her support on the CLIC4 assignment and for providing raw CLIC4 – Digoxin data, in addition to being a great lab mate. Special thanks to Matt R, Will, Dr. Joe Cassar, Hannah and Vicky for providing a great work environment and being some of the best people I've worked with.

Special mention to Sheila Gonzalez Salvatierra for providing never-ending positivity and energy to the entire lab and providing me with the opportunity to learn some Spanish (including Dr. Jose Ortega Roldan and Angela).

Lastly, I'd like to thank my family and friends at home who have always supported my scientific journey and will continue to be behind me all the way, even if that includes taking some time off (Matt and Dean).

Table of Contents

Table of Figures

Table of Tables

Abbreviations

ADH = Anti Diuretic Hormone

ALK1 = Activin Receptor-like Kinase 1

Arf = ADP ribosylation factor

ATP = Adenosine Triphosphate

AVT = Acute Pulmonary Vasoreactivity Test

BH4 = Tetrahydrobiopterin

BMJ = British Medical Journal

BMPR-II = Bone Morphological Protein Type II

cAMP = Cyclic Adenosine Monophosphate

CCB = Calcium Channel Blocker

CF = Cystic Fibrosis

cGMP = Cyclic Guanosine Monophosphate

CLIC4 = Chloride Intracellular Channel 4

COPD = Chronic Obstructive Pulmonary Disease

COXs = Prostaglandin G/H Synthases

CSP = Chemical Shift Perturbations

DAG = Diacylglycerol

DP = Prostaglandin D2 receptor

ECE = Endothelin-converting Enzyme

ECG = Echocardiogram

ENG = Endoglin 1

ER = Endoplasmic Reticulum

ERA = ET Receptor Antagonists

ET1 = Endothelin-1

FAD = Flavin Adenine Dinucleotide

FDA = Food and Drug Administration

FID = Free-Induction-Decay

GAP = GTPase Activating Factors

GEF = Guanine nucleotide Exchange Factors

GIT = Arf GTPase-activating protein

GPCR = G-Protein Coupled Receptor

GST = Glutathione S-Transferases

GTP = Guanosine Triphosphate

HADDOCK = High Ambiguity Driven protein-protein DOCKing

HIF1α = Hypoxia-Inducible Factor 1α

H-NOX = Heme-Nitric Oxide domain

HSQC = Heteronuclear Single Quantum Coherence

IAA94 = Indanyloxyacetic acid

IP = Prostacyclin receptor

IP3 = Inositol Trisphosphate

IPAH = Idiopathic Pulmonary Arterial Hypertension

IPTG = Isopropyl-β-D-thiogalactopyranoside

IV = Intravenous

LB = Luria Broth

LPA = Lysophosphatidic acid

MR = Molar Ratio

MST = Microscale Thermophoresis

NADPH = Nicotinamide-Adenine Dinucleotide Phosphate

NFκB = Nuclear Factor Kappa-light-chain-enhancer of activated B cells

NICE = National Institute for Health and Clinical Excellence

NMR = Nuclear Magnetic Resonance

NO = Nitric Oxide

NOS = Nitric Oxide Synthase

OD = Optical Density

PAEC = Pulmonary Arterial Endothelial Cells

PAH = Pulmonary Arterial Hypertension

PASMC = Pulmonary Arterial Smooth Muscle Cells

PDB = Protein Data Base

PDE-5 = Phosphodiesterase-5

PGI_2 = Prostacyclin

PH = Pulmonary Hypertension

PIP_2 = Phosphatidylinositol bisphosphate

PKA = Protein Kinase A

PKC = Protein Kinase C

PKG = cGMP-dependent protein kinases

PLC = Phospholipase C

PPHN = Persistent Pulmonary Hypertension of the Newborn

PVR = Pulmonary Vascular Resistance

RF = Radiofrequency

RHC = Right Heart Catheterisation

ROS = Reactive Oxygen Species

SDS-PAGE = Sodium Dodecyl Sulphate-Polyacrylamide Gel Electrophoresis

SEC = Size Exclusion Chromatography

sGC = soluble Guanylate Cyclase

TALOS = Torsion Angle Likeliness Obtained from Shift and Sequence Similarity

TB = Tuberculosis

TEV = Tobacco Etch Virus

TGF-β = Transforming Growth Factor β

TP = Thromboxane receptor

TTE = Transthoracic Doppler echocardiography

TXA_2 = Thromboxane

VEGF = Vascular Endothelial Growth Factor

WHO = World Health Organisation

1. Abstract

Pulmonary Arterial Hypertension (PAH) is a high-mortality disease centred on the progressive dysfunction of the right ventricle, as a result of pulmonary artery lumen narrowing and increased pulmonary vascular resistance. Chloride intracellular channel (CLIC) 4 has been recently suspected to play a role in the development of PAH pathogenesis via the propagation of vascular remodelling, a hallmark of PAH. CLIC4's involvement is linked to a newly-hypothesised CLIC4/Arf6 pathway, involving the protein Arf GTPase-activating protein (GIT) 1. This thesis shows the investigation into CLIC4 interactions with inhibitor Digoxin, and GIT1, which was modelled by assigning CLIC4 residues to a 2D Heteronuclear Single Quantum Coherence (HSQC) NMR spectrum. The results allowed a binding site on CLIC4 to be predicted manually and computationally, and CLIC4-GIT1 interactions were determined which strongly suggests CLIC4:GIT1 interactions *in vivo.* Overall, this thesis provides evidence of CLIC4's involvement in vascular remodelling pathways, and its viability as a therapeutic target and supports the novel Arf6/CLIC4 pathway believed to propagate PAH development. With this, the study provides new ideas into combatting PAH development, in a bid to reduce PAH-related mortality.

2. Introduction

2.1 Pulmonary Arterial Hypertension and CLIC4's involvement in disease progression

2.1.1 Pulmonary Arterial Hypertension

Pulmonary Hypertension (PH) is a term used to describe elevated blood pressure in the vascular tissue of the lungs (1). PH is characterised by a narrowing of the pulmonary arteries, this narrowing can drastically increase resistance against blood flow from the pulmonary artery to the left atrium, this is termed Pulmonary Vascular Resistance (PVR, see **Figure 1** (2,3)).

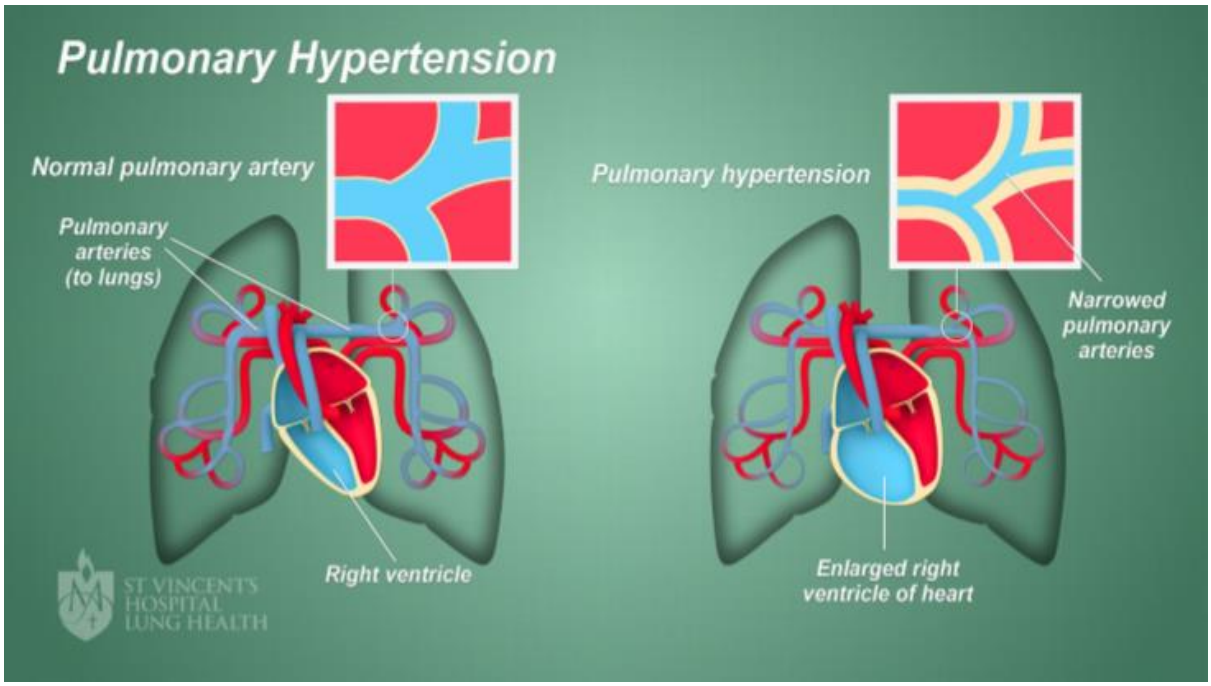

Figure 1 - Comparison of normal pulmonary vasculature vs pulmonary hypertension. *(Left): Normal pulmonary circulation in the lungs showing clear arteries carrying deoxygenated blood from a typical sized right ventricle to the lungs. (Right) Pulmonary Hypertension state of pulmonary arteries in the lungs, with blood flow constricted buy narrowed blood vessels. This causes back-pressure and subsequent enlargement of the right ventricle. Adapted from: https://www.svhhearthealth.com.au/conditions/pulmonary-hypertension*

For example, a 50% reduction in arterial radius results in a 16 times increase in PVR(4). PVR increases can substantially reduce blood flow to the lungs, resulting in an increased workload by the heart and thus an increase in the size of the right ventricle and back-pressure into the right atrium (1). The cascade outlined above discusses the increasing size of the right ventricle, which leads to higher pressure output from this ventricle specifically in the pulmonary artery. There are many types of PH, which can be classified into subsets which are; Group 1 – Pulmonary Arterial Hypertension (PAH), Group 2 – Pulmonary Hypertension due to Left Heart Disease, Group 3 – Pulmonary Hypertension due to Lung Disease, Group 4 – Pulmonary Hypertension due to Chronic Blood Clots in the Lungs (or thromboembolic PH (5), and Group 5 – Pulmonary Hypertension due to Unknown Causes (Idiopathic PH)(6). Given these definitions, the form of PH described above is Pulmonary Arterial Hypertension (PAH) (7). PAH is defined by the measurement of the pressure experienced by the pulmonary arteries to have increased to 25mm Hg and above at rest and more than 30mmHg when under heavier load (exercise) (7,8). It is also characterised by a reduction in Nitric Oxide and Prostaglandin I2, and increased production of Endothelin and Thromboxane (9) Increased pressure output results in increased overall strain on the right ventricle, and if left undiagnosed and untreated, leads to a spiralling morphological restructuring of the right ventricle into a more spherical ventricle ultimately resulting in failure of the right ventricle (known as “Right heart failure”) and cardiac failure (1,8,10). In 2004, the number of patients diagnosed with PH in the UK was 1,539. by 2021 this had risen to a total of 7,876 which is an estimated 500% increase in cases (11). As PAH is classified in group 1 out of 6 subsections of the World Health Organisation (WHO) PH classification system, the average life expectancy of untreated PAH is 2 to 3 years from diagnosis (7) and so carries a high mortality (7). Therefore, there is an urgent need to find effective treatments for PAH, as currently the disease is classified as incurable. There are, however, treatments such as calcium channel blockers e.g. diltiazem and nifedipine, that aim to improve quality of life amongst patients via monitoring improvements to time and distance covered in a “6-minute walk” test (7,12).

2.1.2 Symptoms

The most common symptoms of PH are chest pains, shortness of breath and fatigue (2). PAH symptoms can also include heart palpitations, dizziness, fainting and lips and fingers turning blue (2,13) Symptoms do not necessarily display quickly; there is usually a delay of months/years between the onset of additional symptoms (14). As the disease progresses, dyspnoea (feeling of running out of air/not breathing enough) can occur even after bending down, coupled with syncope (loss of consciousness for a short time) after a short exercise (14). Due to this state becoming life-threatening, it is imperative that early diagnosis is achieved. However, treatment is dependent on the precise classification of PAH that the patient has, hence the underlying cause of PAH is paramount (14).

2.1.3 Causes and Diagnosis of PAH

2.1.3.1 Causes of PAH

The British Medical Journal (BMJ) concluded that in 2018, the prevalence of PAH varied from 11 to 26 cases per million adults, and although it is regarded as a rare disease, survivability is low, especially in the fact that chances of survival are significantly worse in men than women (15). PAH is widely divided into 7 sub-categories, categorised based on the underlying cause of the issue (5). These are Idiopathic PAH (IPAH), Heritable PAH, Drug/Toxin-induced PAH, PAH associated with various diseases (e.g. HIV, connective tissue disease), PAH in long-term calcium channel blocker patients, PAH with capillary/venous involvement, and PH of the newborn (1,5).

Heritable PAH is suspected to account for around 6-10% of all recorded PAH cases (15), but genetic discoveries in the year 2000 have revealed that over 300 mutations in the gene *BMPR2*, encoding the protein Bone Morphological Protein Type II (BMPR-II), could be responsible for a reported 70-80% of all heritable PAH incidences (15,16). *BMPR2* is part of the Transforming Growth Factor β (TGF-β) superfamily which includes Activin Receptor-like Kinase 1 (*ALK1*) and Endoglin 1 (*ENG*) (17). BMPRII expression promotes anti-inflammatory action and inhibits over proliferation of smooth muscle cells (18). The mutations are classified as loss-of-function, leading to reduced cellular signalling and

hyperproliferation of vascular smooth muscle cells (16). When compared to PAH patients who were genetically screened to show no mutations in BMPR-II, mutation carriers were diagnosed remarkably younger, presented with more severe symptoms and were at an increased risk of death as a result (15,16). However, the *BMPR2* mutations are not solely responsible for the development of PAH, as other genetic and environment factors are required for the onset of PAH even in those with *BMPR2* mutations (15). One source also suggests the PAH with capillary/venous involvement may be a subsection of Heritable PAH, due to the capillary/venous involvement including vascular remodelling based on similar genetic mutations (e.g. *BMPR2)* and as such suggests they are not two distinct categories (19)

Drug or Toxin-induced PAH is defined as the development of PAH upon exposure to any form of drug/toxin (20). As with the above variants, it usually leads to heart failure in 70% of diagnosed drug-induced PAH patients and is potentially fatal. The discovery of drug-induced PAH was attributed to the development of PAH in patients that were taking pharmaceutical treatments for obesity in 1965 (21) The drug aminorex fumarate, known commercially as Menocil, was correlated to an increase in PH with 1-2 users developing PAH in 1,000 (a much higher rate than an estimated 1-2 cases per million per year for idiopathic/heritable PAH (15,21). Many amphetamine-like pharmaceuticals such as Phentermine and Aminorex purposed as anorexiants (drugs designed to suppress appetite), have been identified to contribute to PAH (22,23). Particularly, the use of Fenfluramine (commonly prescribed with phentermine to create a “Fen-phen” mixture) was concluded to act as an instigator for the development of PAH (21,24). In regards to toxin-induced PAH, there is no surprise that the idea of tobacco smoking could induce vascular remodelling and hence arterial restriction. In animal studies, pulmonary arteriole cell proliferation is induced following acute exposure to tobacco smoke, and prolonged smoke exposure leads to arterial wall thickening (21). In humans, a 2013 study of 472 PAH patients was compared against a healthy control group in terms of smoking habits (21). The outcome revealed that a significant amount of PAH patients were active smokers, with a higher active and

passive smoke exposure than the healthy, non-PAH control group. Thus, the study suggested a pathogenic component of smoking in the development of PAH, especially in male patients (21,25)

Certain underlying medical conditions can also cause PAH, such as connective tissue disease (26) One disease, scleroderma, is a progressive condition which causes the skin to become tighter and harder, which can affect the heart, lungs and digestive system. (27) It is a rare autoimmune disease that carries significant mortality rates on its own, but due to the nature of the disease affecting the lungs it can increase the blood pressure in the pulmonary vascular system via morphological changes to the vasculature (27,28) This, in turn, causes PAH to develop, with a 2023 publication stating that connective tissue diseases (in particular scleroderma) are the leading cause of PAH (28). Furthermore, PAH is accountable for a 30% mortality, despite a prevalence of 7% to 19%, in patients with scleroderma (28) In addition to scleroderma, HIV infections have emerged to be a contributor to PAH development. HIV infection increases risks for many lung-related diseases, such as tuberculosis (TB) which carries a high morbidity rate when coinfected with HIV (29,30). Therefore, it is no surprise that a study in 2000 concluded unexplained cardiopulmonary symptoms of a patient to be attributed to their HIV-positive status and their development of PAH (31). Current understanding of the pathogenesis of HIV-PAH is not fully understood, but it is suggested that HIV viral proteins induce inflammation, oxidative stress and proliferation of endothelial cells in the pulmonary vasculature which causes endothelium re-modelling (30,32). Viral proteins present in the blood, in addition to hypoxic conditions, were shown to increase arterial pressures in animal models (32). However, there is no conclusive strategy for treating HIV-PAH, and further pathogenic studies are required to collate treatments for HIV-PAH (32).

Some PAH patients who are originally diagnosed with IPAH respond well to long-term calcium channel blockers (CCB), provided a high dosage is administered (33). Long-acting CCBs usually prescribed include nifedipine or diltiazem (8). This was predicted in a 1992 study, suggesting that pulmonary artery pressure and vascular resistance could improve when CCBs are regularly taken over a five-year

course (34). These patients are identified as vasoreactive, determined by a positive Acute Pulmonary Vasoreactivity Test (AVT) in which vasodilators (Nitric oxide, pure oxygen, Intra-venous adenosine) are administered (35). If a reduction in mean pulmonary artery pressure of more than 10 mmHg, to reach an absolute value of less than 40 mmHg providing an increased or unchanged cardiac output is reached, then this is considered a positive result (35). These vasoreactive patients are known as calcium channel blocker responders, but the majority of patients with IPAH exhibit a negative AVT test and hence do not respond to CCB treatments (33). Despite CCBs being a pioneer in viable PAH treatments, it has been shown that 5% of PAH patients or less will gain a significant positive effect long-term (36). Recent studies have shown that even "responders" experience a loss of CCB response in a little as one year of treatment (37). Therefore, newer compounds termed "advanced vasodilator agents" are required for "non-responder" PAH patients, primarily prostacyclin derivatives but also includes upcoming treatments such as phosphodiesterase-5 inhibitors and endothelin receptor agonists (36).

PAH of the newborn, also known as Persistent Pulmonary Hypertension of the Newborn (PPHN), is a rare disorder that occurs during the transition from the foetal circulation state to an extrauterine one (38). Before the lungs of the foetus are expanded and contribute to gas exchange (pre-birth), they are collapsed, hence vascular resistance is high (39). However, when the umbilical cord is clamped, the first few breaths are taken which clears foetal lung fluid (39). This causes a rise in arterial oxygen tension, which causes PVR to decrease, increasing pulmonary blood flow (39). The failure of adaptation between the two states prevents an essential increase in pulmonary blood flow due to the inability of the PVR to fall (40) The sustained higher PVR is the hallmark of PAH of the newborn, which can cause newborns to exhibit respiratory failure within 12 hours of birth (38). Patients are then at a high risk of asphyxia leading to neurological damage and potentially death (40). Thankfully, this complication can be reversed in the early days of life but it relies on the administration of nitric oxide (NO) (40) However, 40% of infants fail to respond to this vasodilator (40). Further treatments are

therefore required, but these utilise new drugs still in an experimental phase, or those approved for PAH in adults (40).

2.1.3.1 Diagnosis of PAH

The diagnosis of PH is initiated by investigations of an Echocardiogram (ECG), a Transthoracic Doppler echocardiography (TTE) and chest radiography with a particular emphasis on the use of TTE for patients suspected of heritable PAH or connective tissue-associated PAH (41). TTE utilises ultrasound waves to image the four chambers, heart valves and nearby blood vessels of the heart (42). Primarily, the diagnostic tool measures the pressure difference between the right atrium and right ventricle, which can be used to estimate pulmonary arterial pressure (systolic) ((41). PAH can then be diagnosed if the estimated systolic pulmonary arterial pressure is above 36 mmHg (41). Additional testing such as lung function tests, ventilation lung scanning, CT scans and X-Rays of the chest, and the "6-minute walk" test can also help reinforce a suspected PAH diagnosis (26,41). However, the only definitive way of making a clear diagnosis is via Right Heart Catheterisation (RHC), which allows for a more detailed definition when diagnosing PAH. This definition is "*mean pulmonary arterial pressure of >25mm Hg at rest or >39 mmHg during exercise with a pulmonary capillary wedge pressure of <15 mmHg and pulmonary vascular resistance of > 3 wood units"* (1,7,8,19,41). Once diagnosed, the patient will be subject to vasodilator tests, known as an acute vasodilator challenge, to determine the relaxation of pulmonary blood vessels and the effect of the relaxation on pressure in the right atrium of the heart (43). If the patient responds well, then calcium channel blockers may be prescribed as treatment, otherwise inhaled vasodilators will be used to treat the disease (43). However, it is important to note that treatment of PAH heavily relies on the underlying cause, and is usually diagnosed via testing and elimination of other underlying causes e.g. asthma, Chronic Obstructive Pulmonary Disease (COPD) and heart failure (5). PAH cannot be diagnosed until the other PH subsets have been ruled out (28).

2.1.4 Molecular mechanisms of PAH

Despite multiple factors contributing to the development of PAH, the disease is hallmarked by extreme pulmonary vasoconstriction and over-proliferation of vascular tissue (smooth muscle cells, endothelial cells, fibroblasts) (17). 3 main pathways act on the vasodilative/vasoconstrictive deregulation of the pulmonary vasculature in PAH which are: The Endothelin Pathway, the Nitric Oxide (NO) pathway and the Prostacyclin (PGI_2) pathway.

2.1.4.1 Endothelin Pathway

Endothelin-1 (ET1) is a 21-amino acid polypeptide that is largely produced by endothelial cells situated in pulmonary vasculature (44). Production of ET-1 can be influenced by cytokines, hypoxia, steroids and growth factors such as TGF-β and cytokines (45). **Figure 2** shows how ET1 acts on two ET1 G-protein-coupled receptors situated on the smooth muscle cell surface, ET_A and ET_B (44,46).

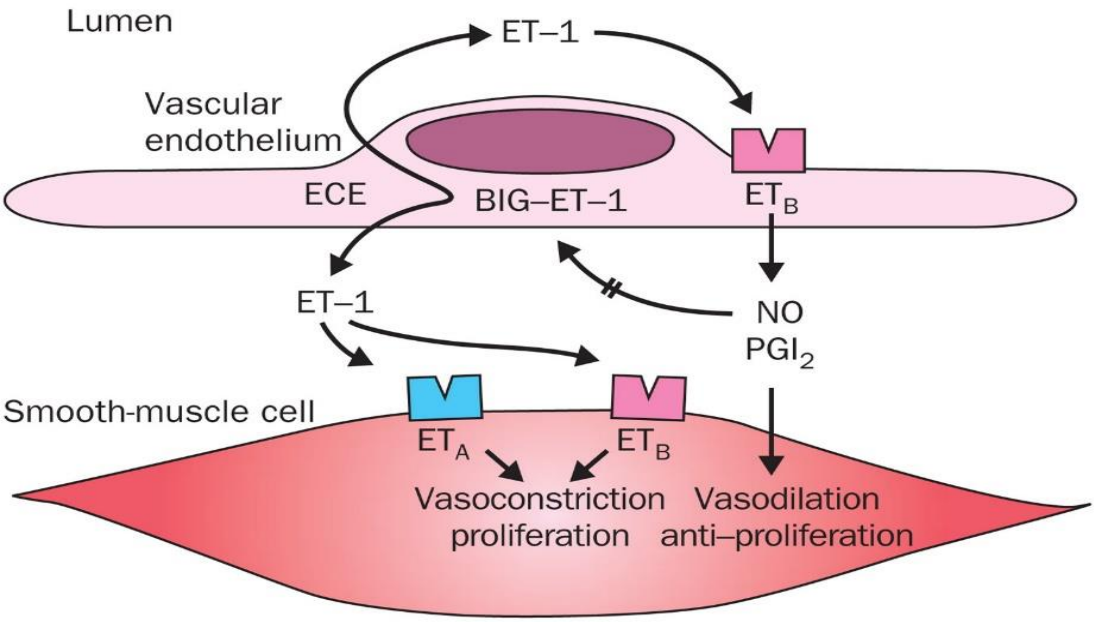

Figure 2 - Endothelin Pathway on regulation of vasoconstriction in smooth muscle cells. *Endothelin-1 (ET-1) acts on both ET_A and ET_B receptors on the smooth muscle cell surface to promote vasoconstriction or on ET_B receptors on the surface of vascular endothelium to promote vasodilation. BIG-ET1 is converted into additional ET-1 via Endothelin-converting Enzyme (ECE). Source: Dupuis, J (2001)*

When both receptors are stimulated by ET1, signalling cascades located within smooth muscle cells lead to vasoconstriction and muscle cell proliferation. ET1 can also cause inflammation, extra-cellular matrix proliferation and hypertrophy (47). However, ET_B receptors are also present on the endothelial surface, and interactions with ET1 produced via endothelial cells (autocrine system (48)) stimulate the production of NO and PGI_2 which acts on the smooth-muscle cells to influence vasodilation (44,46,49). Additionally, proliferation of muscle cells is inhibited (46). ET_B is also thought to contribute, via a negative feedback loop, to the modulation and clearance of ET1 concentrations within the pulmonary lumen as a result of NO interactions with BIG-ET1 (inhibitory effect, less protein produced) (46). BIG-ET1 is a pre-protein that is converted to ET1 via an endothelin-converting enzyme (ECE), a metalloendopeptidase (50). In patients with PAH, it is thought that endothelial ET_B receptors are either downregulated or non-functional as a result of morphological dysfunction of the endothelium. Therefore, there is a lack of NO-dependent vasodilation, and NO cannot act on BIG-ET1 leading to an increase in ET-1 and lack of successful clearance of ET1 from the pulmonary blood (47,51). This in turn causes increased vasoconstriction and smooth-muscle cell dysregulation. Therefore, elevated ET1 levels are strongly associated with disease progression, severity and prognosis.

2.1.4.2 Nitric Oxide (NO) Pathway

Nitric oxide (NO) is endogenously synthesised via nitric oxide synthases (NOS) enzymes from precursor L-arginine, reduced Nicotinamide-Adenine Dinucleotide Phosphate (NADPH), calmodulin and Flavin Adenine Dinucleotide (FAD) (52). In addition to the antioxidant Tetrahydrobiopterin (BH_4), NOS produces L-citrulline and NO (52).

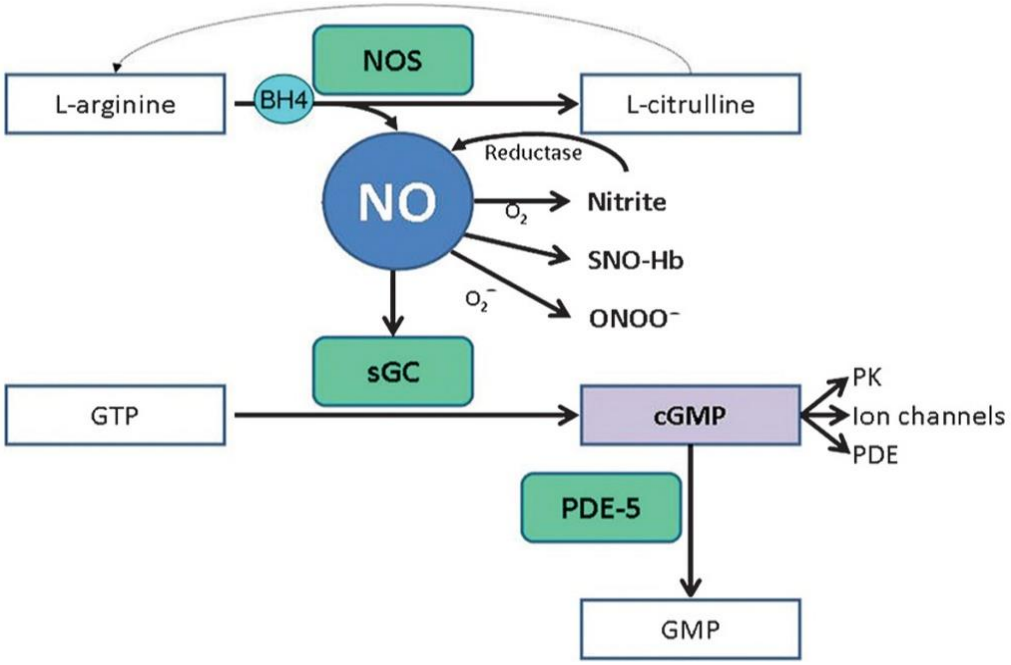

Figure 3 - Nitric Oxide (NO) synthesis and signalling pathways. *NO synthesis from precursor amino acid L-arginine causes soluble Guanylate Cyclase (sGC) to convert Guanosine Triphosphate (GTP) to cyclic guanosine monophosphate (cGMP) leading to downstream signalling cascades and vasodilation. Source: Tonelli, A et al. (2013).*

As **Figure 3** shows, NO binds to soluble Guanylate Cyclase (sGC) and activates the conversion of Guanosine Triphosphate (GTP) to cyclic guanosine monophosphate (cGMP). The natural oxidation of NO can occur, which produces nitrite that can be recycled via nitrate reductase (52) with its reactivity upregulated during hypoxia, driving vasodilation for survival (52). NO can also bind to haemoglobin, forming S-nitrosylated haemoglobin that exerts vasorelaxant effects. When NO binds to sGC, enzymatic activity is increased several hundred fold compared to its basal enzymatic rate, allowing cGMP levels to rise significantly that can further influence protein kinases (cGMP-dependent) and

cGMP-regulated phosphodiesterase and ion channels (52). cGMP interactions with potassium channels can inhibit calcium influx into smooth muscle cells via hyperpolarisation of the cell membrane, causing vasorelaxation of the smooth muscle cell (52).

Cyclic adenosine monophosphate (cAMP) production activates cGMP-dependent protein kinases (PKG) which causes downstream Ca^{2+} concentrations to fall, leading to smooth muscle cell relaxation (**Figure 4** (53)) (52,54). However, Phosphodiesterase-5 (PDE-5) degrades cGMP into GMP, causing PKG activity to fall and vasodilation to decrease in intensity (52). In PAH, PDE-5 is significantly upregulated, causing increased degradation of cGMP which leads to lack of vasodilation. In addition, the bioavailability of NO is severely limited due to reduced NOS expression within the endothelial cells, further limiting the activation of sGC and the conversion of GTP to cGMP (53). Due to inhaled NO being very short-lived in its therapeutic effect, it is deemed more advantageous to the patient to increase cGMP via inhibition of PDE-5 rather than try to increase endogenous NO concentrations (53). Hence, PDE-5 inhibitors are a viable treatment option for PAH sufferers.

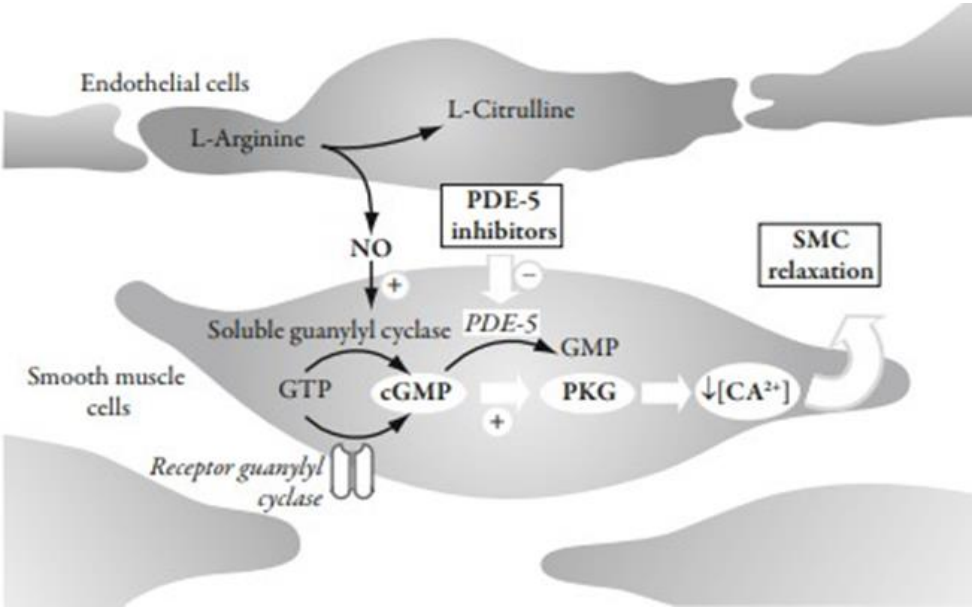

Figure 4 - The effect of Nitric Oxide production on downstream signalling cascades leading to smooth muscle cell (SMC) relaxation. *NO has an indirect on Ca^{2+} levels within SMCs, which can be dysregulated in PAH following Phosphodiesterase-5 (PDE-5) upregulation recycling cGMP to GMP. This is prevented via PDE-5 inhibitors. Source: Montani, D et al. (2009)*

2.1.4.3 Prostacyclin (PGI_2) Pathway

Prostaglandins are produced in the vascular endothelial cells via the metabolism of unsaturated arachidonic acid (55). The prostaglandin G/H synthases (also known as COXs) produce Prostacyclin (PGI_2) and Thromboxane (TXA_2) which act on varying receptor types on smooth muscle cells of the pulmonary vasculature (55).

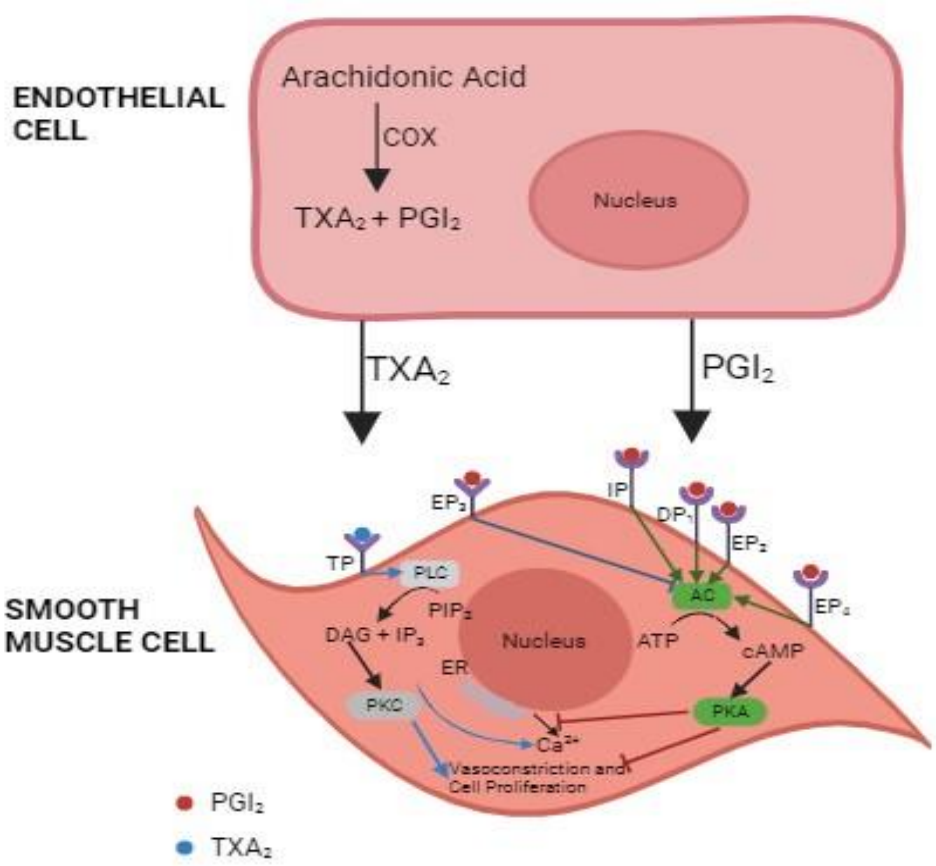

Figure 5 - Prostacyclin (PGI_2) and Thromboxane (TXA_2) Pathway in smooth muscle cells. *PGI_2 and TXA_2 are synthesised from arachidonic acid in the endothelial cell, which bind to receptors on the surface of the smooth muscle cell, causing either vasoconstrictive effects (TXA_2, blue pathway) or vasodilative effects (PGI_2, red pathway). AC = adenylyl cyclase. DAG = diacylglycerol. ATP = adenosine triphosphate. cAMP = cyclic adenosine monophosphate. DPx = prostaglandin D2 receptor. EPx,= prostaglandin E2 receptor. ER = endoplasmic reticulum. IP = prostacyclin receptor. IP3 = inositol trisphosphate. PIP2 = phosphatidylinositol bisphosphate. PKA = protein kinase A. PKC = protein kinase C. PLC = phospholipase C. TP = thromboxane receptor. Adapted from: Lindegaard, M et al. (2020)*

In **Figure 5**, 4 prostaglandin receptor types associated with cAMP modulation bind PGI_2 and its analogues that contribute to activation or inhibition of cAMP production via modulation of adenylate cyclase (9,56). Stimulation of the IP, DP1, EP2 and EP4 receptors causes adenylate cyclase activity to initiate, resulting in increased concentrations of cAMP within the cell and activating protein kinase A (9). Protein kinase A (PKA) activity then initiates downstream signalling effects that act to cause Ca^{2+} concentrations to decrease leading to vasorelaxation of the smooth muscle cells.

Contrastingly, TXA_2 receptors can bind TXA_2 which stimulates phospholipase C (PLC) to convert Phosphatidylinositol bisphosphate (PIP_2) into Inositol Trisphosphate (IP_3) and Diacylglycerol (DAG) (56). Whilst IP_3 directly modulates the concentration of Ca^{2+} inside the cell, DAG acts on Protein Kinase C (PKC) to promote vasoconstriction and smooth muscle cell proliferation (figure **Figure 5**)) (56). Therefore, non-disease state control of vasodilation and vasoconstriction of the pulmonary arteries is mediated by the balance of PGI_2 and TXA_2 production.

In PAH, there is limited prostacyclin production as a result of a lack of PGI_2 synthase (COX that produces PGI_2) (9) This causes inadequately stimulated Prostacyclin receptors, with negative downstream effects on the production of cAMP and loss of vasoconstriction (76). In addition, PAH patients experience an increased synthesis of TXA_2, further increasing vasoconstriction and smooth muscle cell proliferation via the constrictive pathway of phospholipase C (**Figure 5**) (56). To combat this, prostacyclin analogues and prostacyclin receptor agonists aim to increase cAMP production within the smooth muscle cell, increasing PKA activity and downstream vasodilative effects.

2.1.5 Treatments currently available

Treatments available to help alleviate symptoms in both PAH and PH generally can be split into Primary and Supportive treatments (57). For PAH and PH, a first-call supportive treatment is the use of diuretics (a compound that increases the volume of urine) which treats the fluid retention typically seen in the lungs, but also reduces the blood volume of the pulmonary system (57–59). Due to the vasoconstriction of the pulmonary arterial wall causing PVR increase and right ventricle expansion, the cardiac output falls due to reduced stroke volume leading to the release of anti-diuretic hormone (ADH) (60). Ultimately, ADH release acts on the renin-angiotensin-aldosterone to promote fluid retention (61). Unfortunately, fluid retention increases the volume of blood entering the right ventricle causing a right-ventricle volume overload, preventing effective cardiac output and reducing left ventricle filling (60,61). Consequently, left untreated, this will result in overall cardiac failure. Diuretics, such as furosemide and torsemide, can be used to control the blood volume entering the left ventricle (60,61). This can be used to control pulmonary arterial pressure, the reduction in right ventricle dilation and reduce the risk of catastrophic right ventricle failure (60–62). Although documented evidence shows that these diuretics have a positive effect on pressure and fluid management within PAH patients, these drugs are administered with caution due to the risk of arrhythmia induction via hypokalaemia (low blood potassium level) as well as metabolic alkalosis (raising of body pH) (58).

Inhaled pure oxygen combined with CCBs is another viable option to be used as a supportive therapy (26,59,63). However, inhaled oxygen is only recommended for patients who exhibit hypoxaemia, despite being an effective pulmonary vasculature-selective dilator, due to the efficacy being dependent on the state of the lungs which can deteriorate as a result of other lung complications e.g. COPD (63). It is also not practical as a long-term solution, as the patient would have to constantly carry oxygen equipment around which would cause increased fatigue (63). Primary Treatments like Trepostinil allow the pulmonary vasculature to dilate, reducing arterial pressure and allowing an

increase in oxygenation to the lungs (64). However, usage of this drug in combination with other therapies (antihypertensives, vasodilators and diuretics) could cause hypotension systematically (9).

Trepostinil is a Prostaglandin I2 (PGI_2) analogue, which is included in 1 of 5 classes of current therapeutic strategies aimed at targeting PAH and its underlying causes (65). These are Endothelin Receptor antagonists, Phosphodiesterase-5 inhibitors, Soluble guanylate cyclase stimulators, Prostacyclin analogues and Prostacyclin receptor agonists (65). **Figure 6** displays an overview of the multiple treatments and their molecular targets regarding each vascular dysregulation pathway (i.e. NO pathway, Prostacyclin pathway, Endothelin pathway) (17).

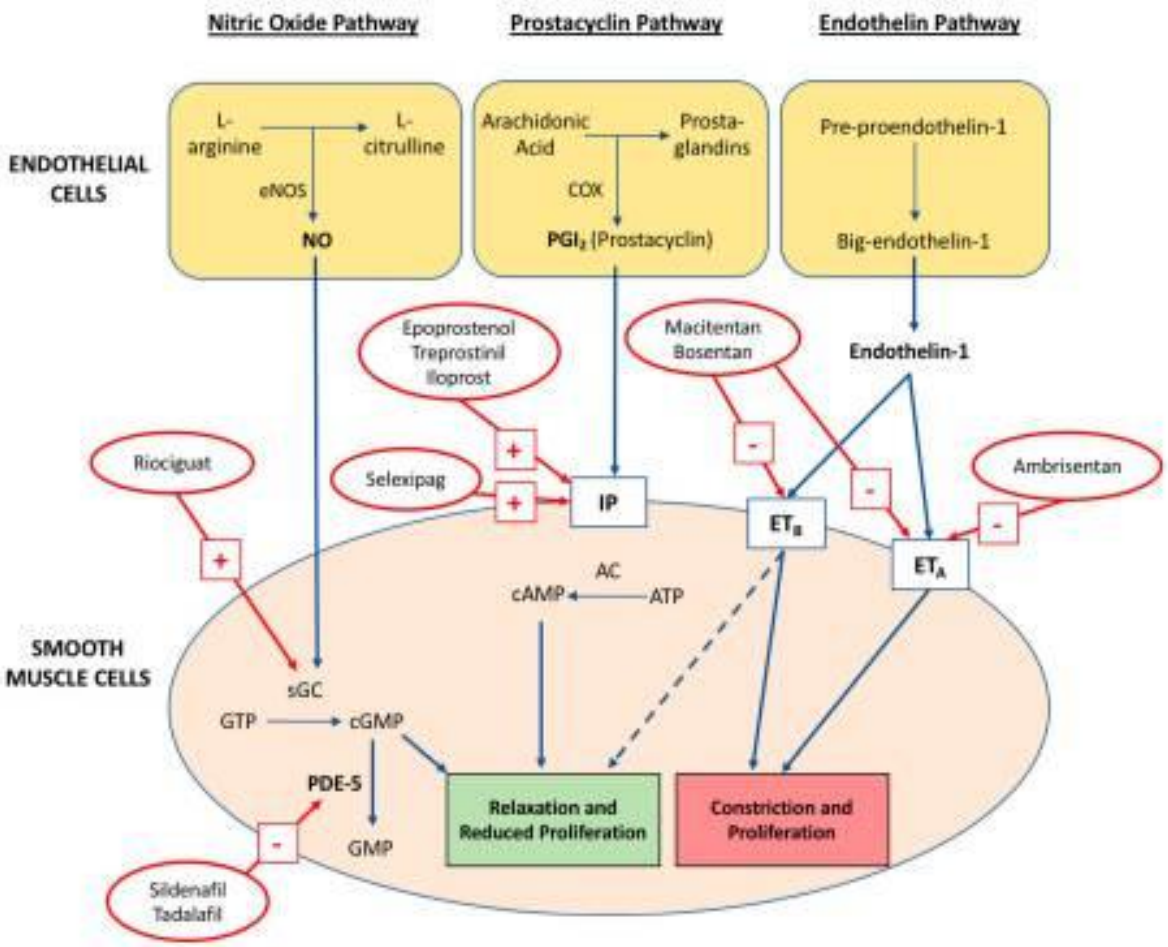

Figure 6 - Overview of Treatment options for each pathway involved in smooth muscle cell control. *Each pathway and its effects on smooth muscle cell control, with pharmaceutical treatment options (red circles) outlined. The dashed line relates to Nitric Oxide (NO) and Prostacyclin (PGI_2) action as a result of ET_B activation. AC = adenylyl cyclase. ATP = adenosine triphosphate. cAMP = cyclic adenosine monophosphate. cGMP = cyclic guanosine monophosphate. ET_x = Endothelin receptor. GTP = guanosine triphosphate. IP = prostacyclin receptor. PDE-5 = Phosphodiesterase-5. PKA = protein kinase A. PKC = protein kinase C. Source: Lan, N et al. (2018)*

2.1.5.1 Endothelin-1 (ET) Receptor antagonists

Current ET Receptor Antagonists (ERAs) are split into two categories: Selective drugs and Unselective/dual antagonist drugs (44). With selective compounds, candidates on the market typically bind to the ET_A receptor and prevent ET1 from interacting (58). This prevents vasoconstriction and cell proliferation, with clinical data showing that ET_A blockades reduce these ET1 negative effects (47) Such selective drugs, e.g. Ambrisentan and Sitaxentan, have shown promising results in improving exercise tolerance, breathing, delaying disease progression, PVR and overall quality of life (26,28,44,58). Sitaxentan was the previously used ET_A-selective drug used to improve exercise capacity and PVR via prevention of vasoconstriction and was well-tolerated up to 2 years of treatment (47,66). The selectivity of these drugs is highly advantageous, due to the non-interactions with ET_B resulting in ET1 being able to interact with ET_B on the endothelium and causing vasodilation (57). However, Sitaxentan was removed from the market shortly after 2011 due to two confirmed cases of fatal hepatotoxicity, with clinical trials ceasing thereafter (44,58). Ambrisentan is the most common drug of choice but does still carry hepatotoxic behaviour and is high-risk for those who are pregnant (67).

Unselective/dual antagonist drugs bind to both ET_A and ET_B receptors (**Figure 6**) to prevent vasoconstriction. Due to this, it has been hypothesised that selective drugs may be less effective at preventing vasoconstriction and alleviating PAH symptoms because ET_B receptors on the smooth muscle cells can still cause vasoconstriction when stimulated by ET1 (51). Bosentan is a dual antagonist drug that displayed a significant improvement in the exercise capacity of PAH patients, whilst increasing the time taken for symptoms of PAH to progress (68). Bosentan was modified structurally to increase safety, as it was shown that the drug had high incidences of adverse liver function (44,69) This modified variant, Macitentan, was discovered to possess higher affinity and longer-duration receptor binding but did exhibit preference for the ET_A receptor (44) A reduced risk for health-related quality of life deterioration was also observed in clinical trials (28). However, it is still classed as a dual antagonist and has been evaluated to be the first ERA to reduce the risk of mortality for PAH (44).

2.1.5.2 Phosphodiesterase-5 inhibitors

PDE-5 inhibitors primarily aim to raise cGMP concentrations within smooth muscle cells surrounding pulmonary arteries, to aid PKG activity and downstream vascular relaxation (53). One of the most famous PDE-5 inhibitors is sildenafil, a drug manufactured by Pfizer to treat erectile dysfunction (53,70). Although the drug is mainly used for treating erectile dysfunction, it has been repurposed to treat PAH as a result of the smooth-muscle cell relaxation mechanism in the lungs being similar (70). However, one study did recommend caution when prescribing sildenafil with PAH, due to the mortality effects are not fully documented (58). Two other PDE-5 inhibitors, Tadalafil and Vardenafil, are also very effective at inducing vasodilation. Tadalafil has a longer-lasting effect, with a half-life of 17.5 hours and is usually only taken once a day, in comparison to sildenafil and vardenafil, taken multiple times a day with a half-life of 4 hours. Sildenafil and Tadalafil have similar safety profiles, and both are well tolerated with few serious adverse effects (71). Tadalafil does carry additional symptoms such as coughing/Upper respiratory tract infections, and back pain (71). Vardenafil Is a more potent version of sildenafil, but is comparable to Sildenafil and Tadalafil in side effects and safety but possesses lower bioavailability due to low water solubility (71–73). Another downfall of PDE-5 inhibitors is that in patients with low NO production (e.g. diabetic patients), cGMP levels are further decreased so the efficacy of these inhibitors is reduced (74).

2.1.5.3 Soluble guanylate cyclase stimulators

Referring back to **Figure 4** (53), soluble guanylyl cyclase (sGC) enzymatically promotes cGMP production from GTP which allows downstream intracellular calcium levels to fall and subsequent relaxation of smooth muscle cells (53,75). PAH results in decreased cGMP concentrations as a result of PDE-5, leading to the characteristic vasoconstriction, but expression levels of sGC are increased compared to healthy lung donors (53,75). This makes sGC a viable target for pharmaceutical intervention (75). The structure of sGC is shown in **Figure 7** (74), with an α-subunit, a β-subunit, a dimerisation domain, and a catalytic domain (74). In physiological conditions, NO would bind to the Heme-Nitric Oxide domain (H-NOX) situated on the β-subunit and induce a conformational change

(74). This change would stimulate the catalytic domain to form cGMP from GTP. A lack of NO production as a result of PAH prevents cGMP production via desensitisation of sGC, so sGC stimulators act on the α-subunit to induce the conformational change required for cGMP production (74,76,77) If stimulators are combined with supportive therapeutics to boost NO production, a synergistic effect is seen to further increase cGMP concentrations and promote vasodilation (74).

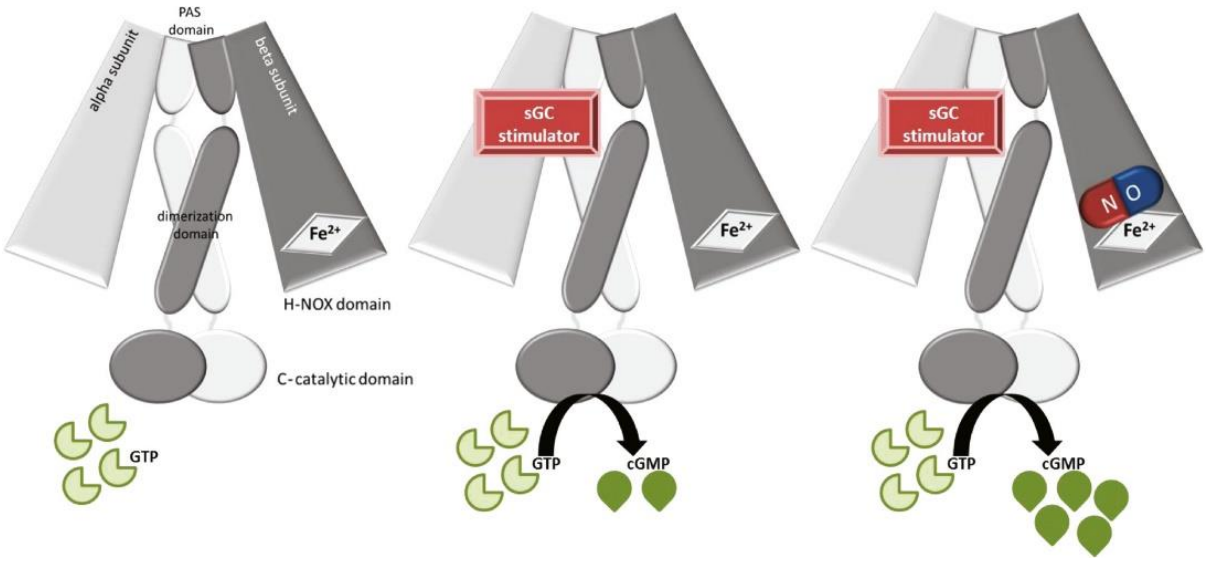

Figure 7 - A simplified structure of the heterodimeric soluble guanylyl cyclase (sGC) and its catalytic activity on GTP. *sGC consists of a α-subunit, a β-subunit containing the heme-nitric-oxide (H-NOX) domain, a dimerisation domain and a catalytic C terminal (left side). When GTP binds, it is converted to cGMP, which can be enhanced when NO is absent/decreased as is in PAH (middle). When NO is present, synergistic properties are experienced and a higher concentration of cGMP is observed (right). Source: Sandner, P (2018).*

The first Food and Drug Administration (FDA) approved sGC stimulator is Riociguat (76). This drug provides a dual effect: it binds to sGC and promotes cGMP production independently of NO, but also promotes cGMP production when NO is present (76). Thus, this treatment exhibits a higher efficacy of inducing vasodilation in comparison to PDE-5 inhibitors which makes sGC stimulators a favourable choice of treatment. Although Riociguat is the only approved drug on the market, additional compounds are undergoing research testing and clinical trials to provide alternatives (76,77). One such compound is Mosliciguat, an sGC activator that binds directly to the H-NOX domain, mimicking a bound NO and catalysing the cGMP reaction. The drug has been shown to improve circulation and aid bronchodilation, which could be beneficial for those suffering from PAH and PH (77). It has also been

shown to possess high pulmonary efficacy and improve PVR/airway resistance making this treatment a favourable alternative to other therapeutics that exhibit limitations i.e. PDE-5 inhibitors and endothelin-receptor agonists.

2.1.5.4 Prostacyclin Analogues (e.g. Prostanoids)

Prostacyclin analogues aim to induce the same effect that endogenous prostacyclin has on the smooth muscle cells, in its absence as a result of PAH progression (78). Within PAH treatments, PGI_2 analogues have been regarded as the "gold standard" since the 1990s, hence their reservation as a first-line drug in patients with PAH (9). The first approved synthetic PGI_2 designed for PAH sufferers was Epoprostenol, which binds to multiple IP receptors non-selectively situated on smooth muscle cells. However, due to the non-selectivity of Epoprostenol to the IP receptor, the Phospholipase C signalling cascade can become active following alternative prostanoid receptor activation (**Figure 8**) (56). Phospholipase C increases Ca^{2+} concentrations, counteracting the cAMP inhibition, leading to vasoconstriction (56). However, prostacyclin analogues also bind to the EP_3 receptor, which inhibits Adenylate cyclase and prevents vasodilation (56).

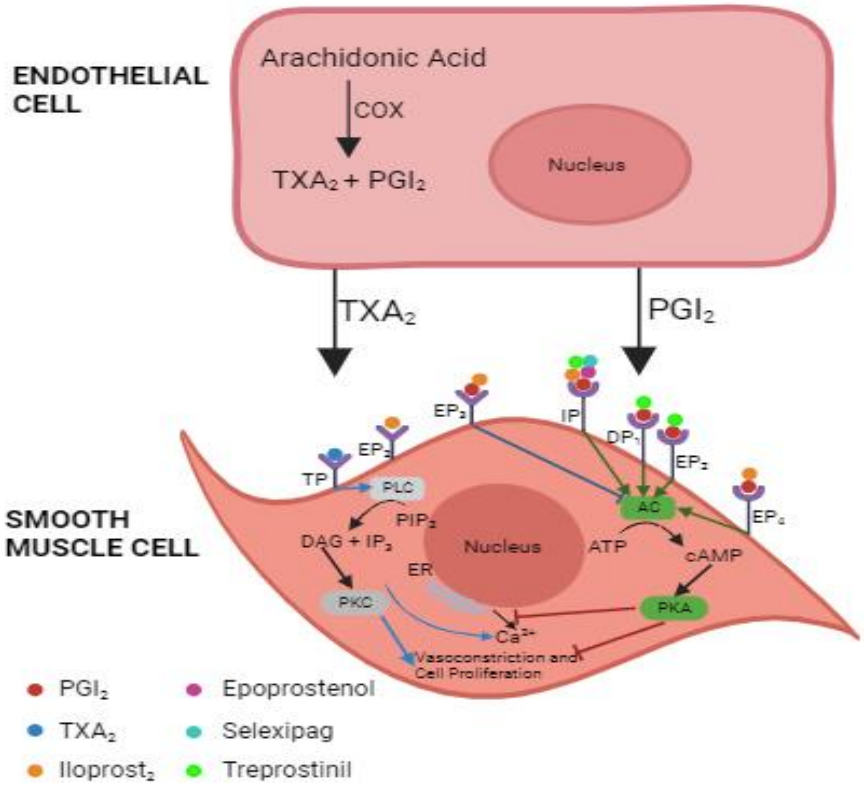

Figure 8 - The action of Prostacyclin Analogues on the Prostacyclin (PGI_2) and Thromboxane (TXA_2) Pathways and smooth muscle cell regulation. *Blue denotes vasoconstrictive pathways. Green denotes vasodilatory pathways. Red denotes inhibition. AC = adenylyl cyclase. DAG = diacylglycerol. ATP = adenosine triphosphate. cAMP = cyclic adenosine monophosphate. DP_x = prostaglandin D2 receptor. EP_x= prostaglandin E2 receptor. ER = endoplasmic reticulum. IP = prostacyclin receptor. IP3 = inositol trisphosphate. PIP2 = phosphatidylinositol bisphosphate. PKA = protein kinase A. PKC = protein kinase C. PLC = phospholipase C. TP = thromboxane receptor. Adapted from: Lindegaard, M et al. (2020)*

Epoprostenol is the only drug that has demonstrated a significant survival benefit in randomised controlled trials, via decreasing PVR and improving overall exercise capacity in the 6-minute walk test (79). This led to the reduced need for further, more drastic measures for advanced PAH (i.e. lung transplantation) (80). However, the major drawback of Epoprostenol is the need for constant IV infusions via catheter, as a result of its instability and short half-life (around 6 minutes) (79,80). Interruption of constant IV infusions may result in a surge of PAH-related symptoms that could prove life-threatening (80). Additionally, side effects such as headaches, diarrhoea, local administration site

infection and sepsis lead the drug to not be considered a holistic treatment (58). Supplementary drugs are required for long-term treatment of severe PAH, such as Iloprost and Treprostinil.

Iloprost occupies similar efficacy in its vasodilative effects when compared with Epoprostenol as a result of its homology to Epoprostenol's binding to the prostacyclin receptor (IP) (81). The drug is vastly improved in viability over Epoprostenol, as Iloprost is stable at room temperature and has an extended half-life of around 25 minutes (81). It is also aerosolised and administered via inhalation, an easier administration method when compared to IV Epoprostenol. However, the side effects are similar and after around 10 minutes from inhalation, the drug is metabolised into an inactive compound. Therefore, nebulisers are required to be used by the patients up to 12 times a day (81). Iloprost also binds to the EP_3 receptor (see **Figure 8**), which inhibits adenylate cyclase leading to inhibition of vasoconstriction (9). It also binds to the EP_1 receptor as part of phospholipase C modulation, which has downstream effects leading to vasoconstriction, detrimental to PAH patients (9).

Treprostinil can be administered Intravenously (IV), by inhalation and orally providing less burdensome administration methods (9) This drug has shown an increased affinity for the IP receptor, in addition to binding to DP_1 and EP_2 receptors (see **Figure 8**) which further induces a rise in cAMP and vasodilation as a result (9). Aside from this, Treprostinil has similar pharmacological abilities to the gold standard Epoprostenol (82). The major drawback with this drug is that when administered via IV, it causes intense pain at the site of entry which has caused patients to withdraw from this therapy (83).

2.1.5.5 Prostacyclin receptor agonists

Unlike prostacyclin analogues that can bind to other prostanoid/prostacyclin receptors, prostacyclin receptor agonists are highly specific to IP receptors (80). Therefore, prostacyclin receptor agonists prevent the induction of adverse side effects that prostacyclin analogues possess (80).

One prostacyclin receptor agonist is Selexipag (84). Once hydrolysed by microsomes situated in the hepatic cells of the liver, its metabolite ACT-333679 binds to the IP receptor with a 130-fold stronger affinity that binds to other prostaglandin receptors (**Figure 8**) (84,85). The result of this causes a significant increase in cAMP levels within the cell, inducing smooth muscle relaxation and improving right ventricle systolic pressure and endothelial dysfunction (86). The increased selectivity has proven to be advantageous in the treatment of PAH, with one study showing increased benefits in the treatment of PAH on top of a baseline regimen of two drug treatments that patients were already receiving (87). It has also been prescribed in patients as a third treatment option when endothelin receptor antagonists and PDE-5 inhibitors failed to control PAH symptoms (86). However, the incidences of common side effects associated with drugs affecting the prostacyclin pathway (receptor agonists, analogues) were increased with the administration of Selexipag in comparison to a placebo (86). It also did not improve the survival of critical PAH patients compared with a placebo. Overall, it was shown that Selexipag did greatly reduce the risk of death due to a complication related to PAH, suggesting viability as an upcoming, first-in-class treatment for PAH sufferers (86).

2.1.6 Last-line therapies and a new therapeutic target: Chloride Intracellular Channel (CLIC) 4

Despite extensive treatment options, PAH still carries a high mortality rate. A study in 2022 discovered that out of 935 patients with PAH, 121 (12.9%) died during the follow-up after receiving pharmaceutical vasodilative treatments (88). Therefore, there is still an urgent need to find more advanced therapeutics and disease inhibition strategies to curb the mortality rate of PAH globally.

In 2010, tissue samples from peripheral regions of the lung were taken from 20 PAH patients at lung transplantation and proteomic analysis was conducted (89). It was found that a Chloride Intracellular Channel (CLIC) protein was upregulated in PAH lung tissues, particularly the epithelium of bronchioles and bronchi (89). This CLIC protein was identified to be CLIC4, which is linked to varying signal pathways including bone morphological proteins (e.g. BMPR-II) and TGF-β interactions suspected to be a contributing factor to the diagnosis of heritable PAH (89). It also plays a role in RhoA (Ras Homolog gene family member A) signalling cascades leading to endothelial remodelling and proliferation of pulmonary artery smooth muscle cells (89). Further investigations concluded that CLIC4 was partly responsible for the development and progression of endothelial dysfunction in PAH, and has presented itself as a potential target for therapeutic strategies to prevent PAH development (90).

2.1.7 CLIC4 and PAH

2.1.7.1 CLIC 4: Overview, Structure and Function

Chloride Intracellular channel 4 (CLIC4) is a globular protein that belongs to a family of 6 individual CLIC proteins (CLIC1-6). Structurally, CLICs are related to omega-class Glutathione S-Transferases (GSTΩ), a group of cytosolic enzymes responsible for the detoxification of any toxic metabolites, antioxidants and carcinogens within the cell (91). CLICs were originally discovered following investigations into cystic fibrosis (CF) ion channels responsible for the aforementioned disease (92). Using indanyloxyacetic acid (IAA94) to inhibit a chloride channel within bovine kidney membrane vesicles, a membrane protein was purified which was known as p64 (but became CLIC5B). This protein carried chloride channel activity and is located in intracellular/apical membranes but did not resemble

any known ion channels (92). Following on from this discovery, two proteins that displayed homology to p64 but lacked an extensive N-terminal region were characterised, which became known as CLIC1 and CLIC4. These two are the most widely expressed and extensively studied of all the CLIC proteins (93). When the *CLIC2* gene was identified, comparisons to p64 and p64H1 (original name of CLIC4) transcripts allowed the renaming of all proteins associated with the *CLIC2* gene as CLICs, aiding the viewpoint that CLICs function as chloride channels (92). However, permeability and conductance experiments concluded that CLICs have a poor selectivity for Cl^- ions, and therefore their ability to perform as an ion channel is limited, eluding to CLICs possessing other functions within the cell (92,94).

The structure of CLIC4 is shown in **Figure 9**, using the Protein Databank (PDB) 3D structure entry 2AHE, and has a molecular weight of approx. 28.8 kDa (95).

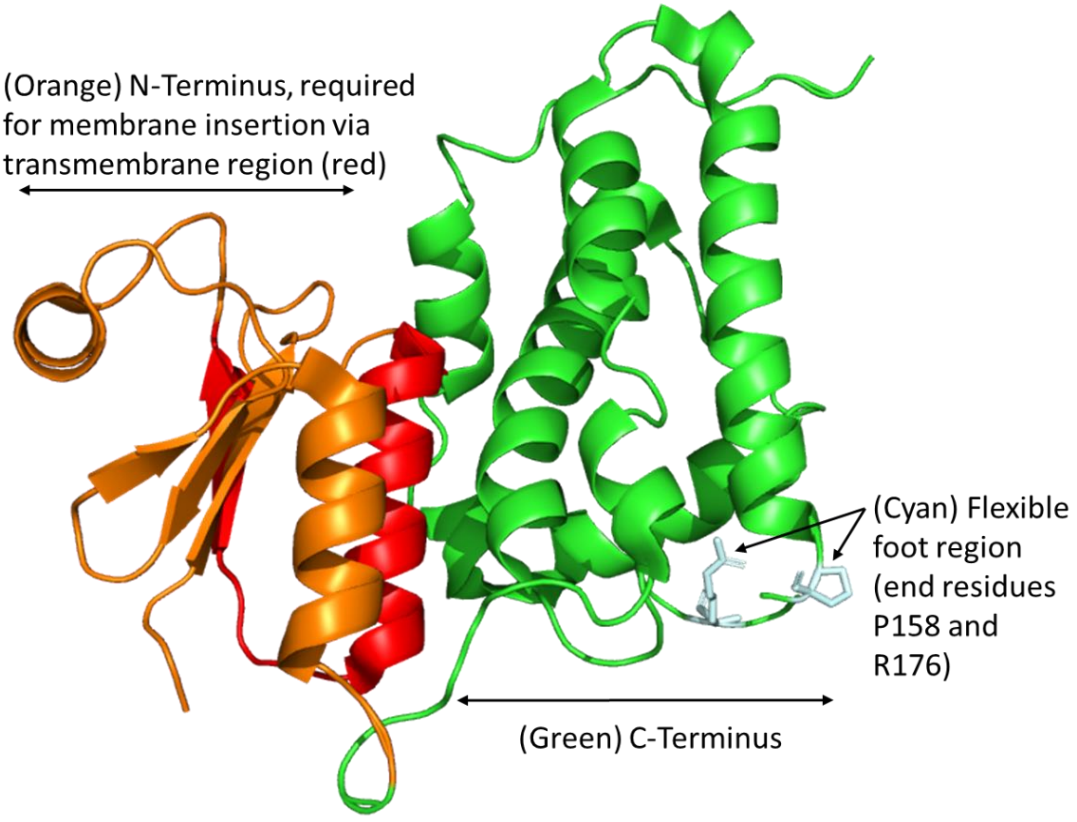

Figure 9 - The structure of Chloride Intracellular Channel (CLIC) 4. *Obtained from PDB entry 2AHE and modelled in Pymol, CLIC4 contains an N-Terminus (orange) which possesses a Transmembrane region required for membrane insertion aided by divalent cations (not shown). The C-terminus (green) contains a "flexible foot region" which is marked by border residues P158 and R176 (cyan) due to missing residues on the PDB file.*

Sequence alignments have shown that CLIC1 and CLIC4 are closely similar, with one key difference between the two isoforms being attributed to CLIC4 lacking a Cys24-Cys59 disulphide bond of which CLIC4 has, required for CLIC1 homodimerisation (96). The N-terminus of CLIC4 (Orange, **Figure 9**), possess a thioredoxin fold, involving residues 16-105 which is believed to undergo conformational changes inducing structural reorganisation that allows for insertion into a bilayer, via the exposure of hydrophobic residues that forms a single transmembrane segment (Red, **Figure 15**) (95,96). Hence, this region is highly flexible and may aid the oligomerisation of CLIC4 into dimers, trimers etc (96). The C-terminus is all α-helical domain and contains a nuclear localisation signal (residues 199-206) required for translocation to the nucleus within the cell (97). Despite sharing high homology with the GSTΩ in terms of folds (Thioredoxin fold in the N-terminus that is similar to the protein Glutaredoxin), CLICs contain a "flexible foot" region that is situated within the C-Terminus (95). This site is indicated in **Figure 9** in cyan, but only the "border" residues of P158-R176 due to missing residues on the PDB file (95,98). However, this flexible region makes the CLICs unique, as this region is not seen in any GSTs (95).

CLIC4 exists as a dimorphic protein; A soluble form within the cytosol almost entirely, as well as an insoluble form once inserted into a lipid bilayer (99,100). This insertion was originally thought to be based on the oxidation state of the protein, via the oxidation of the Cys24-Cys59 disulphide bond (100,101). However, CLIC1 was recently discovered to be redox-independent regarding membrane insertion, with the mechanism being reliant on divalent cations such as Zn^{2+}(100). This is thought to translate to CLIC4 (100,101). CLIC4 expression is typically ubiquitous throughout the cell, found in the nucleus, cytoplasm, ER, mitochondria, Golgi, intracellular membrane (hence its name) and cytoskeleton (associated) (102). One of the most important locations is the plasma membrane, where cytosolic CLIC4 has been shown to translocate to the plasma membrane to modulate cell migration and adhesion via its association with β_1 Integrin (98). Another key localisation of CLIC4 is endosomal and secretory vesicles, where it is linked to endosomal/vesicular trafficking and membrane remodelling (102,103).

As such, CLIC4 has been widely speculated to be involved in numerous subcellular functions (including cell proliferation and apoptosis), with links to diseases such as squamous cell carcinogenesis, breast cancer and neuronal degeneration (93,104). This is due to the high expression of CLIC4 in the skin and brain (102). However, CLIC4's function as a signalling cascade mediator, particularly its role in angiogenesis, has placed it under investigation for its role in PAH (104).

2.1.7.2 Signalling Cascades and development of PAH

CLIC4 is well documented in its signalling cascades within the pathogenesis of certain diseases. In certain cancers, such as the aforementioned squamous cell carcinogenesis. Upon keratinocytes becoming stressed (via reactive oxygen species (ROS), DNA damage etc.), CLIC4 has been known to rapidly translocate to the nucleus and enhance TGF-β signalling, by preventing dephosphorylation of phospho-Smad 2 + 3 and initiating cell arrest and apoptosis (93,105). Thus, CLIC4 has been described as a tumour cell suppressor in cancer (105).

Soluble CLIC4 is known to be localised to endothelial cells in the development of PAH vascular lesions, allowing for altered endothelial survivability and angiogenesis in those endothelial cells (106). CLIC4 has been reported to target RhoA G-protein coupled receptors (GPCR) involved in the RhoA signalling pathways (103). Specifically recruited via the activation dependence of G_{α} -13 RhoA receptors, CLIC4 seems to influence signalling cascades with downstream effects on tubulogenesis and angiogenesis (107,108). When Lysophosphatidic acid (LPA) binds to G_{α} -13 RhoA GPCR, CLIC4 binds to NHERF2, a scaffold protein that connects the actin cytoskeleton (polymerised by Rho) to transmembrane GPCRs, causing cytoskeletal changes leading to endothelial cell restructuring and vascular lesion development (93,98,106). It has also been shown that reduced CLIC4 expression in endothelial cells in umbilical veins led to the normalisation of cell proliferation and capillary lumen formation (108). This suggests CLIC4's role in vascular remodelling/responses and the link to PAH development, however, the downstream role CLIC4 plays in the RhoA signalling cascade remains unsolved (108).

Pulmonary Arterial Smooth Muscle Cells (PASMC) migrate as a result of atherogenesis in response to vascular injury (106,109). This is partly governed by the expression of the gene *BMPR2*, which as discussed previously, has been linked to the development of PAH due to mutations present in heritable and idiopathic-diagnosed patients (see section: Causes and Diagnosis of PAH). A 2019 study outlaid how mutations in *BMPR2* result in reduced expression of BMPRII, which maintains CLIC4 concentration within PASMCs (18,106,109). Previously, CLIC4 has been linked to the activation of RhoA but it also activates Rac1, causing downstream cytoskeleton remodelling for increased PASMC migration. This is also aided by the direct activation of Rac1 and RhoA by the action of the cell surface receptor RAGE (receptor for advanced glycation end products) (106).

The pathogenic mutations in *BMPR2* have a more involved effect in the Pulmonary Arterial Endothelial Cells (PAECs), where reduced expression of BMPII proteins causes downstream Nuclear Factor Kappa-light-chain-enhancer of activated B cells (NFκB) and TGF-β upregulation (106). The effect of upregulated NFκB results in a direct modulation of Hypoxia-Inducible Factor 1α (HIF1α) which in turn causes Vascular Endothelial Growth Factor (VEGF) and ET1 to drive inflammation, PAEC over-proliferation and PAH symptom acceleration (18,106). The TGF-β expression has the same effect on phospho-Smad 3 as in squamous cell carcinoma, but this causes an opposite effect; in PAECs, phospho-Smad 3 inhibits apoptosis, allowing survivability of PAECs and dysregulation of angiogenesis and pulmonary vasculature to continue (106). CLIC4 is predicted to feed into BMPR2 expression, by causing lysosomal degradation of the BMPR2 protein. Thus, a negative cycle of vascular dysfunction is observed, placing CLIC4 at the heart of the pathogenesis (106).

The downstream NFκB effects, modulated by CLIC4 within the PAEC, involve an intermediatory protein along the same pathway. This intermediatory protein is Arf6 and was recently proposed to be linked to PAH via its interactions with CLIC4 (106,110). This discovery provides some explanation of the effects of CLIC4 on the signalling pathways that ultimately lead to the progression of PAH, opening up potential therapeutic targets and strategies for future development (110).

2.1.8 Arf6/CLIC4 Pathway

ADP ribosylation factor (Arf) 6 is a small G-protein belonging to the Ras family, which regulates the cytoskeleton of the cell via its activity as a guanine nucleotide binding protein (111). Hence, it is a GTPase, switching between the GDP-bound (inactive) and GTP-bound (active) forms **Figure 10** shows the proposed influence of CLIC4 on the Arf6 pathway, starting with hypoxia, ROS and DNA damage upregulating CLIC4 expression.

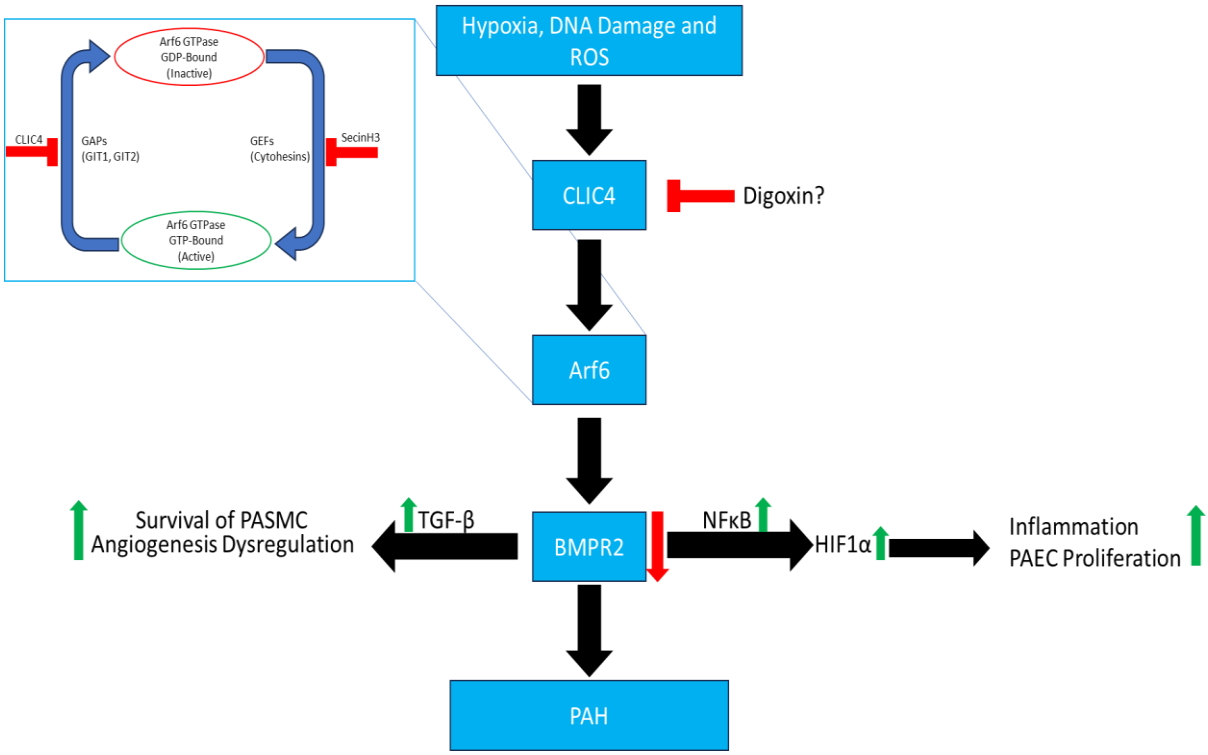

Figure 10 - The Arf6/CLIC4 Pathway. *Hypoxia, DNA damage and Reactive Oxygen Species (ROS) triggers a signalling cascade that results in Arf6 overstimulation and Bone Morphological Protein Type II down-regulation. This causes up-regulation of inflammatory molecules, Pulmonary Arterial Endothelial cells (PAECs), survival of Pulmonary Arterial Smooth Muscle Cells (PASMCs) and angiogenesis dysregulation. Arf6 activation is the consequence of GAP/GEF dysfunction via CLIC4 over-expression leaving Arf6 GTPase in an "always-on state" (blue box, left). Green arrows = Up-regulation. Red arrows = Down-regulation. Red "T" = Inhibition. HIF1α = Hypoxia-Inducible Factor 1α. NFκB = Nuclear factor kappa-light-chain-enhancer of activated B cells. TGF-β = Transforming Growth Factor β. Source : Abdul-Salam, V et al. (2019).*

Arf GTPase-activating protein (GIT) 1 and 2, known as GTPase activating factors (GAPs) are thought to bind to Arf6 in the active form, to promote transition to its inactive form (hydrolysis of GTP) and prevent downstream PAH development, certainly in PAECs (110,111). Conversely, cytohesin proteins that act as Guanine nucleotide Exchange Factors (GEFs) trigger the inactive to active Arf6 conversion

(110,111). Thus, these GAPs and GEFs act to “switch on” or “switch off” Arf6. (110). With Arf6 now active, the signalling cascade can then promote the negative impacts of PAH via vascular remodelling, cell proliferation etc. This is achieved by Arf6 causing an increase in BMPR2 expression, leading to increased NFκB and TGF-β concentration and PAH development (110). Some preclinical studies have shown that the cytohesin inhibitor SecinH3 has prevented inflammation and over-proliferation of the pulmonary endothelial cells, by preventing Arf6 activation and keeping Arf6 in the inactive state (110). However, this is potentially outweighed by the effect of CLIC4 on the progression of PAH, both its involvement in driving pathogenesis via the RhoA signalling, negative regulation of BMPRII and dysfunctional Arf6 “always-on” activation. This “always-on” interaction is predicted to be due to CLIC4 -GIT1 interactions, preventing GAP activity. Therefore, CLIC4 presents itself as a therapeutic target for the reduction of PAH symptoms for patients, in addition to uncovering the mechanisms behind aberrant vascular morphology.

2.1.9 The search for CLIC4 Inhibitors: Digoxin

The inhibition of CLIC4 provides a promising outlook on the regression of both PAH and cancer, on the condition that CLIC4 inhibitors can be identified. IAA94 is a known CLIC inhibitor, based on a GST inhibitor (ethacrynic acid) given the homology between GSTs and CLICs, that has proven to reduce the progression of other disease states, such as neurodegeneration and carcinogenesis (98). This is achieved via a mechanism of action of partially blocking the chloride channel (98,112). However, the drug is non-specific and acts on multiple CLICs (e.g. CLIC1, CLIC3 and CLIC5) (98). Therefore, further research is required to identify chemical compounds with increased specificity to CLIC4, to formulate into effective inhibitors. In addition, novel molecules and successful inhibitory interactions with CLIC4 can be studied to further ascertain CLIC4’s functional role in pathogenesis development in PAH, but also carcinogenesis and neurodegeneration.

A paper published in 2022 by Dr. Abdul-Salam and Dr. Ortega-Roldan reported screening for compounds that had potential inhibitor effects when allosteric sites on CLIC4 were discovered (98).

Their results concluded that out of 1615 compounds, the compound they deemed yielded the most inhibitory potential (based on binding energy affinity) was Digoxin (98). This was among other compounds, such as Amphotericin B and Rapamycin (98). The compound was predicted to bind to a site that is situated around the "flexible foot region" displayed in **Figure 9** (see section: 2.1.7.1 CLIC 4: Overview, Structure and Function). However, the study also revealed a site in the N-terminus (the GSTΩ Thioredoxin-like domain) that was suggested to be a better-suited allosteric site and possessed higher "druggability" (98). In comparison to digoxin, IAA94 performed poorly regarding its binding affinity and hence is not a very CLIC-4 selective chloride channel inhibitor (98). The result of the study provided insight into the suggested allosteric binding sites that CLIC4 could possess and their respective ligands that warrant further research into inhibition potential. This could be confirmed by studying interactions with CLIC4 and Digoxin and detecting binding within regions of the protein to model interactions computationally. If evidence then suggests Digoxin is suitable as a CLIC4 inhibitor, especially if the "flexible foot region" is indeed the allosteric site, then CLIC4 translocation and motility within the cell could be greatly hindered (98). Thus, prevention of disease progression could be a reality, via perturbing the signalling cascades mentioned prior (BMPRII, RhoA, TGF-β etc.) and subsequent improvement of quality of life for multiple disease types, particularly PAH.

2.1.10 GTPase Activating Protein (GIT) 1 and CLIC4

As mentioned previously (See section: Arf6/CLIC4 Pathway), a GIT1:CLIC4 interaction could be responsible for the progression of dysfunctional vasculature remodelling and inflammation, a signature of PAH. Thus, it is hypothesized by Abdul-Salam et al. that interactions between CLIC4 and GIT1 cause Arf6 to remain GTP bound (or in its "active" state", see **Figure 10** section: 2.1.8 Arf6/CLIC4 Pathway), driving the Arf6 pathway and PAH progression. The same study also reported that early K_d values for GIT1:CLIC4 are similar to that of GAP-Arf interactions (110). Therefore, GIT1 and its interactions may play a significant role in PAH pathogenesis.

Figure 11A displays the structure of GIT1, obtained from an Alphafold prediction based on sequence with a molecular weight of approx.. 86.0 kDa (113). No PDB file is available as the crystal structure of GIT1 has been obtained yet, however, 3 clear domains are predicted with a very high per-residue confidence score (pLDDT) of >90 (**Figure 11**A, dark blue). The structure displayed in Pymol shows these distinct domains categorised into their proposed functions (**Figure 11**B: Red C-terminus (residues 642-762) is proposed to interact with Paxillin (involved in focal adhesions and signalling pathways) and TGF-β, Orange coiled-coil domain involved in dimerisation (residues 422-472), and the Blue N-Terminus (Residues 1-356). The latter contains the Arf-GAP domain, which involves residues 1-124 and is responsible for the interactions with Arf6 and CLIC4 (114). This domain also contains signature ankyrin repeat motifs (residues 132-228). Primarily expressed in the brain, PASMCs and lung bronchi, GIT1 is responsible for VEGF signalling hence its potentially pathogenic role in PAH development via angiogenesis and cell proliferation (114).

Due to GIT1 playing a role in the hypothesised Arf6/CLIC4 pathway on the progression of PAH detailed above (see section: 2.1.8 Arf6/CLIC4 Pathway), investigating the binding between GIT1 and CLIC4 would initiate some perspective on the intricate signalling cascades that hallmark PAH development. Both CLIC4-Digoxin and CLIC4-GIT1 binding events can be determined via the use of Nuclear Magnetic Resonance (NMR), a spectroscopic technique utilising NMR-active nuclei present with proteins to visualise the movement of residues upon interaction with ligands and other proteins.

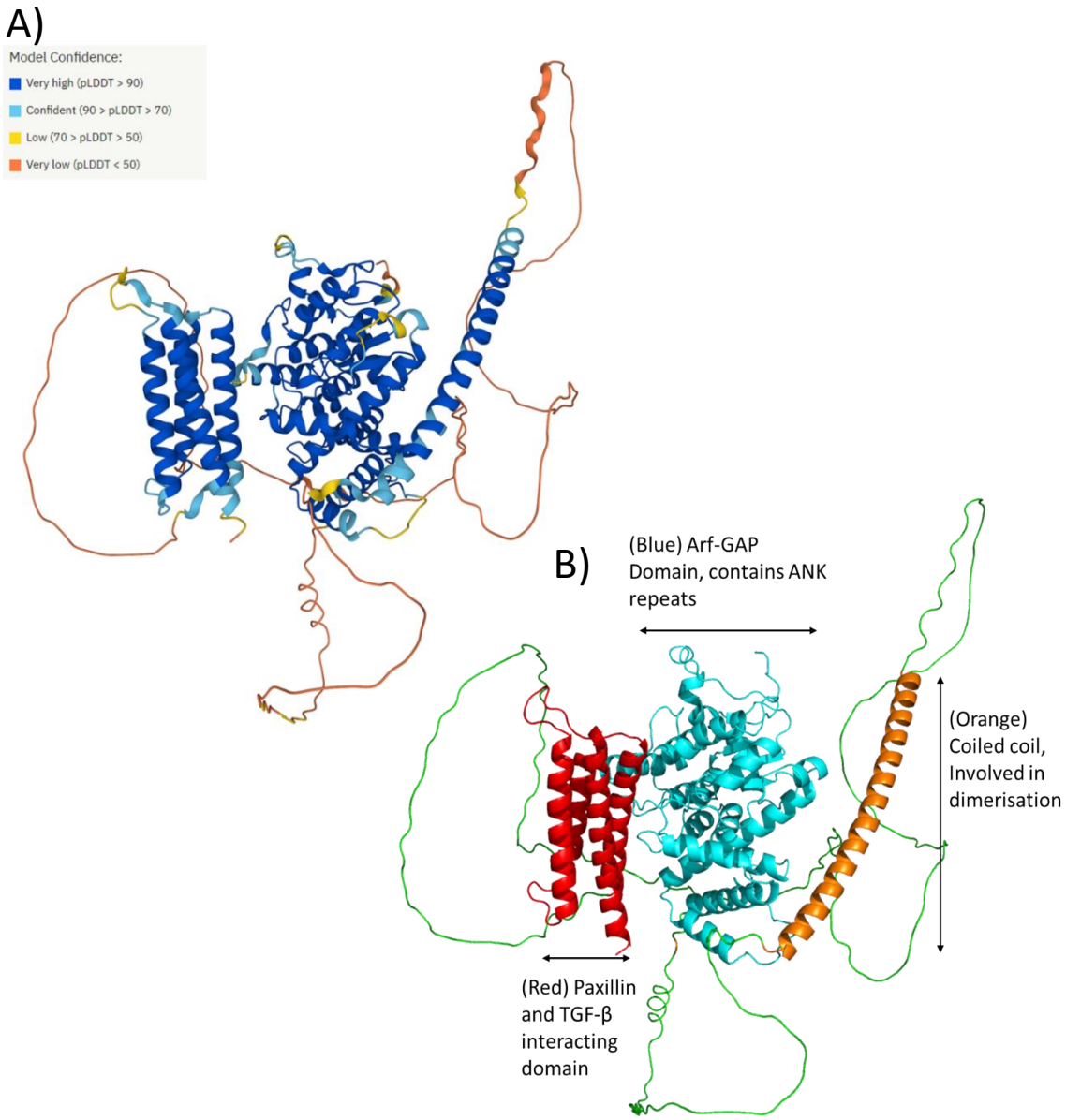

Figure 11 - The Structures of Arf GTPase-activating protein (GIT) 1. *A) Alphafold prediction model based on protein sequence, as no known crystal structure has been obtained. Each residue (and the secondary structure they form) has been colour-coded based on a per-residue confidence score (pLDDT), key of colours corresponding to confidence score shown above. 3 clear domains are seen in GIT1, with detail shown in the second panel. B) Pymol model of GIT1, based on the Alphafold model in panel A. The 3 domains are coloured, and functions detailed: Red = Interacts with Paxillin and TGF-β, Orange = coiled coil domain involved with dimerisation, and Blue = Arf-GAP domain responsible for binding GEFs and GAPs (and CLIC4).*

2.2 Nuclear Magnetic Resonance (NMR)

2.2.1 Analysing Proteins via NMR

Nuclear Magnetic Resonance (NMR) is a spectroscopic technique that was previously utilised for determining the structure of biological molecules in place of crystallisation for X-ray crystallography (115). However, the biological applications can also elucidate protein-protein and protein-ligand interactions, which can be determined due to how atoms within a molecule respond to electromagnetic waves and their effect on the environment around an individual atom (116).

To identify NMR signals, the molecule of which one is studying is required to contain atoms that are "magnetic" or "active" nuclei. This is dependent on their spin state (116). Atoms contain protons and neutrons which in themselves have "intrinsic angular momentum" (AKA "spin") (117). In atoms with even mass numbers (therefore even proton and neutron numbers), the spins cancel out resulting in a whole integer net spin (116,117). However, those atoms with odd mass numbers (e.g. ^{1}H, ^{15}N, ^{13}C) possess a net half-integer spin, which causes a magnetic moment to form in a particular direction known as "spin states" which can be +1/2 (spin up) or -1/2 (spin down) (116,117). When these atoms are in the presence of a strong magnetic field, they align their magnetic moment in the same vector as the magnetic field, which is termed B_0. They wobble on the z-axis whilst in line with this magnetic field, called precession (117). When a radiofrequency pulse (short burst of electromagnetic energy, termed "Rf") is passed perpendicular to the B_0, the nuclei will re-orientate themselves along the X-Y axis from which the Rf originates, provided the Rf pulse is the same frequency as the magnetic nuclei's precession rate (which is correlated to the resonant frequency) (117). This re-orientation, or change in magnetisation vector, is the signal to which the detector coil in an NMR machine responds. A graphical representation is shown in **Figure 12**.

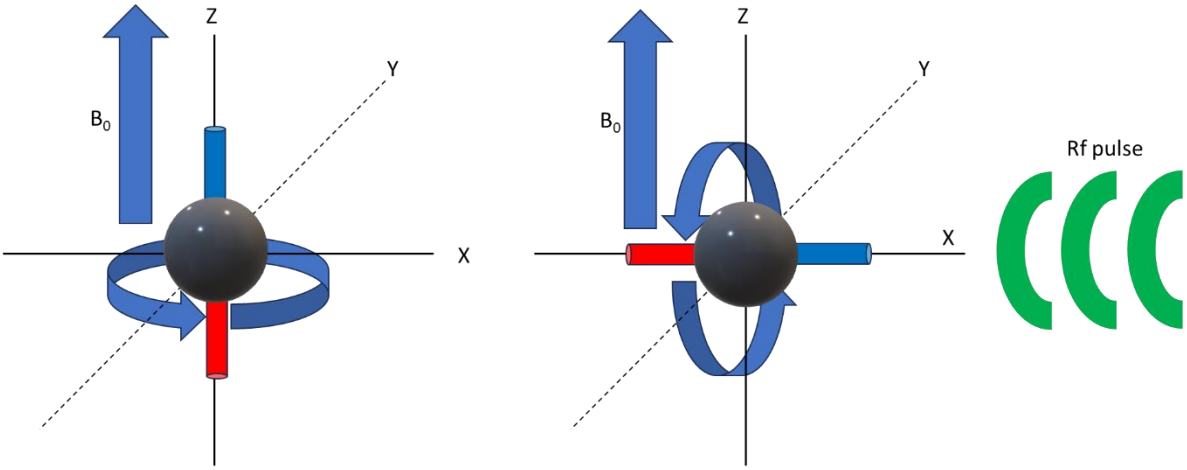

Figure 12 - Simplified Diagram of Nuclear Magnetic Resonance. *(Left panel): When magnetic or "active" nuclei (grey sphere) are present in a magnetic field, their magnetic moment is aligned with the vector of the magnetic field (B_0) along the Z-axis and spin on the X axis, called precession. (Right Panel): When a radiofrequency pulse (Rf), that is of the same frequency as the precession rate of the nuclei (green waves) is passed perpendicular to the B_0, the spinning nuclei re-aligns its magnetic moment along the X-Y axis. This change in magnetisation vector emits a signal which is picked up in the NMR machine.*

The signal is a typical sine wave, decreasing in amplitude as the signal deteriorates as the nuclei re-align with B_0 (116,117). The signal generated as a result is known as Free-Induction-Decay (FID), presented within the time domain. This FID is processed via a Fourier Transform equation into a spectrum along the frequency domain to output 1-dimensional and 2-dimensional spectra peaks (116).

Therefore, each magnetic nuclei in a protein, such as ^{15}N atoms in the backbone of each protein residue, will emit a different FID trace as a result of each atom being present within a different chemical environment (115–117). This effect is the consequence of shielding, where a magnetic nucleus will be more/less sensitive to the Rf pulse depending on the electron density around it. A higher electron density means its resonance frequency is lower due to a lower magnetic field effect, so a lower FID frequency (116–118). Over the entirety of a protein, different atom resonant frequencies can be built up to display a spectrum with "peaks" corresponding to each atom (117). The resonance frequency of each peak is known as chemical shift, and in the context of proteins, each residue will have a different chemical shift as a result of the electronic environment around it, which is affected amongst other factors by the tertiary structure. In the case of a protein labelled with 15N,

any folding events within the protein that change the environment of a 15N atom of a residue will result in a change in signal, or a chemical shift perturbation (CSP). These chemical shifts can then be seen on a 2D Heteronuclear Single Quantum Coherence (HSQC) so that each peak correlates to an individual residue of the protein sequence (117,119).

CLIC4 structure is well known via the crystallisation of the protein (see section: 2.1.7.1 CLIC 4: Overview, Structure and Function). However, the structural changes as a result of protein-ligand or protein-protein binding that would be investigated cannot be aided by the protein crystal (no information on binding and chemical shifts can be extracted from the crystal). As such, the change in the chemical environment around magnetic nuclei located within the CLIC4 protein, which would indicate binding interactions, is recorded via NMR assays. Hence, the display of CLIC4 protein peaks on a 2D spectrum, such as a 2D HSCQ spectrum, is paramount to begin to understand protein-protein and protein-ligand binding. The HSQC shows all H-N correlated nuclei of each residue on the backbone of a protein and is regarded as a "fingerprint" of the protein being analysed. The HSQC gives information about the quality of the protein sample (does the sample need deuteration) and whether higher field strengths are required (for better resolution of each peak)

2.2.2 Predicting CLIC4 interaction sites with ligands/proteins: The problem

Simply running a 2D HSQC on CLIC4 is the first step, but identifying the residues concerned with binding events is more complicated. To start with, the standard procedure to identify a protein-ligand or protein-protein binding site would be to grow a labelled protein sample (e.g. protein backbone labelled with ^{15}N) and titrate with an unlabelled ligand or another protein (120). If the ligand is titrated in excess, binding site saturation will occur leading to CSPs of peaks associated with residues situated within or near the ligand binding site (120). CSPs are shifts between two peaks associated with one residue, as a result of its chemical environment changing upon protein-protein or protein-ligand interactions occurring (120). By tracking how peaks shift across an HSQC spectrum, it is possible to identify significantly shifted peaks via their CSP value, hence suggesting involvement in binding site

interactions. Alternatively, significant CSPs can be attributed to allosteric interactions, or secondary structure modulation due to backbone conformational changes (120).

Tracking CSPs of residue peaks relies on the exchange rate of bound protein-ligand and free protein present in the solution. If we consider that in a protein-ligand titration, [P] is free protein, [L] is a free ligand and [PL] is a bound protein-ligand, then we can express the binding and dissociation of the complex as:

$$[P] + [L] \leftrightharpoons [PL]$$

Where [P] + [L] association rate is k_{on} and [PL]→ [P] +[L] dissociation rate is k_{off}. Therefore, the dissociate constant K_d is given by $K_D = \frac{k_{off}}{k_{on}}$ (120,121). If the exchange rate is fast, so k_{off} is faster than the chemical shift difference of [P] and [PL], then there is a distinctive peak shift from the free protein spectrum to that of the bound protein spectrum. Likewise, if the exchange rate is slow (k_{off} is slower than the chemical shift difference of [P] and [PL]) then the free protein spectrum peak disappears and the bound protein spectrum appears, almost like the peaks are "stacked" (120,121). This is shown in **Figure 13** (121).

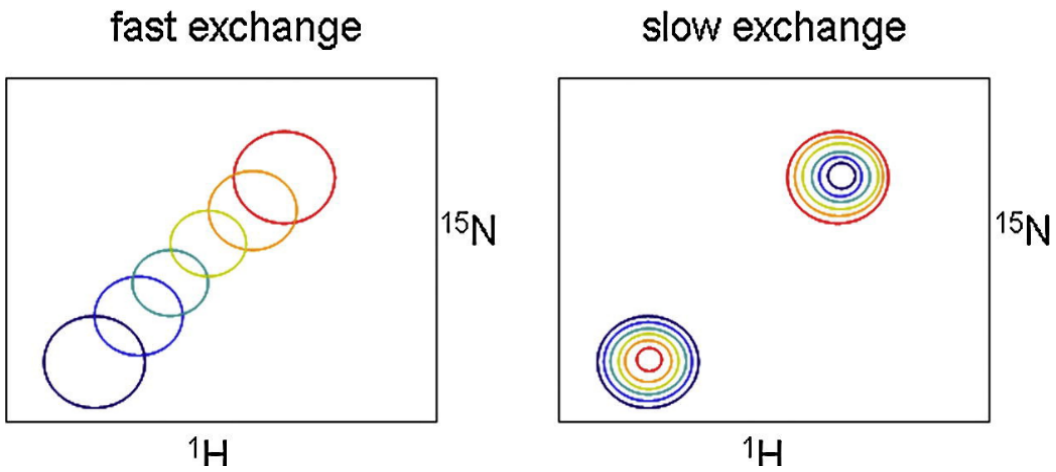

Figure 13 - Types of exchange rate on a 2D ^{1}H – ^{15}N HSQC spectrum. *(Left) Fast exchange occurs when the dissociate rate (k_{off}) of a protein-ligand interaction is faster than the chemical shift difference of free protein [P] and protein-ligand complex [PL]. This can cause peaks to shift from blue (unbound) to red (bound) states with weighted average of the chemical shifts in the middle. Slow exchange occurs when k_{off} is slower than the chemical shift difference of [P] and [PL], then strong signals for either unbound (blue stacked peak) or bound (red stacked peak) are seen. Source: Maity, S et al. (2019).*

CSPs are calculated using the equation:

$$CSP = \sqrt{(\Delta 15N/7.142)^2 + (\Delta 1H)^2}$$

Where value 7.142 is the scaling difference between ^{15}N and ^{1}H axis on the HSQC spectrum, and Δ is the difference in the axis value of the unbound and bound spectra (120,121). By calculating the CSPs, each residue CSP value can be statistically analysed for significance based on standard deviation and mean comparison. Hence, those residues with statistically significant CSPs suggest binding site locations and structural conformational changes.

However, the value of CSPs relies on knowing which peak present on an HSQC is which residue in the CLIC4 sequence. Therefore, CLIC4 must have its residue peaks assigned. Without these assignments, the modelling of a binding site and its interactions with ligands cannot be predicted. Such assignments must be made with additional spectra, which allows each residue's Cα, Cβ, and C=O to be attributed to its perceived chemical environment peak.

2.2.3 Residue Assignment of CLIC4

Residue assignment utilises a triple-labelled (^{15}N for backbone, ^{13}C for Cα and Cβ and D_2O for hydrogens) of which multiple NMR spectra are collected (119). This is because each spectrum collected gives different information about the residue you are trying to assign (119). The spectra used are 3D spectra, meaning that they are based on a 2D HSQC but incorporate a third dimension which is the ^{13}C dimension (119). Using an example of one 3D spectrum, an HNCACB, the axis set-up is such that the ^{1}H is on the X-axis, ^{13}C on the Y-axis and ^{15}N on the Z-axis.

What one looks at is a 2D ^{1}H-^{13}C spectrum, but has the ^{15}N dimension on the Z-axis. The ^{15}N dimension is crucial for identifying each residue, as this correlates to the H-N nuclei of each residue in the protein sequence. Thus, each residue is identified by its ^{15}N frequency (119). When assigning residues one can isolate peaks that display a particular ^{15}N and ^{1}H frequency, and "zoom in" on that peak. However, the

entire ^{13}C height is available for identification of Cα, Cβ etc (119). This is what is known as a "strip", with the concept of strip design shown in **Figure 14**.

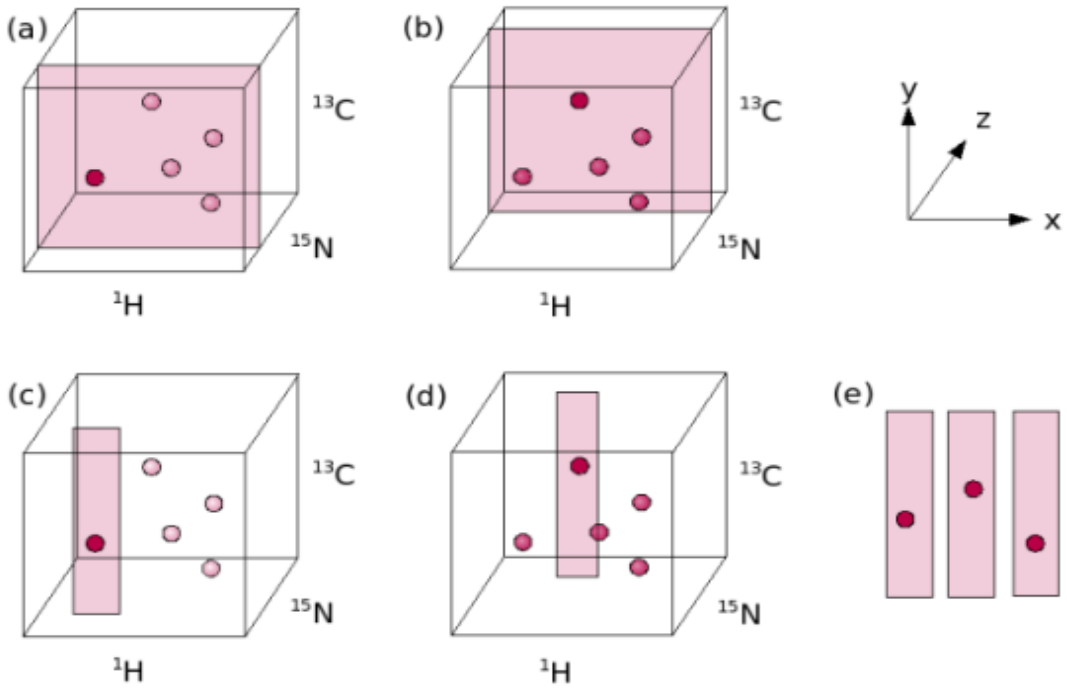

Figure 14 - Simplified diagram of visualising 3D NMR spectra as "Strips". *A) In a 3D spectrum, one peak will be present in one particular ^{15}N z-plane (dark red peak). B) Peaks with similar ^{15}N ppm values will lie just above or below the plane one looks at. C and D) If you trim the ^{1}H dimension down you can focus on just the region containing the peak desired, across different ^{15}N ppm values. E) The 2D HSQC will define each peak via ^{1}H and ^{15}N values, so you can pick out strips for each HSQC peak and align them next to each other comparison. Source: Higman, V (2012)*

As **Figure 14** shows, the strips containing certain residue atom peaks (either Cα, Cβ or C=O) can be seen across each ^{15}N frequency and therefore every residue in a protein sequence (119). In a spectrum like an HNCACB, each strip will have two intense peaks (one Cα, one Cβ) of the current residue being examined (i). There are also two weaker peaks, which are still for Cα and Cβ but for the preceding residue (i-1). If one (i) strip is adjacent to a HNCOCACB which only contains (i-1) peaks, it is possible for the stronger peaks seen in the HNCACB (i) to match their ^{13}C frequencies with the peaks in the HNCOCACB (i-1). In this way, one can "walk down the backbone" of the protein as you match the residues together, and assign each ^{15}N frequency to a residue in the protein sequence. After this is completed, a residue (e.g. Alanine, A26) can be assigned to a particular peak on the HSQC as one now

knows the ^{15}N frequency and ^{1}H frequency of A26 (119). A figure displaying this concept is shown in **Figure 25** (see section: 5.2.2 CLIC4 Assignment via "strips" – Backbone, Cα and Cβ (1 mM)).

For the protein ^{15}N HSQC resonances to be fully assigned, ^{15}N backbone, Cα, Cβ and C=O resonances need to be assigned, and various spectra have to be collected. The information gathered from each spectrum can be attributed to the way the magnetisation flows through the residue and which atoms are involved in signal detection (119).

2.2.3.1 Assignment Spectra Overview

Figure 15 shows all magnetisation flow diagrams for each spectra listed below.

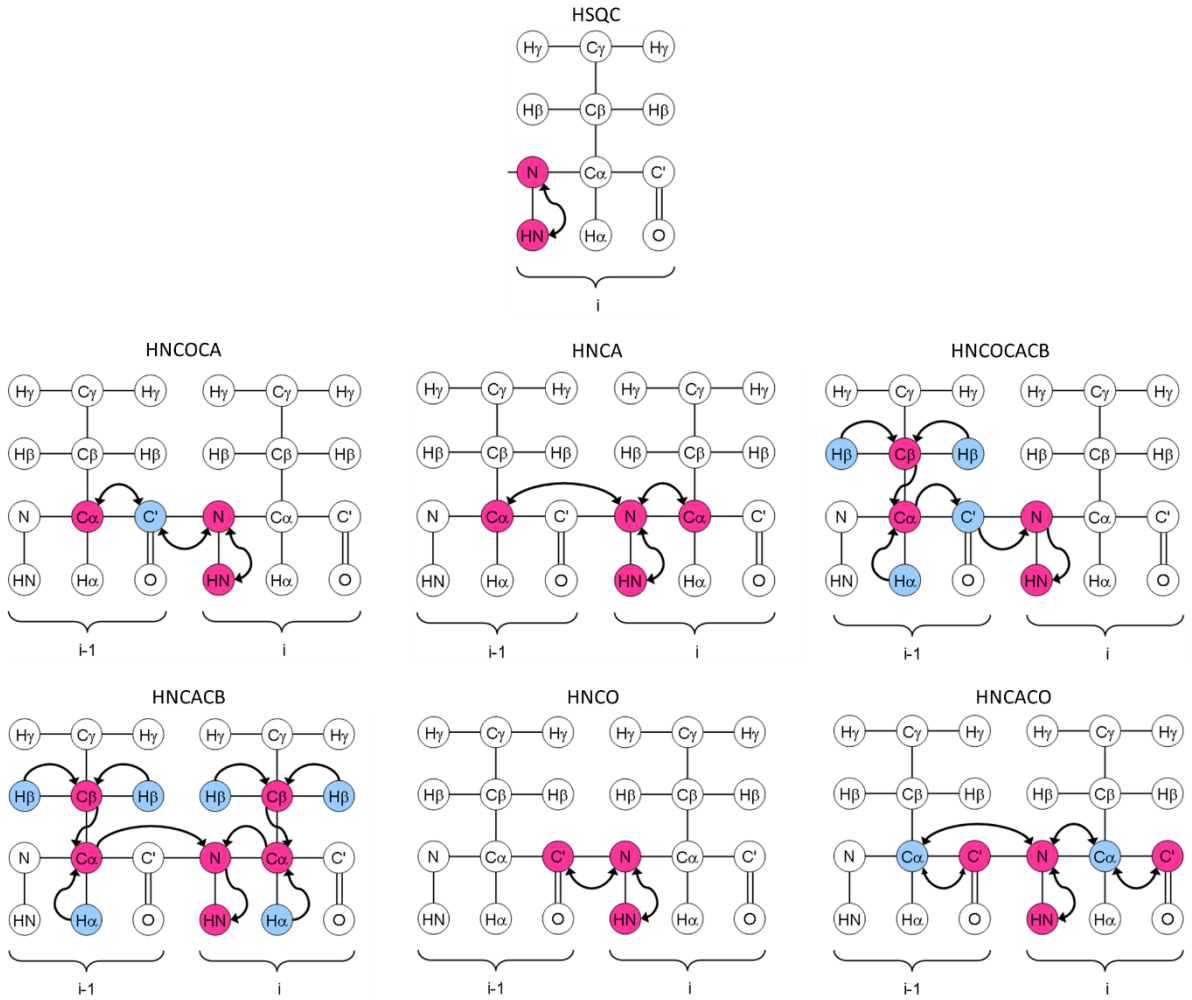

Figure 15 - Overview of magnetisation flow between nuclei in each 2D and 3D spectra. *Red Nuclei = atoms directly contributing to chemical shift evolution (signal). Blue Nuclei = atoms that are involved in magnetisation transfer, but do not directly contribute to chemical shift evolution (signal). Note that the HSQC is the only 2D NMR spectrum as only 2 nuclei are involved in chemical shift evolution.*

2.2.3.2 ^{1}H-^{15}N HSQC

With an HSQC (see **Figure 15** for magnetisation flow visual), the magnetisation from the Rf pulse is transferred from the ^{1}H nuclei of the amide group ($^{1}HN_i$) to the $^{15}N_i$ nuclei (119). This induces a chemical shift (these peaks display on the spectrum), and magnetisation is transferred back to the $^{1}HN_i$ which is then detected. This occurs on the current residue being examined within the protein (i) (119). This spectrum allows the identification of all residues via their backbone amides (except Proline)(119). As chemical shift evolution only involves 2 nuclei, this is a 2D spectrum (119). An example of a protein (ubiquitin α-synuclein fusion protein) 2D HSQC spectrum is shown in **Figure 16** showing individual peaks corresponding to each residue of the protein complex (122).

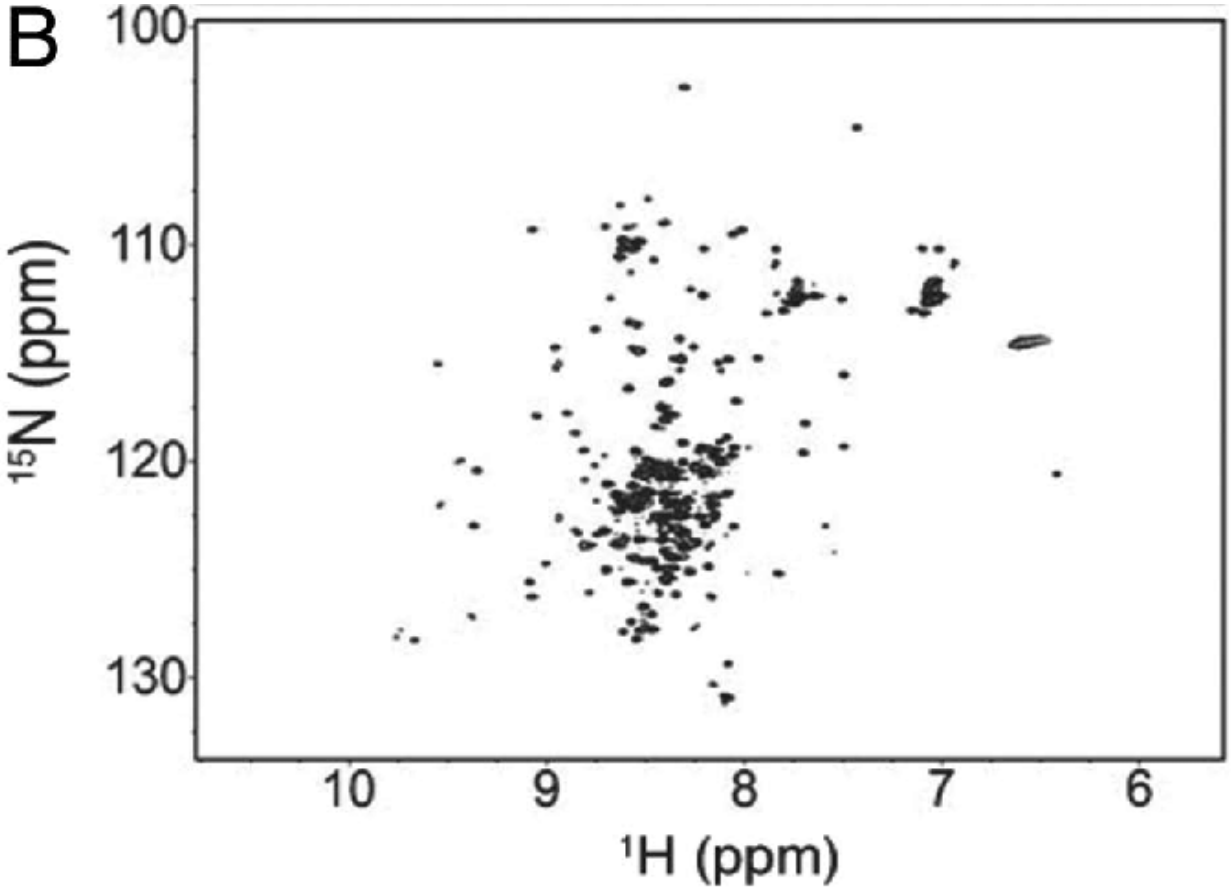

Figure 16 - 2D ^{1}H - ^{15}N HSQC spectra of ubiquitin-α-synuclein fusion protein. *The spectrum displays individual clear peaks, which correspond to the ^{1}H and ^{15}N values of each residue present in the protein sequence. Adapted from: Alderson, T et al. (2013)*

2.2.3.3 HNCOCA

Figure 15 shows that with an HNCOCA, magnetisation originating from the $^{1}HN_{i}$ nuclei is transferred to the $^{15}N_{i}$ nuclei. Magnetisation flows to the C=O situated on the i-1 residue, which transfers to the $C\alpha_{i-1}$ and back through ^{15}N nuclei to the ^{1}H nuclei on the (i) for detection and chemical shift experienced (119). However, the chemical shift and peaks displayed only arise from the $C\alpha_{i-1}$, $^{15}N_{i}$ and HN_{i}. Thus, this spectrum selects the Cα residing on the previous amino acid (119).

2.2.3.4 HNCA

Magnetisation flow starts at the HN_{i}, moving towards the ^{15}N nuclei on the (i) residue. The chemical shift is evolved and displays the relevant peaks once magnetisation is transferred to the $C\alpha_{i}$ and back to the $^{15}N_{i}$ nuclei and ^{1}HN nuclei for signal detection. With this spectrum, the ^{15}N nuclei also pass magnetisation to the $C\alpha_{i-1}$. This results in the spectra displaying two Cα, with the most intense peak being a (i) and the weaker one being (i-1) (119). HNCA is usually combined with the HNCOCA for Cα identification (119). An overview is shown in **Figure 15**.

2.2.3.5 HNCOCACB

HNCOCAB spectrum mainly reports peaks situated on the (i-1) residue. As **Figure 15** shows, the Rf pulse excites the $^{1}H\alpha_{i-1}$ and the two $^{1}H\beta_{i-1}$ present, and magnetisation is transferred to the $C\alpha_{i-1}$ and $C\beta_{i-1}$ respectively (119). The $C\beta_{i-1}$ also transfers its magnetisation to the $C\alpha_{i-1}$, which then passes it to the C=O and onto the ^{15}N (i) before being detected as magnetisation is finally transferred to the ^{1}H nuclei of HN (i). The chemical shift experienced comes from the $C\alpha_{i-1}$ and $C\beta_{i-1}$ simultaneously in one dimension, alongside the ^{15}N and ^{1}HN. There is no chemical shift evolution on the C=O or the $^{1}H\alpha_{i-1}$ and $^{1}H\beta_{i-1}$ (119). Due to the HNCOCACB providing information on the ^{15}N and ^{1}HN of the (i) residue and the Cα and Cβ of the previous residue, this spectrum is one of the most important for backbone assignment as it is used alongside the HNCACB. It can also be complemented by the HNCO for the C=O assignment of residues (119).

2.2.3.6 HNCACB

The HNCACB is twinned with the HNCOCACB for being essential for backbone assignment, due to the chemical shift evolutions arising from the magnetisation flow through the nuclei. Regarding the (i-1) residue, magnetisation is transferred through the same nuclei as in the HNCOCACB, with the exception that the $C\alpha_{i-1}$ transfers to the $^{15}N_i$ directly, with no C=O involvement (119). In addition, a similar magnetisation transfer occurs on the (i) residue, with the $^{1}H\alpha_i$ and the two $^{1}H\beta_i$ transferring magnetisation to the $C\alpha_i$ and $C\beta_i$ respectively before being transferred to the $^{15}N_i$ and then to the ^{1}HN nuclei for detection. Within the spectrum, there are two Cα and Cβ peaks visible, allowing the identification of which peaks belong to either (i) or (i-1) when combined with the HNCOCACB (119). **Figure 15** summarises this magnetisation pathway (119).

2.2.3.7 HNCO

As **Figure 15** shows, HNCO magnetisation starts at the $^{1}HN_i$ nuclei and is transferred to the $^{15}N_i$. This is passed to the C=O of the (i-1). For detection, magnetisation is passed back through the $^{15}N_i$ to the $^{1}HN_i$. This experiment is not crucial for backbone assignment but is useful for obtaining C=O chemical shifts for secondary structure prediction via computational structure prediction software (119).

2.2.3.8 HNCACO

With magnetisation starting at the $^{1}HN_i$ nuclei and transferring to the $^{15}N_i$ nuclei, the $C\alpha_{i-1}$ receives the magnetisation and passes it to the C=O of the (i-1) residue. Detection is then facilitated via magnetisation being transferred back the same way it came through. However, the chemical shift evolution is only on the $^{1}HN_i$, $^{15}N_i$ and the C=O with the $C\alpha_{i-1}$ not evolving. As a result of the $^{15}N_i$ magnetisation, this also gets passed to the C=O on the (i) residue via the $C\alpha_i$. When the spectrum is produced, the result is two C=O peaks appearing on the same dimension but with the (i) C=O peak being more intense (119). This spectrum is usually paired with the HNCO for carbonyl assignment.

By combining all of the above spectra, one can identify each residue and where each residue's peak resides on an HSQC. Thus, CSPs can be calculated following protein-protein and protein-ligand interactions and binding site information can be obtained.

3. Aims and Hypothesis

This thesis aims to assign CLIC4 residues to an HSQC spectrum collected using a triple-labelled CLIC4 sample. The assignment of the backbone Cα, Cβ and C=O of each residue will be completed via the use of triple-resonance 3D assignment spectra. Once each residue is assigned, a titration of CLIC4 with a suspected CLIC inhibitor (digoxin) collected as an HSQC will be analysed for chemical shift perturbations, leading to the identification of a potential inhibitor binding site. Any identified residues proposed to be involved in binding will be modelled on CLIC4 via a 3D model in Pymol, in addition to a comparison of the secondary structure of CLIC4 based on sequence and NMR CSPs.

A second titration experiment will investigate CLIC4's interaction with GIT1, both full-length and Arf-GAP-specific domain, using the CLIC4 assignments to identify key residues involved in GIT1 binding. The residues will be analysed the same way as the CLIC4-Digoxin experiment to model interacting residues on Pymol.

4. Materials and Methods

4.1 Growth Medias

Table 1 shows all bacterial growth media used within the expression of CLIC4 and GIT1, detailing the pH of each media and the concentrations of each component required.

Table 1 - Bacterial Growth Medias used for CLIC4/GIT1 cell growth and protein induction. *The media pH, components and concentrations per litre are listed.*

Media	pH	Component	Concentration / L
Luria Broth (LB)	7.4	Tryptone NaCl Yeast Extract	10g 10g 5g
Luria Broth Agar (for Plates)	7.4	Tryptone NaCl Yeast Extract Agar	10g 10g 5g 15g
M9 Minimal Media (M9)	7.0	Sodium Phosphate (Monobasic) Potassium Phosphate (Monobasic) NaCl Magnesium Sulphate ($MgSO_4$) Calcium Chloride ($CaCl_2$) Thiamine-HCl ^{15}N Ammonium Chloride ^{13}C D-Glucose	55mM 24mM 9.4mM 1mM 0.2mM 1mM 18mM 22mM

4.2 Buffers

Table 2 details buffers used within the expression and purification of CLIC4 and GIT1. **Table 2** also lists the constituents of the SDS-PAGE loading dye used to prepare samples for Sodium Dodecyl Sulphate-Polyacrylamide Gel Electrophoresis (SDS-PAGE).

Table 2 - List of Buffers used in the harvesting and purification of CLIC4/GIT1 proteins. *The buffer pH, components and concentrations per litre are listed. Note: SDS-PAGE loading dye, although not a harvesting and purification buffer, is listed for clarity of SDS-PAGE sample preparation.*

Buffer	pH	Component	Concentration / L
Lysis Buffer	7.4	NaCl Tris-Base EDTA DTT	150mM 50mM 1mM 1mM
Wash Buffer	Same as Lysis Buffer		
Elution Buffer	8.0	Same as Lysis Buffer, with the addition of: Imidazole	 500mM
Dialysis Buffer	7.4 (TEV) / 8.0 (Non-TEV)	NaCl Tris-Base EDTA DTT	50mM 50mM 1mM 1mM
CLIC4 SEC Buffer	7.4	Potassium Phosphate (Monobasic) NaCl	20mM 20mM
SDS-PAGE Loading Dye (5X)	6.8	Sodium Dodecyl Sulphate (SDS) DTT Glycerol Tris-HCl Bromophenol Blue	300mM 10mM 2500mM 200mM 0.7mM

4.3 Transformation of Competent cells

4.3.1 CLIC4

2µl of CLIC4 DNA (containing 6xHis-Tag within a pET28 bacterial plasmid carrying Kanamycin resistance) was transferred into one vial of competent commercial BL21 DE3 cells and placed on ice for 25 minutes. were then heat shocked in a pre-warmed 42°C water bath for 1 minute, and then placed on ice for 20 minutes as part of the bacterial recovery phase. 600µl of Luria Broth (LB) (See section: 4.1 Growth Medias, **Table 1**) was added to the cells and incubated in a 37°C, 200RPM shaking incubator for 1hr. Media was spun down at 13,000 RPM (16,060 x g) for 3 minutes using a Heraeus® Biofuge® Pico centrifuge, 500µl of supernatant was removed and a pre-warmed (37°C) LB Agar plate (containing 1mM Kanamycin) was inoculated with 100 µl of cell culture. LB Agar plate was incubated at 37°C overnight and was sealed with Parafilm™ and kept in the fridge the subsequent day for future use.

4.3.2 GIT1 Full-length

2µl of GIT1 Full-length (Protein MW = ~90kDa) DNA (containing 6xHis-Tag within a pET28a bacterial plasmid carrying Kanamycin resistance) was transferred into 1 vial of competent commercial T7 Express cells. All other Transformation steps are identical to the BL21 DE3 transformation with CLIC4 DNA.

4.3.3 GIT1 Truncated

2µl of GIT1 Truncated (Protein MW = ~41kDa) DNA (containing 6xHis-Tag within a pET28a bacterial plasmid carrying Kanamycin resistance) was transferred into 1 vial of competent commercial Rosetta 2 DE3 cells, containing Chloramphenicol resistance. LB Agar plate used for transformation of Rosetta 2 DE3 cells contained 1mM Kanamycin and 1mM Chloramphenicol. All other Transformation steps are identical to the BL21 DE3 transformation with CLIC4 DNA.

4.4 Non-labelled Protein expression and purification

All CLIC4 and GIT1 proteins were prepared using the media and buffers listed above. Any reference to any media and its constituents in the following methods is listed in **Table 1** (See section: 4.1 Growth Medias), and reference to any buffers can be found in **Table 2** (See section: 4.2 Buffers)

4.4.1 Starter Culture / Overnight Preparation

10mL of autoclaved sterilised LB (see **Table 1**) was added to 4 x 50ml Falcon tubes, with 10µL of 1M filter-sterilised Kanamycin antibiotic (using a 0.2µm filter) added to each tube. A colony of CLIC4-Transformed BL21 DE3 cells was picked via a sterile pipette tip from an LB Agar plate (See **Table 1**) and deposited into each falcon tube. All tubes were then placed in a 37°C, 200 RPM shaking incubator overnight to create starter cultures for inoculation of LB flasks the following day.

4L of LB (see **Table 1**) was split into 4 X 1L baffled flasks, covered with tin foil, and sterilised via autoclave, then stored in a cold room until the following day.

4.4.2 Bacterial Growth and Protein Induction

The 4 x 1L LB flasks were allowed to warm up to room temperature before 1ml of 1M filter-sterilised Kanamycin antibiotic (using a 0.2µm filter) was added to each flask. Each flask was then inoculated with 1 overnight starter culture and placed back into a shaking incubator set to 37°C, 200 RPM until the optical density of the media (OD) reached 0.7 at wavelength 600nm. This was tested by taking 1mL samples at regular time intervals and comparing them against 1ml of sterilised LB using a bench-top spectrophotometer. In addition, a 20µL sample of cell culture was taken from a flask and added to 20µL of Loading Dye (See section:

4.2 Buffers) and 40µL of 8M Urea, labelled "PRE-IPTG" and kept in a 4°C fridge for confirmation of protein expression test via SDS-PAGE.

Once each flask reached OD 0.7, 1ml of 1M Isopropyl-β-D-thiogalactopyranoside (IPTG) (Filter-sterilised using a 0.2µm filter) was added to induce protein transcription via the *lac operon* model of protein transcription. Each flask was then re-covered and placed in a 30°C, 200 RPM shaking incubator overnight

4.4.4 Bacterial Cell Lysis and Extraction of Soluble Proteins

Following overnight induction, a "POST-IPTG" SDS-PAGE sample was collected from a flask and added to 20µL of Loading Dye and 40µL of 8M Urea. Each flask was poured into multiple 500ml Nalgene™ centrifuge bottles and balanced, before being centrifuged at 6,000 RPM (6,440 x g) in a JA-10 Rotor for 15 minutes at 4°C. The supernatant was poured off, and two bottles containing bacterial cell pellet was re-suspended in 25 ml CLIC4 lysis buffer each. Once resuspended, the cell pellet solutions were transferred to any remaining bottles containing cell pellets, to be resuspended. All resuspended pellets were transferred to a sonication vessel (metal beaker) and 1-2 Pierce™ Protease Inhibitor Mini tablets, in addition to a pinch of powdered DNAse, were added to the solution. The resuspended pellets were then lysed via sonication at amplitude 55 for 30 seconds on, and 30 seconds off for 5 minutes (10 minutes total).

The cell lysate was transferred to 26.3ml Beckman-Coulter Polycarbonate Ultra Centrifuge Bottles, balanced, and spun at 40,000 RPM (143,104 x g) in a Beckman-Coulter Type 45Ti Fixed-Angle Rotor for 1hr at 4°C to separate the insoluble and soluble fractions of the cells. The supernatant was then poured off and kept, and a 20 µL sample was taken and added to 20µL of Loading Dye to create an SDS-PAGE sample entitled "Ultra Supernatant".

4.4.5 Purification via Ion Affinity Chromatography

Ni^+ Sepharose High-Performance beads (cOmplete His-Tag Purification Resin) at a volume of 5mL were added to a plastic gravity column with a filter at the bottom. The beads were washed with 25ml of Milli-Q water twice and then equilibrated with 50ml of Lysis buffer. Once equilibrated, the column had the ultra-centrifuge supernatant (containing soluble proteins) passed through it allowing the His-tagged CLIC4 to bind to the beads, with the flow through collected in a 50ml falcon tube and labelled "Column Flow Through". 25 ml of Wash Buffer was passed through the column to elute any loosely bound proteins/cell debris, and the flow through collected in a 50 ml falcon tube and labelled "Wash Buffer Flow through". 25 ml of Elution Buffer was passed through the column, and elutions were collected in 5 x 15 ml falcon tubes in 5 ml aliquots. SDS-PAGE samples were collected, with 20 µl of "Column Flow Through", "Wash Buffer Flow through" and the CLIC4 elutions being added to 20 µl of Loading Dye each.

SDS-PAGE samples that were collected and 5µl of PageRuler™ Plus Prestained Protein Ladder (10 – 250kDa) were then run through a 12% Polyacrylamide gel at 200V, 400mA. The gel was stained with Coomassie blue, to visualise protein bands that were then compared to the protein ladder for indication of protein molecular weight in each sample, and each sample's relative expression of CLIC4 (MW = 30kDa, uncleaved). Ni^+ gravity column elutions containing CLIC4 were then selected for overnight dialysis.

4.4.6 Dialysis and TEV Cleavage

A section of SnakeSkin™ Dialysis tubing was cut to accommodate the total volume of all elutions from the Ni^+ gravity column containing CLIC4, as identified by the SDS-PAGE gel (see above). The section cut was measured in accordance with the specified volume per cm of tubing of 3.8ml. One end was folded over and clamped with a dialysis tubing clip, before being securely wrapped with Parafilm™. The selected CLIC4 elutions and 1ml of Tobacco Etch Virus (TEV) protein were pipetted into the tubing, and the other end was clamped and wrapped with Parafilm™ in the same manner. Tubing was then

placed in 5L of “TEV” Dialysis buffer and covered with tin foil. Buffer was placed in a cold room for overnight dialysis. This step is to ensure TEV cleaves the 6xHis-Tag on CLIC4 and remove imidazole from the sample to prevent aggregation.

4.4.7 Reverse Ion Affinity Chromatography (Removal of TEV)

The same gravity column used the previous day for the purification of CLIC4 was utilised. 50ml of lysis buffer was added to equilibrate the column, and all elutions that had been dialysed overnight were taken out of the SnakeSkin™ Dialysis tubing and were added to the column with the flow through collected (which was the CLIC4, as TEV has bound to the column). 25 ml of Wash buffer was passed through the column, and then 25 ml of Elution buffer was added to the column to elute the TEV protein.

SDS-samples of the reverse Ion affinity purification step were collected, termed “After dialysis”, “Flow Through”, “Wash Buffer” and “Elution (TEV) and ran in the same manner detailed above (see section: 4.4.5 Purification via Ion Affinity Chromatography)

4.4.8 Size Exclusion Chromatography (SEC) Purification

CLIC4 elutions were concentrated using 10K Amicon® Ultra-15 Centrifugal Filters, centrifuged at 4,000 RPM (3,220 x g), 10 minutes at 4°C using an Eppendorf™ 5810 R Centrifuge to a CLIC4 concentration of 10-15mg/ml in 5ml samples. Meanwhile, a HiLoad™ 16/600 Superdex™ 200 pg column was equilibrated with 1L of CLIC4 SEC Buffer for 2 hours. Following equilibration, 5ml samples of CLIC4 were loaded into the column and ran for 2 hours with the elutions collected. The chromatogram displayed by the SEC indicated which elutions contained CLIC4, and those elutions were collected at the end of the SEC run and concentrated in 10K Amicon® Ultra-15 Centrifugal Filters using an Eppendorf™ 5810 R Centrifuge run at 4,000 RPM (3,220 x g), 10 minutes at 4°C to obtain CLIC4 samples ready for experimental testing.

4.5 Isotopically - Labelled CLIC4 Expression

All labelled CLIC4 samples were prepared in the same manner as the above (See section: 4.4 Non-labelled Protein expression and purification) except for the specific preparation stages listed below:

4.5.1 Triple Labelled (^{15}N, ^{13}C, D_2O)

4.5.1.1 Bacterial Growth and Protein Induction in M9 Minimal Media

M9 Minimal Media (M9) was prepared as above and made up to 900ml using D_2O excluding the Thiamine HCl, ^{15}N Ammonium Chloride and ^{13}C D-Glucose. Then, ^{15}N Ammonium Chloride was dissolved in 50 ml autoclaved D_2O, and the ^{13}C D-Glucose and Thiamine HCl were dissolved in separate 50 ml autoclaved D_2O. Both 50ml solutions were passed through a 0.2 µm filter into the 900 ml M9 to make a total volume of 1L M9 Minimal Media.

Following the growth of BL21 DE3 cells in LB media until OD = 0.7, the bacterial growths were poured into multiple 500 ml Nalgene™ centrifuge bottles and balanced, and then centrifuged at 6,000 RPM (6,440 x g) in a JA-10 Rotor for 15 minutes at 4°C. The supernatant was poured off, and two bottles containing bacterial cell pellet was re-suspended in 50 ml M9 media. Once resuspended, the cell pellet solutions were transferred to any remaining bottles containing cell pellets, to be resuspended. All resuspended pellets were transferred into the M9, and the vessel was inverted to ensure homogeneous resuspension. The M9 was then split into 2 x 1L autoclaved sterilised baffled flasks with 500 ml of M9 in each. The flasks were placed in a shaking incubator set at 30°C, 200 RPM for 45 minutes. 500µl of 1M IPTG was added to each flask and incubated overnight at 30°C, 200 RPM.

4.5.1.2 Dialysis and TEV Cleavage

Samples prepared for NMR analysis were dialysed without the addition of TEV, therefore elutions were dialysed in 5L of "Non-TEV" dialysis buffer. Reverse Ion Affinity Chromatography was not carried out the following morning as a result.

All other growth, induction and purification stages (including SDS-PAGE sample preparation) for triple-labelled CLIC4 remain the same as non-labelled CLIC4.

4.5.2 Single Labelled (^{15}N)

4.5.2.1 Bacterial Growth and Protein Induction in M9 Minimal Media

M9 used for single labelled CLIC4 did not use ^{13}C D-Glucose and instead used ^{12}C D-Glucose. In addition, the M9 media did not use any D_2O to make up the solution to 900ml, nor used in the dissolving of Thiamine HCl, ^{15}N Ammonium Chloride, and ^{12}C D-Glucose. Here, the D_2O was substituted with Milli-Q H_2O.

4.5.2.2 Dialysis and TEV Cleavage

Samples prepared for NMR analysis were dialysed without the addition of TEV, therefore elutions were dialysed in 5L of "Non-TEV" dialysis buffer. Reverse Ni^+ Ion Affinity Chromatography was not carried out the following morning as a result.

All other growth, induction, and purification stages (including SDS-PAGE sample preparation) for single-labelled CLIC4 remain the same as non-labelled CLIC4

4.6 GIT1 (Full-length/Truncated) Expression and Purification

4.6.1 Starter Culture / Overnight Preparation

10 ml of autoclaved sterilised LB was added to 4 x 50 ml Falcon tubes. Two of the tubes were labelled "GIT1 FULL" and had 10µl of 1M filter-sterilised Kanamycin antibiotic (using a 0.2 µm filter) added. The remaining two tubes were labelled "GIT1 STOP" and had 10 µl of 1M filter-sterilised Kanamycin antibiotic and 10 µl of 1M Chloramphenicol added to each tube. A colony of GIT1 Full-length T7 Express cells was picked from an LB Agar Plate and deposited into the labelled "GIT1 Full" tubes, whilst a colony of GIT 1 Truncated Rosetta 2 DE3 cells were picked from an LB Agar plate and deposited into the labelled "GIT1 STOP" tubes.

All tubes were then placed in a 37°C, 200 RPM shaking incubator overnight to create starter cultures for inoculation of LB flasks the following day.

4L of LB was split into 4 X 1L baffled flasks, covered with tinfoil and sterilised via autoclave, then stored in a cold room until the following day.

4.6.2 Bacterial Growth and Protein Induction

The 4 x 1L LB flasks were allowed to warm up to room temperature before 1 ml of 1M filter-sterilised Kanamycin antibiotic (using a 0.2µm filter) was added to each flask. Then, 1 ml of 1M Chloramphenicol was added to two of the flasks and labelled “GIT1 STOP”. The two remaining flasks were labelled “GIT1 Full”. Each flask was inoculated with the starter culture that matched its designated protein growth (e.g. flask labelled “GIT1 STOP” was inoculated with the starter culture that was labelled “GIT1 STOP”).

The GIT1 Sample preparation then proceeded in the same manner as the non-labelled CLIC4 preparation, including purification and dialysis. The only aspect that varied from the non-labelled CLIC4 sample preparation protocol was the Dialysis and TEV Cleavage and the SEC stages.

4.6.3 Dialysis and TEV Cleavage

Both GIT1 Full-length and Truncated protein samples were dialysed overnight in 5L of GIT1 Dialysis buffer (20 mM Potassium Phosphate, 150 mM NaCl, 1 mM EDTA, 1 mM DTT pH 7.4). This did not include the addition of TEV.

4.6.4 Size Exclusion Chromatography (SEC) Purification

The SEC purification and concentration of GIT1, both Full-length and Truncated versions, were carried out in the same manner as the non-labelled CLIC4 with the exception that the column was equilibrated and run with GIT1 SEC buffer (20 mM Potassium Phosphate, 150 mM NaCl, pH 7.4).

4.7 GIT1 Bioinformatics: Predicting Interactions with CLIC4

4.7.1. ColabFold with CLIC4

The three-dimensional structure of GIT1 was obtained from a predicted Alphafold structure from UniProt (Entry number: Q9Y2X7) and analysed in Pymol (123) for domain structure and interactions with other biological elements, and a domain that is known to be involved in the Arf6 pathway was selected to test against CLIC4 for any binding interactions. The sequence of this Arf6 domain was joined with a linker to CLIC4, and both protein sequences were run in ColabFold (Alphafold2 using MMseqs2 (113)) to predict CLIC4:GIT1 interactions. The resulting PDB file was then opened in Pymol, and inspected for interacting regions between GIT1 and CLIC4.

4.7.2 Construct design

Following Pymol analysis of the ColabFold results, two constructs were designed on SnapGene software (www.snapgene.com); One construct of the entire GIT1 protein termed "Full-length" and one of the Arf-GAP domain only, termed "GIT1 Truncated". Constructs were ordered, and plasmids were prepared via the company GenScript®.

4.8 Nuclear Magnetic Resonance (NMR) Sample Preparation

^{15}N CLIC4 and GIT1 samples were concentrated to required protein concentrations using 10K Amicon® Ultra-15 Centrifugal Filters and stored in 300 µl aliquots. Samples required for NMR experimentation had 5% D2O and 0.01mM DSS as an NMR standard added. The sample was then loaded into a 5mm Shigemi NMR tube, secured with Parafilm™, and loaded into a 600 MHz Bruker™ NMR Spectrometer with a TCIP-CryoProbe at 303°K based at the University of Kent Wellcome Trust NMR facility.

Triple-labelled CLIC4 preparation differed from the above, due to the need for increased resolution on some of the spectra (See Results: 5.2 Using Nuclear Magnetic Resonance (NMR) Spectra to assign CLIC4 residues). Triple-labelled samples were concentrated and prepared with the same 5% D2O and 0.01mM DSS NMR standard, and the HNCA, HNCOCA, HNCACB and HNCOCACB were collected with a

1 mM sample at The Crick Institute, run on an 800MHz Bruker™ NMR Spectrometer with a TCIP-CryoProbe at 303°K. The HSQC in addition to the HNCO and HNCACO spectra used for carbonyl assignment was collected using a 500 mM sample at the University of Kent Wellcome Trust NMR facility at 600 MHz.

All samples run on each spectrometer, and the spectra collected were facilitated via the use of Bruker Topspin 3.6.1 (124). Phasing and processing of the spectra was carried out using NMRPipe via NMRBox and analysed for both assignment and binding of proteins via NMRViewJ (125–127).

4.9 Microscale Thermophoresis (MST) Sample Preparation

Microscale Thermophoresis (MST) was conducted on samples of GIT1 (His-Tag Uncleaved) and non-labelled CLIC4 (His-Tag Cleaved). The affinity of the His-Tag labelling dye (RED-tris-NTA 2nd Generation Dye) was determined using GIT1 Full-length uncleaved. 8 ml of Milli-Q H_2O was added to the stock 5 x PBS-T buffer to obtain a working 1 X PBS-T solution. The stock dye solution was suspended in 25 µl of 1 X PBS-T to create a 5 µM dye solution. 2 µl of the 5µM dye solution was added to 198 µl of 1 X PBS-T to make a 50 nM dye solution. A 4 µM solution of GIT1 Full-length was prepared, and 20 µl of this was pipetted into the first PCR tube in the first well of the 96-well plate. 10 µl of the 1 X PBS-T was pipetted into PCR tubes 2-16, and 10 µl of GIT1 in tube 1 was transferred into tube 2. Here, the solution was mixed via pipette, and 10 µl was transferred to tube 3. This was repeated as a serial dilution until tube 16, with the extra 10 µl left over being discarded (See **Figure 17**). Each PCR tube then has a Monolith NT.115 Standard Treated Capillary (K002) loaded into it, with each capillary then loaded into the Monolith NT.115 MST, set to 40% excitation power at 25°C.

Once the affinity of the dye had been determined to possess a suitable K_D for the GIT1 protein, the GIT1 (both Full-length and truncated proteins) were incubated with the dye to ensure complete binding of the dye to the His-Tag. This was carried out by firstly preparing 100 µl of 200 nM GIT1, and 100 µl of 100 nM dye solution (2 µl of 5 µM dye to 98 µl PBS-T). 90 µl of 200 nM GIT1 was mixed with 90 µl of 100 nM dye, and incubated for 30 minutes at room temperature. After centrifuging the sample

for 10 minutes at 4°C at 15,000 x g (in Heraeus® Biofuge® Pico centrifuge), the supernatant was transferred to a new microcentrifuge tube ready for the GIT1:CLIC4 binding assay.

20 µl of CLIC4 was loaded into PCR tube 1 (concentration at 300 µM), and 10 µl of 1 X PBS-T was pipetted into PCR tubes 2-16. 10 µl of PCR tube 1 was transferred to PCR tube 2 and mixed multiple times. 10 µl was then transferred to PCR tube 3 and mixed the same. This continued for each tube in a serial-dilution manner as shown in **Figure 17**. 10 µl of GIT1 Full-length (with dye) was then added to PCR tube 1 (CLIC4 concentration now at 150 µM, GIT1 at 50 µM), and was also added to tubes 2-16 and mixed each time. Each PCR tube then has a Monolith NT.115 Standard Treated Capillary (K002) loaded into it, with each capillary then loaded into the Monolith NT.115 MST and run with the same parameters as above. This process was then repeated for the GIT1 Truncated protein.

MST data was analysed using M0 Affinity Analysis, to determine binding events and K_D.

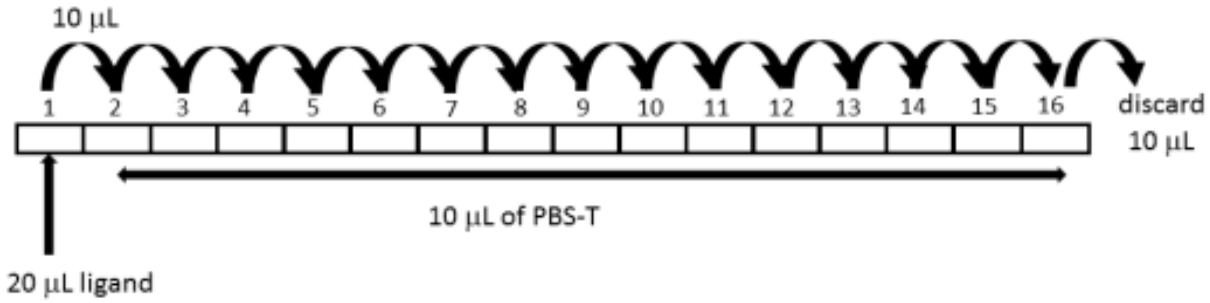

Figure 17 - Schematic of serial dilution steps required for MST sample preparation. *Sample starts at well 1, and is serial diluted continuously until well 16, where the excess is discarded.*

5. Results

5.1 CLIC4 Expression: Non-labelled, Single and Triple-labelled

To obtain protein samples required for CLIC4 NMR assignment and binding site prediction, non-labelled and isotopically labelled samples of CLIC4 were expressed via the growth of BL21 DE3 cells and harvested via the sample preparation method listed above (see section 4.4 Non-labelled Protein expression and purification and section 4.5 Isotopically - Labelled CLIC4 Expression).

5.1.1 Confirmation of CLIC4 production using SDS-PAGE Gels

5.1.1.1 Non-labelled CLIC4

Non-labelled CLIC4 was purified, following the growth, and harvesting of BL21 DE3 cells, via ion affinity chromatography detailed in methods above (see section 4.4.5 Purification via Ion Affinity Chromatography). Samples were dialysed overnight with the addition of TEV and run through a reverse ion affinity chromatography column with SDS-PAGE samples taken. **Figure 18** shows the purification of the non-labelled CLIC4 post-dialysis and post-reverse Ni^+ gravity column.

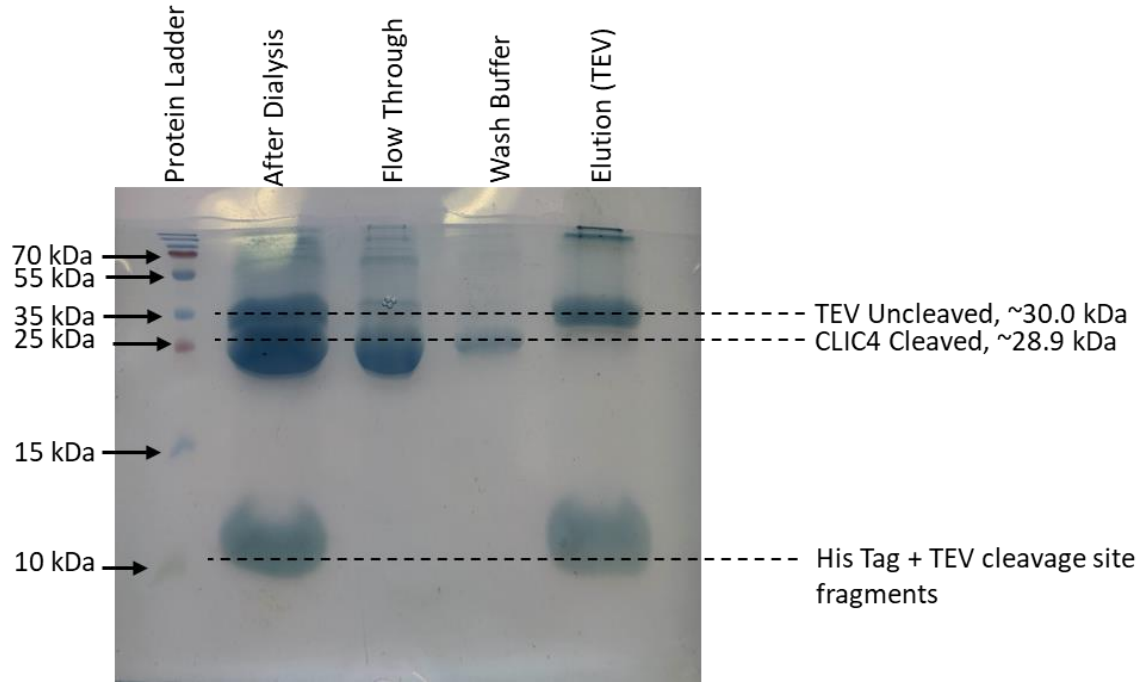

Figure 18 - SDS-PAGE gel of Non-labelled CLIC4 samples after Ion affinity chromatography and TEV cleavage via dialysis. *The samples "After Dialysis" and "Flow Through" (after reverse ion affinity chromatography) show a clear expression band, correlating to TEV-cleaved CLIC4 at approx. 28.9 kDa., estimated via the protein ladder (left). Additional bands are seen in "After Dialysis", which is the TEV enzyme at around 30 kDa (also see in the "Elution" sample).*

Each sample (after dialysis, column flow through, wash buffer and elution) was compared against the protein ladder standard to determine the approximate molecular weight of the protein band present within the SDS-PAGE gel.

From **Figure 18**, the after-dialysis sample contained three thick expression bands. These bands correlate with the molecular weights shown on the left-hand side. The top band in the sample has a molecular weight of approx. 30-35kDa which indicates the presence of TEV (30.0 kDa). The next band is situated between the 25-35kDa protein ladder standards, and below the TEV band. Thus, the protein here is CLIC4, as TEV-cleaved CLIC4 has a molecular weight of 28.9kDa. Appearing at around 10kDa are the remnants of the dialysis TEV-cleavage of CLIC4, which contains the His-Tags and TEV cleavage site fragments. Across the samples, the expected outcome was achieved; TEV is absent in the flow through due to it being bound to the Ni^{+} Sepharose beads, leaving only the CLIC4 band to display in this lane. The wash buffer contained some CLIC4 that was not bound, and the elution only contained

TEV and the dialysis remnants. Therefore, the expression of CLIC4 was achieved for use in the binding assays below.

5.1.1.2 Triple (^{15}N, ^{13}C, D_2O) labelled CLIC4

Following the successful growth of Non-labelled CLIC4, triple-labelled CLIC4 samples were prepared via cell growth in LB and induction in M9 minimal media containing ^{15}N Ammonium Chloride, ^{13}C D-Glucose and D_2O. **Figure 19** displays an SDS-PAGE gel of samples obtained at each stage of the Ni affinity gravity column purification process.

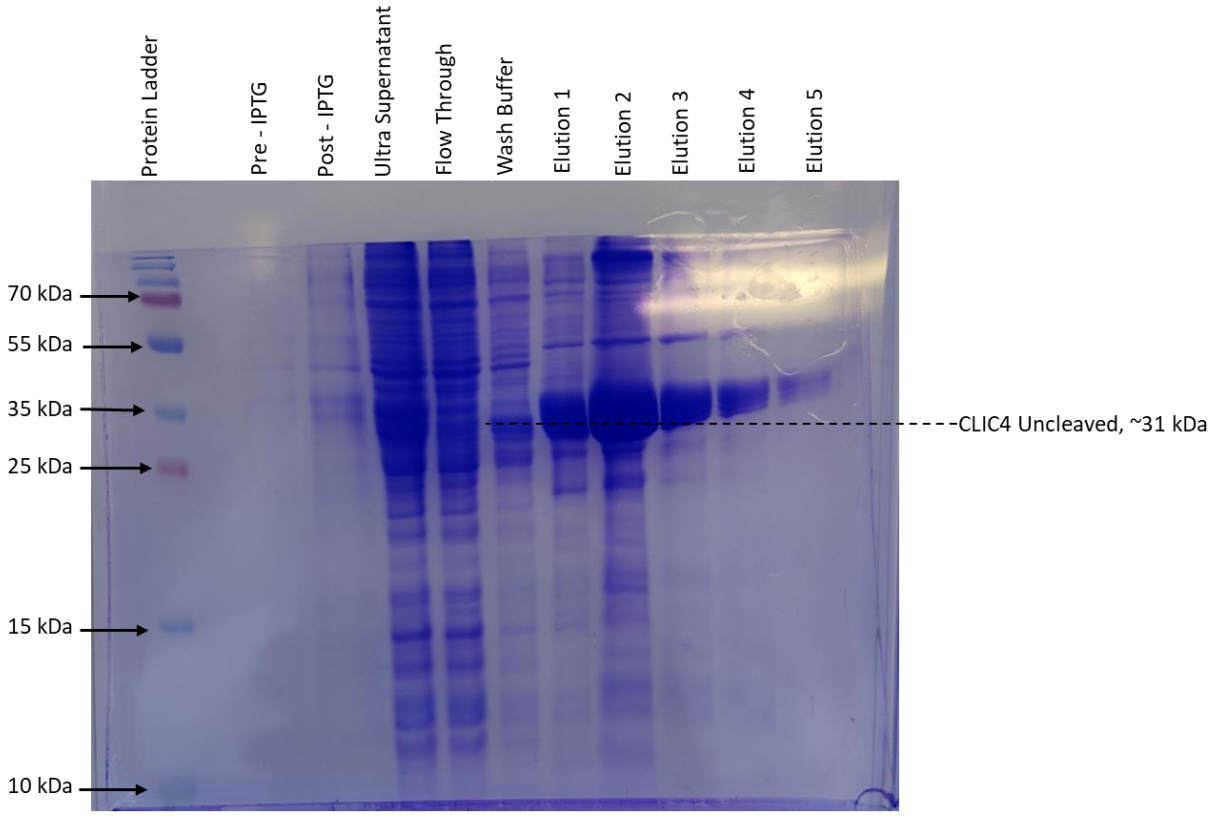

Figure 19 - SDS-PAGE gel of Triple-labelled CLIC4 (Uncleaved), using samples taken from the growth of cells and harvesting/purification of CLIC4. *The "Ultra Supernatant" and "Flow Through" show expression of proteins present within the cells, but clear thick expression bands that correlate to CLIC4 uncleaved (31 kDa) start to appear in elutions 1-4 after the ion affinity chromatography stage. Elutions 4-5 have curved banding patterns indicating a run issue with the gel.*

A reverse Ni^+ affinity gravity column used to remove TEV was not required, as TEV cleavage was not performed on this protein due to the need for the His-Tag to be retained. The gel indicates the expression of cellular proteins, as seen in the "Ultra Supernatant" and "Flow Through" lanes. However,

clear expression of CLIC4 is seen in Elutions 1-4, with thick expression bands correlating to around 31 kDa as shown by the protein ladder. His-Tagged CLIC4 is approx. 31kDa, which assigns the thick expression band as CLIC4 expression. There is also some protein present in the wash buffer, indicating that some CLIC4 was loosely bound to the column and washed through with the rest of the cell debris/proteins.

5.1.1.3 Single (^{15}N) labelled CLIC4

Single labelled CLIC4 was prepared following cell growth in LB, and protein induction in M9 media containing ^{15}N Ammonium Chloride. **Figure 20** highlights the outcome of the protein sample preparation of CLIC4 following cell harvesting, lysis and purification stages.

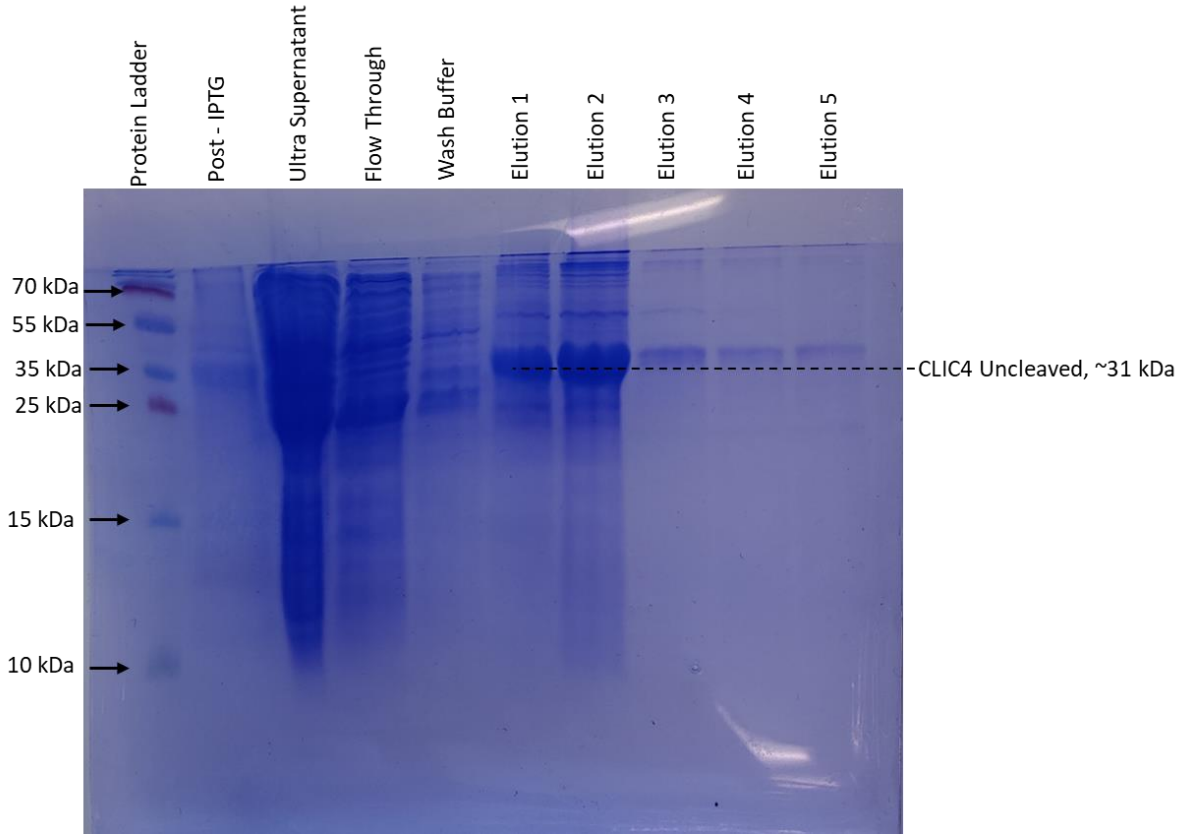

Figure 20 - SDS-PAGE gel of Single-labelled CLIC4 (Uncleaved) using samples taken from the growth of cells and harvesting/purification of CLIC4. *The "Ultra Supernatant" and "Flow Through" samples have clear expression of proteins within the cell, albeit the lanes are smeared. The distinct expression of CLIC4 is seen in Elutions 1-2, with remnant expression in Elutions 3-5. These bands correlate to the CLIC4 uncleaved molecular weight of approx. 31 kDa which is estimated via the protein ladder (left), which has also experiences running issues as the banding separation is not proportional, especially at the top of the gel.*

The SDS-PAGE gel does show expression of cellular proteins in the “Ultra supernatant”, but the lane has smeared so that individual bands are not recognised. The “flow through” is slightly clearer, but has smeared in addition to the bands running at an angle, distorting the bands’ molecular weight classification when compared to the protein ladder. The protein ladder has not run correctly; the spacing of the marked protein bands is not as expected, making identification of any expression bands a harder task. This could have been due to a gel constituent-related issue. However, Elutions 1-5 do show clear expression of a protein which is situated around the 30-35kDa mark. Given the protein ladder has not run correctly, and taking into account **Figure 19**’s clear expression of CLIC4 in a similar location on the SDS-PAGE gel, the banding pattern displayed in **Figure 20** indicates the expression of uncleaved CLIC4 at 31 kDa. To further confirm the expression of CLIC4, SEC purification was carried out for all three conditions (Non-labelled, Triple-Labelled and Single-Labelled).

5.1.2 Purification of CLIC4 using Size-Exclusion Chromatography (SEC) Chromatograms

Following the successful expression of the non-labelled and isotopically labelled CLIC4 samples, each sample was run through the SEC for further purification (see section: 4.4.8 Size Exclusion Chromatography (SEC) Purification for details) and to separate monomeric protein states from oligomers that may have formed.

5.1.2.1 Non-labelled CLIC4

The non-labelled CLIC4 samples were run through the SEC, and **Figure 21** displays the 280nm UV absorbance over the elution volume of an SEC column, possessing a column volume of 120ml. The elutions taken from the Ni^{+} affinity gravity column purification stage were run through the column to remove DNA and other contaminants. Following this, CLIC4 samples collected from the SEC possessed a concentration of 300µM.

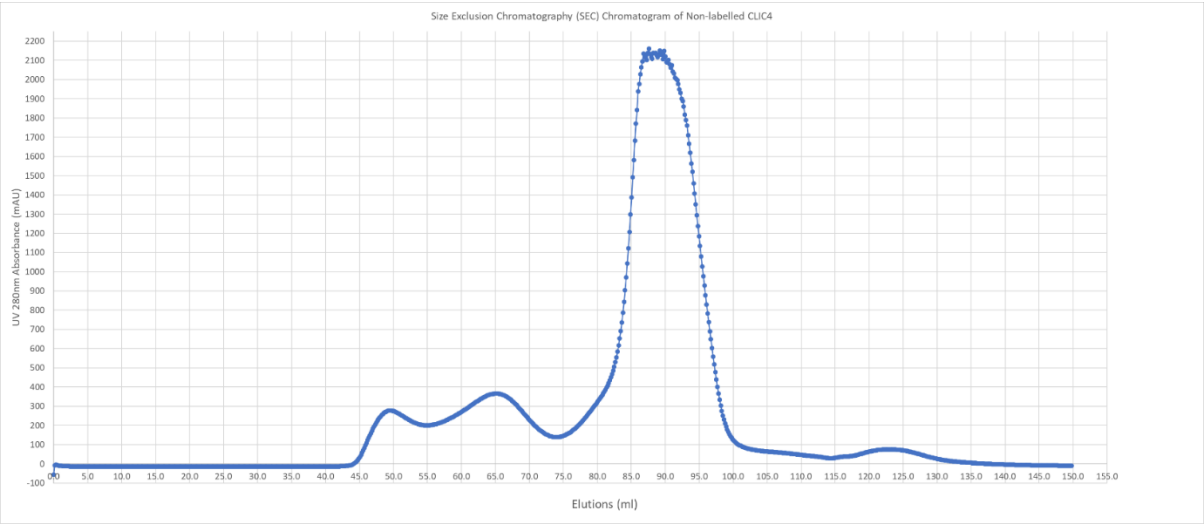

Figure 21 - Size Exclusion Chromatography (SEC) Chromatogram of non-labelled CLIC4 (TEV cleaved). *SEC column has a column volume of 120ml, with the intensity of the 280nm UV absorbance correlating to the concentration of CLIC4 present. A single peak with great intensity (2150 mAU) at 80-100ml elution indicates the presence of monomeric CLIC4. The double peak at 45-75ml may be the result of higher oligomeric states forming, or aggregate formation.*

The graph shows two regions of interest; a double peak located at 45ml-75ml of elution volume, and a single peak 80-100 ml elution volume. The single peak is of great intensity, with a peak 280nm UV absorbance of 2150 mAU. This peak is correlated with the successful elution of CLIC4 in the oligomeric state of a monomer. In contrast, the double peaks at 45-75ml elute at a lower volume. Elutions of lower volumes indicate larger proteins, as smaller proteins take longer to travel through the column's beads, leading to higher elution volumes. Hence, this double peak may be CLIC4 dimers, or other oligomeric states, given the His-Tag of this sample was cleaved by TEV. Therefore, higher dimerisation of CLIC4 has occurred as is it thought the removal of the HisTag promotes oligomerisation of the protein. There is also the possibility this could be aggregate formation. However, the graph shows that the CLIC4 monomer has been purified and is present within the sample run.

5.1.2.2 Triple (^{15}N, ^{13}C, D_2O) labelled CLIC4

Similar SEC purification results of the Triple-labelled CLIC4 sample can be seen in **Figure 22** below. Due to the amount of protein produced by the BL21 *E.coli* cell, and eluted via the Ni affinity gravity column purification stage, two runs of the SEC were required given that the injection loop is 5ml (10ml total sample volume).

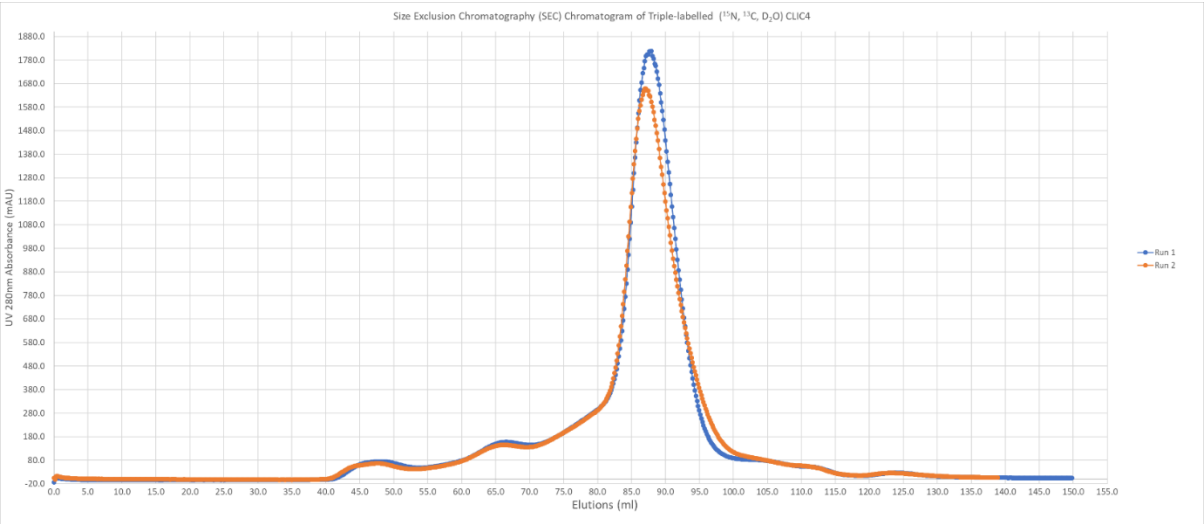

Figure 22 - Size Exclusion Chromatography (SEC) Chromatogram of Triple-labelled CLIC4 (Uncleaved). *SEC column has a column volume of 120ml, with the intensity of the 280nm UV absorbance correlating to the concentration of CLIC4 present. SEC was run twice due to the amount of protein harvested from the sample preparation stage. Run 1 exhibited a single peak with great intensity (1830 mAU) at 75-100ml elution indicates the presence of monomeric CLIC4. Run 2 also displayed a peak in this region of 1650 mAU intensity. There is two peaks present at 45ml and 65ml which could indicate higher oligomeric states or aggregate formation.*

Both SEC traces (Run 1 and 2) above indicate a strong absorbance peak between 75-100ml elution volume, which when compared to the non-labelled sample SEC trace is confirmatory of CLIC4 monomer presence. Run 1 seems to have a higher absorbance peak at 1830 mAU compared to Run 2 at 1650 mAU, indicating a higher concentration of CLIC4 in the first run. There are also traces of higher oligomeric states present in both samples, with peaks at 45ml and 65ml. Again, the presence of these peaks suggests dimer/trimer formation, but could also be aggregate. Overall, both runs contribute to high expression of triple-labelled CLIC4, which was utilised for the acquisition of multiple NMR spectra for assignment.

5.1.2.3 Single (^{15}N) labelled CLIC4

Single-labelled CLIC4 expressed for MST binding assays with GIT1 was purified via SEC in the same manner as the non-labelled and triple-labelled samples. This SEC purification is shown in **Figure 23** below:

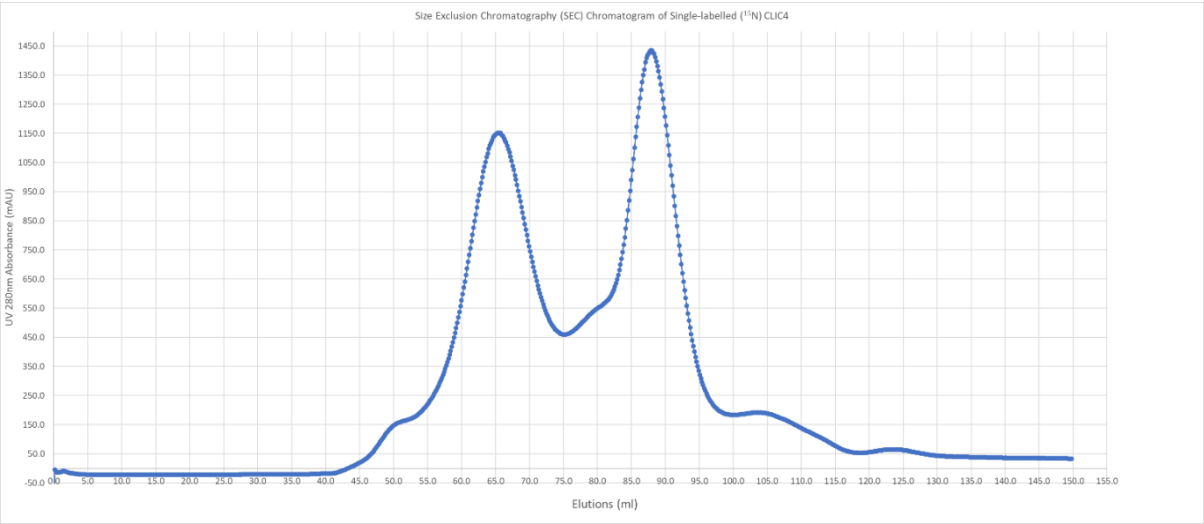

Figure 23 - Size Exclusion Chromatography (SEC) Chromatogram of single-labelled CLIC4 (TEV Cleaved). *SEC column has a column volume of 120ml, with the intensity of the 280nm UV absorbance correlating to the concentration of CLIC4 present. A single peak with significant intensity (1450 mAU) at 75-100ml elution indicates the presence of monomeric CLIC4. However, there is another peak with considerable intensity (1150 mAU) at 55-75ml which could be increased oligomeric state formation, since this sample was TEV cleaved which can promote oligomer formation.*

This SEC trace has one significant difference in comparison to the other SEC traces for the non-labelled and triple-labelled CLIC4 samples, which is the appearance of 2 peaks on the SEC trace. In addition to the CLIC4 monomer peak at 75-100 ml, as seen in the other SEC traces, this sample also contained a significant peak ranging from 55-75 ml. This is indicative of dimer formation, but this sample seems to have a higher dimer concentration when compared to the other samples. **Figure 23** is the SEC trace of ^{15}N CLIC4 sample which was utilised for the CLIC4:GIT1 experiment, and as such had the His-Tag cleaved via TEV. As mentioned previously, the His-Tag is thought to prevent oligomerisation, so its removal in this sample would account for the higher dimerisation peak seen in this SEC trace.

5.2 Using Nuclear Magnetic Resonance (NMR) Spectra to assign CLIC4 residues

5.2.1 2D ^{1}H - ^{15}N HSQC of Triple-labelled CLIC4 - 550µM

A 2D ^{1}H - ^{15}N HSQC NMR spectra of a 550 µM triple labelled CLIC4 sample was obtained at 600MHz, and the results were displayed below:

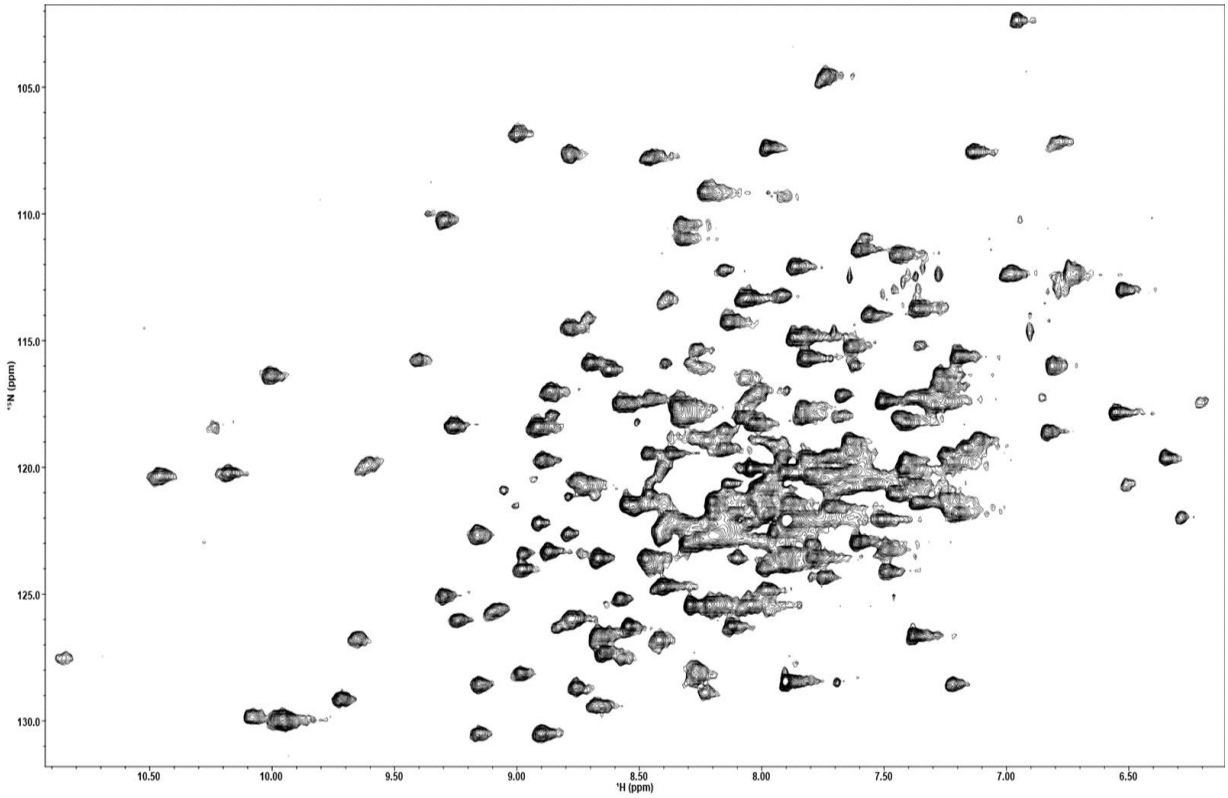

Figure 24 - 2D ^{1}H - ^{15}N HSQC Spectrum of Triple-labelled CLIC4. *Concentration of CLIC4 is 550µM, run at 600 MHz.*

Figure 24 shows peaks relating to ^{15}N frequencies against the ^{1}H frequencies for each residue in CLIC4. Overall, the spectrum shows defined clear peaks around the outside of the spectra, moving inwards towards overlapping and broader peaks correlating to ^{15}N frequencies of buried residues in more of the protein. These overlapping/broader peaks are due to the chemical exchange rate of these innermost residues being slower than the outermost residues, because of the 253-residue CLIC4 tumbling more slowly in solution than a smaller protein.

5.2.2 CLIC4 Assignment via "strips" – Backbone, Cα and Cβ (1 mM)

To assign the backbone of the CLIC4 protein, six 3-Dimensional NMR spectra were collected and arranged into "strips". Each strip has the ^{1}H dimension on the x-axis, ^{13}C dimension on the y-axis and ^{15}N dimension on the z-axis. The strip alignment of each NMR spectra used is shown in **Figure 25**

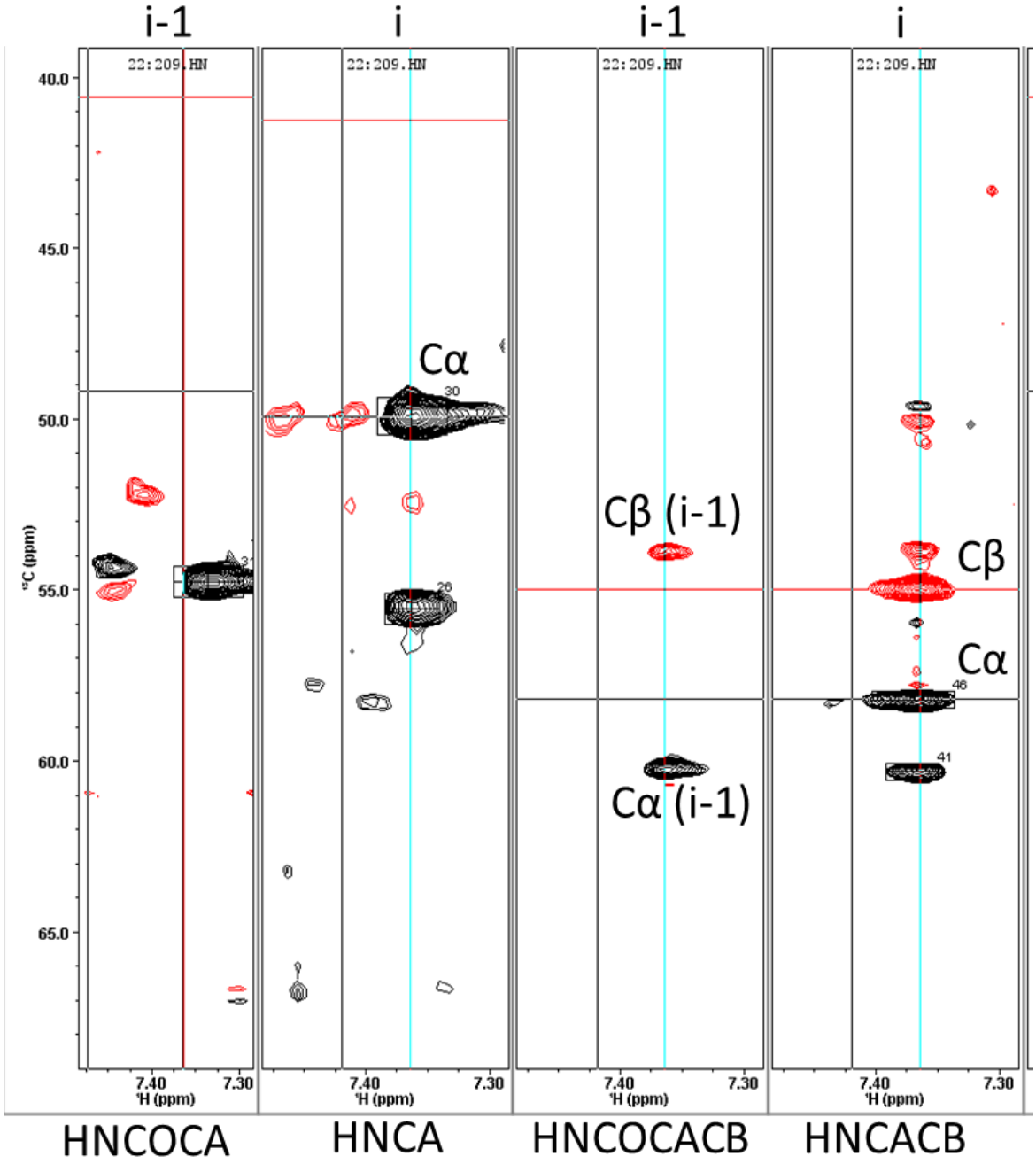

Figure 25 - "Strip" Arrangement of four 3D NMR spectra using Triple -labelled CLIC4 (1mM), indicating Cα and Cβ present on the current residue (i) and the previous residue (i-1). *The HNCOCACB (i-1) and HNCACB (i) work in tandem to assign each Cα and Cβ to their respective residue in the CLIC4 sequence, and peak number on the 2D HSQC. The HNCOCA (i-1) and HNCA (i) confirm the Cα of both the current and previous residue.*

All spectra collected used a 1 mM CLIC4 sample at 800 MHz. Once the above strips were set up, the strategy to assign each residue was to "walk down the backbone" which is detailed in section 2.2.3 Residue Assignment of CLIC4 above. Matching strips as outlined above, this allows the assignment of each ^{15}N frequency peak to a residue number of CLIC4. The result of this is seen in **Figure 24** below.

5.2.3 C=O Residue assignment – 550 µM

Although the ^{15}N frequency backbone peaks of CLIC4 can be assigned via the method above, each residue will have a carbonyl peak (C=O). Here, the assignment of these carbonyl peaks can be completed using HNCO and HNCACO spectra in strips, as shown in **Figure 26**.

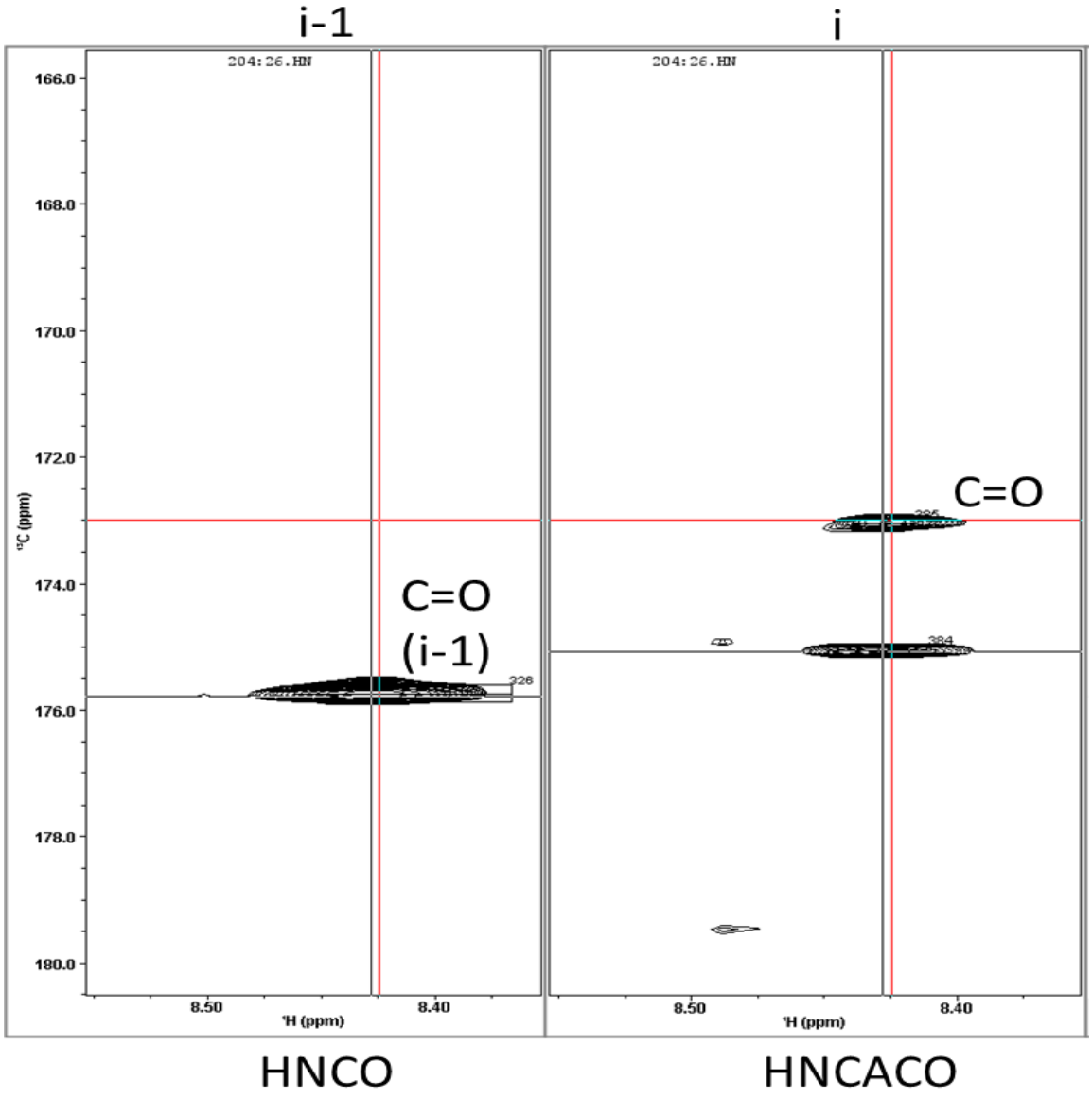

Figure 26 - HNCO and HNCACO "Strip" arrangement to assign C=O peaks to triple-labelled CLIC4 (550µM) residues. *The HNCACO shows the current (i) C=O residue, and the HNCO shows the C=O of the previous residue (i-1). The unlabelled peak in the HNCACO corresponds to the C=O of the previous residue (indicated by the black line).*

The HNCO AND HNCACO spectra were collected using a 550 µM sample at 600 MHz. The HNCACO corresponds to the current residue being examined. Similar to the Cα and Cβ assignment, the C=O residues indicated on the HNCO and HNCACO match as the black line passes through both peaks. Both spectra can be used to match each residue's C=O peak via the same "walk down the backbone" strategy outlined above (details in section 2.2.3 Residue Assignment of CLIC4)

5.2.4 Assigned Backbone peaks on 2D ^{1}H - ^{15}N HSQC CLIC4 - 550µM

Once residues of CLIC4 had been assigned to their ^{15}N and ^{1}H frequencies, the peaks on the HSQC could be related to their designed residue. This is shown in **Figure 27**, with assigned peaks possessing a blue box and a residue number around them.

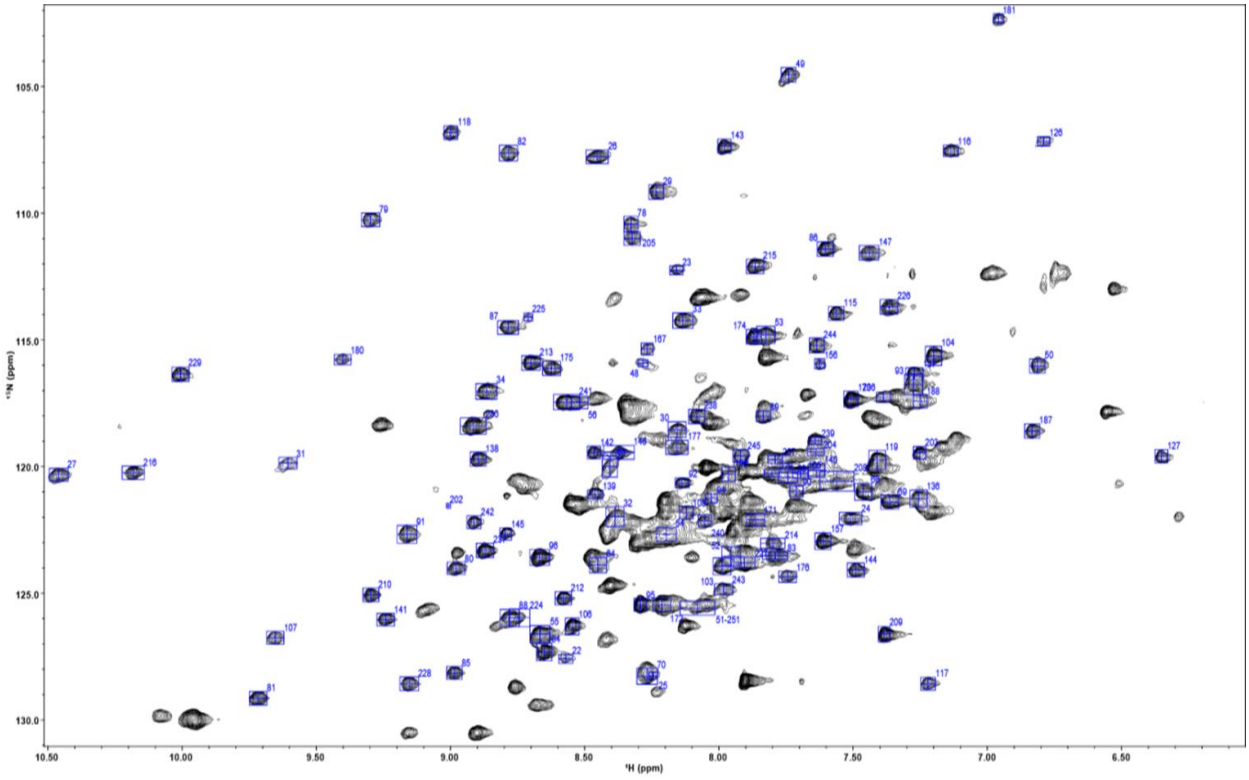

Figure 27 - 2D ^{1}H - ^{15}N HSQC Spectrum of Triple-labelled CLIC4 with backbone assignments. *Concentration of CLIC4 is 550µM, run at 600 MHz. Blue boxes = peaks assigned to a specific residue of the CLIC4 protein sequence.*

The HSQC, using a 550 µM Triple-labelled CLIC4 sample at 600 MHz, shows an interesting observation concerning the residues that are assigned, their location within the protein, and those that are not. The majority of those that are now assigned are located around the outsides of the spectra. However, there are significant amounts of peaks which are unassigned and are situated near the middle of the spectra. As mentioned in relation to **Figure 24**, this space exhibits densely packed residues with crowded chemical environments and hence displayed overlapping peaks on the "strips" (see section: 5.2.2 CLIC4 Assignment via "strips" – Backbone, Cα and Cβ (1 mM)). As a result, these residues were not reliably confirmed and assigned due to ambiguity with Cα and Cβ peaks. Despite this, **Figure 27** does show assigned peaks situated around the centre of spectra in these dense regions of residues, providing some information useful for tracking interactions of CLIC4 ligands/proteins when interactions occur. All assigned peaks present on this spectrum can be mapped onto a computational model, shown below.

5.2.5 Pymol representation of Assigned Residues

The assigned residues of CLIC4 were mapped onto a CLIC4 model, to display the coverage of NMR assigned residues in comparison to the whole protein sequence. The resultant model is shown in **Figure 28**.

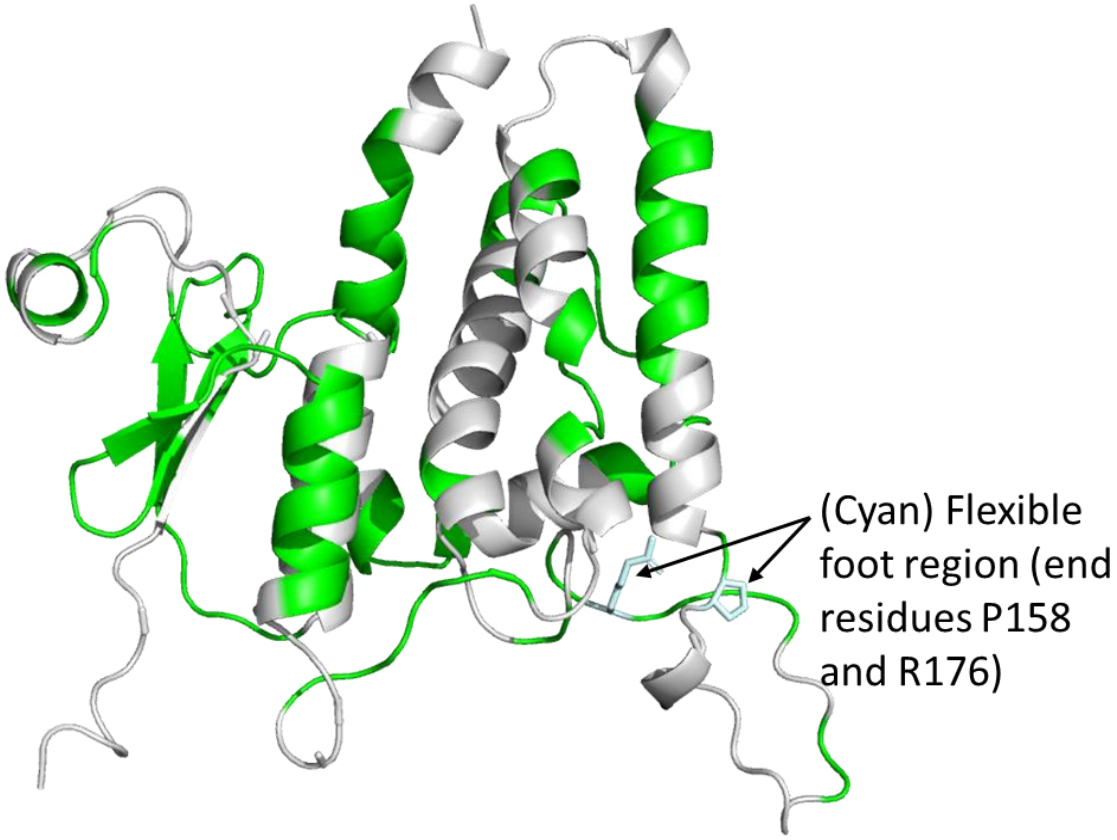

Figure 28 - Pymol model of CLIC4 (Alphafold PDB), showing NMR-determined assigned residues. *Green areas indicate residues that are assigned based on the peak assignment in the 2D HSQC of triple labelled CLIC4. Grey areas indicate unassigned residues. The "flexible foot region" and its border residues P158 and R176 are shown to display assignment cover of that region, as it is a suspected binding region.*

As **Figure 28** shows, there is a significant amount of the protein that has been mapped (117 residues assigned) and can be analysed for ligand/protein binding sites with accuracy to the specific residues involved. Unfortunately, due to protein not being fully assigned, the model shows substantial grey areas relating to unassigned residues where no further analysis of the protein can be undertaken. There are significant amounts of assigned residues situated in key structural areas, such as β-strands and α-helices around the outside of the protein. Some areas of the flexible foot region are also assigned, potentially aiding binding site analysis.

The assignment of residues, and how much of CLIC4 is now assigned which is shown in **Figure 28**, allows the investigation into interactions with ligands and other molecules. However, the prediction of CLIC4 secondary structure based on sequence and NMR assignments is beneficial for determining a comparison between known structure from an X-ray crystal, and computational predictions. As such, this structure prediction can be obtained via the Torsion Angle Likeliness Obtained from Shift and Sequence Similarity (TALOS) program (124).

5.3 TALOS Secondary Structure Predictions

5.3.1 CLIC4 Secondary Structure via X-Ray PDB

TALOS is a protein secondary structure prediction software that calculates the phi and psi (ϕ and ψ) backbone angles depending on the chemical shifts of assigned residues for a protein sequence (128). The structure of CLIC4, according to the PDB file 2AHE, was mapped via the diagram below in **Figure 29**.

Figure 29 – Secondary structure map of CLIC4, based on PDB sequence. *Structure predictions are based on PDB file 2AHE, obtained via X-Ray crystallisation. Secondary structure elements are displayed in top left.*

As shown, 110 residues are involved in α-helices which account for 43% of the CLIC4 protein. 26 residues constitute β-strands which is 10% of the entire protein. Therefore, 47% is either random coils or loops.

5.3.2 CLIC4 Secondary Structure via TALOS sequence and NMR assignment

TALOS was provided with the assigned residues of CLIC4, and run with the full sequence to identify the secondary structure of CLIC4 using both data sets. The results are shown in **Figure 30** below.

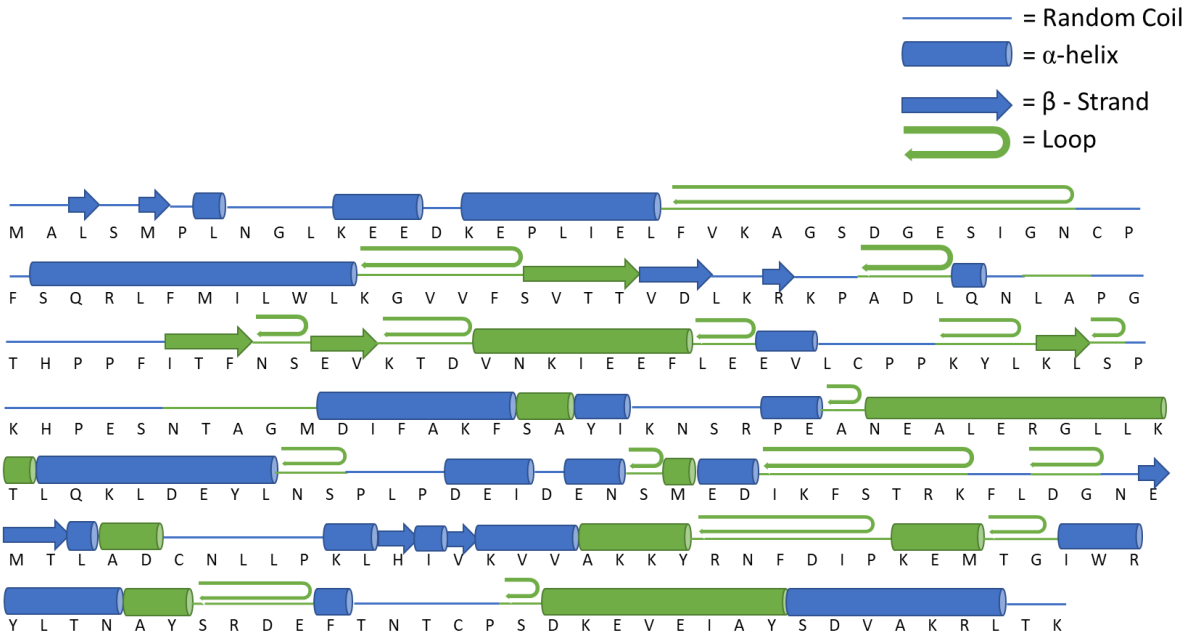

Figure 30 - Secondary structure map of CLIC4 based on NMR-determined residue assignments and CLIC4 sequence. *Secondary structure elements are displayed in top left, with colouration denoting structure prediction origin. Blue = Secondary structure element predicted via sequence of CLIC4. Green = Secondary structure element predicted via NMR-determined residue assignments.*

When comparing the PDB file of CLIC4's secondary structure with TALOS predictions based on NMR assignments, a similar amount of residues are predicted to be associated with α-helices, 111 in total which is 44% of the protein. Of this, 40 residues are from the assignment data, 36% of the total α-helix prediction. However, the location and specific residues concerned with the TALOS prediction are different to that of the PDB structure. One example is the α-helix predicted at sequence "KEE" and "KEPLIEL" which is absent in the PDB structure. Instead, a β-strands is predicted at the end of "KEPLIEL"

starting with residue “I” in that sequence. TALOS also predicts an α-helix at “SDVAKRL”, which is a loop region on the PDB structure.

In regards to β-strands, 22 residues are involved according to TALOS, making CLIC4 8% β-strands, similar to the 26 in the known PDB structure. Of these, 11 are taken from the NMR assignments. Again, their location according to TALOS is a stark contrast to the PDB file. The sequence “KLHIVKVVAKKY” is all part of an α-helix in the PDB, but TALOS predicts a β-strand at residues “H” and “V” in that sequence. Additionally, the sequence “GESI” is a β-strand in the PDB, but is a loop in the TALOS predictions.

Despite the differences between the two structure maps, the NMR assignments have been crucial to the prediction of the secondary structure that TALOS has suggested. These assignments will therefore be vital for identifying and mapping the binding of ligands and other molecules, and what structures they impact as a result.

5.4 Prediction of Digoxin binding site within CLIC4

5.4.1 2D ^{1}H - ^{15}N HSQC of Digoxin-bound CLIC4 – MR 1:1

Following the assignment of the CLIC4 residues, a 2D ^{1}H - ^{15}N HSQC of CLIC4 and bound Digoxin previously collected by a lab colleague (Angela Serrano Sanchez) was overlayed with the CLIC4 assigned residues. This is displayed in **Figure 31**:

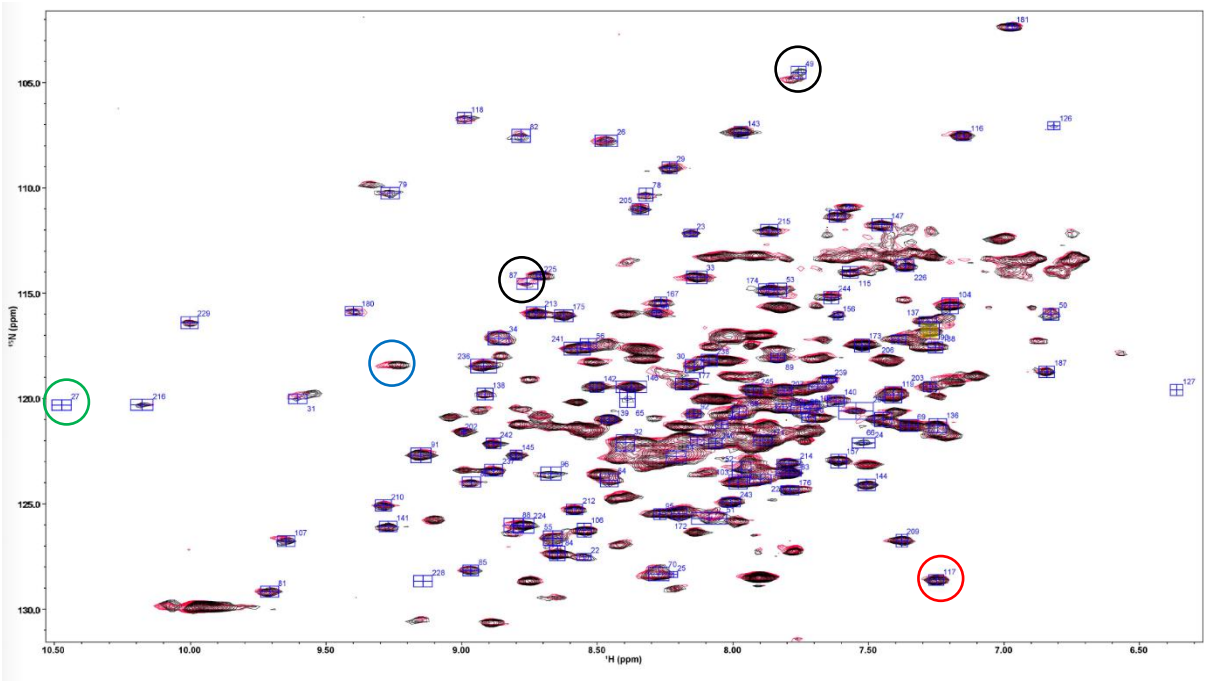

Figure 31 – Overlay of two 2D ^{1}H - ^{15}N HSQC Spectra: One of CLIC4, and one of CLIC4 bound to the drug Digoxin. *Spectra collected at 600 MHz with CLIC4 sample at 375 µM. Black peaks = CLIC4 Control sample. Red peaks = CLIC4-Digoxin (MR 1:1). Significant chemical shift perturbations highlighted with black circles. Disappeared peaks upon Digoxin binding circled in green. Peaks that experience a lack of chemical shift are circled in red. Peaks that have experienced chemical shift perturbations but are not assigned are circled in blue. Blue boxes = CLIC4 assigned residues.*

The CLIC4 used was single-labelled and was bound to Digoxin in molar ratio (MR) of 1:1 (375µM). As **Figure 31** shows, there are a significant amount of peaks that have shifted position when comparing the unbound CLIC4 control sample (black peaks) to the bound CLIC4-Digoxin MR1:1 sample (Red peaks). Notably, peaks 49 and 87 (circled, black) have undergone significant chemical environment changes as a result of digoxin binding. Peak 49 has shifted to the left of the spectrum, and Peak 87 has increased intensity and shifted. This would indicate these peaks are associated with residues that could be directly involved in a ligand binding site or undergo a shift as a result of structure re-orientation within the protein. Some peaks completely disappear, such as peak 27 (circled green). However, some peaks have experienced no chemical shift (e.g. residue 117, circled red) or have shifted but are unassigned (example circled in blue).

Due to the spectra showing chemical environment changes in assigned peaks, their shifts can be calculated and computationally analysed to accurately determine significant chemical shift

perturbations and hence suggest potential binding sites when comparing peak numbers to their residue number allocations.

5.4.2 Chemical shift Perturbations of shifted assigned CLIC4 peaks upon Digoxin Binding

The difference in peak locations between unbound and bound CLIC4 of each assigned residue was compared against the mean shift across all assigned residues, and significant residue shifts (determined via comparison to the standard deviation of the mean) were identified in **Figure 32**.

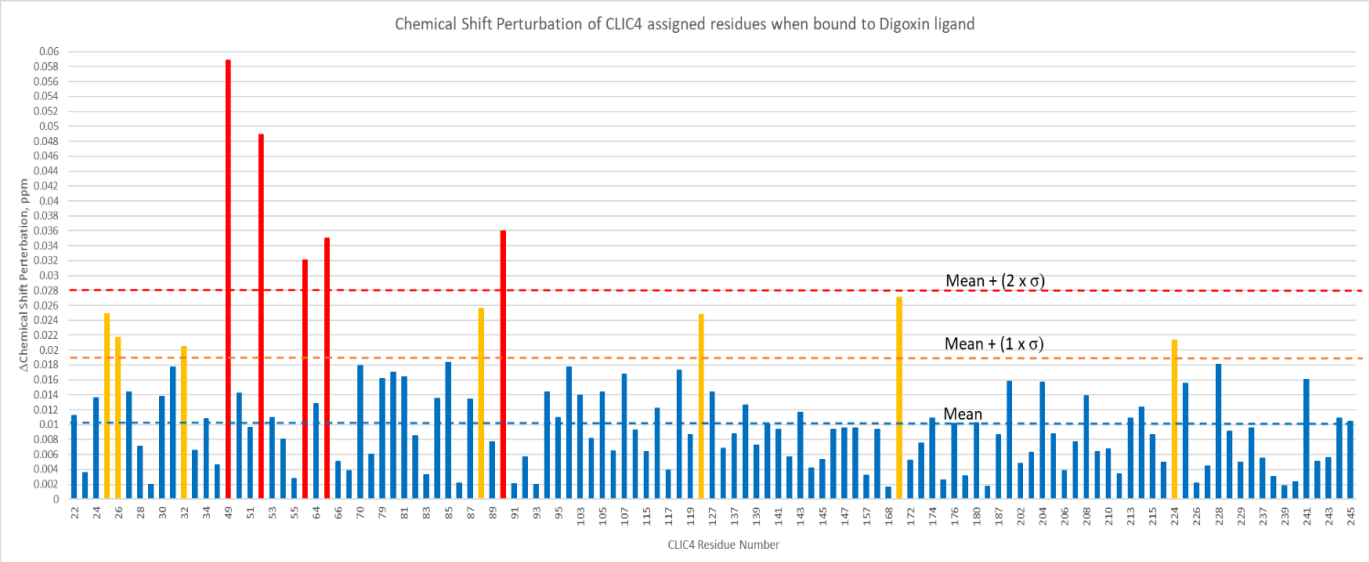

Figure 32 - Chemical Shift Perturbations (CSPs) of CLIC4 assigned residues, upon Digoxin binding. *Residues that have a chemical shift perturbation value around the mean, and are not statistically significant, are highlighted in blue. Those that are statistically significant by shifting more than one standard deviation (σ) from the mean are in yellow. Peaks that have shifted by more than two standard deviations from the mean are highlighted in red. Boundaries of mean, mean + 1 σ and mean + 2 σ are colour coded identically to the bars they represent.*

As shown, certain residues have shifted significantly upon digoxin binding. When comparing significantly shifted peaks (Figure 31) to their correlated residues (Figure 32), residues 25, 26, 32, 88, 126, 171 and 224 are highlighted as statistically significant due to their chemical shift perturbation value lying more than one standard deviation away from the mean (orange bars). In addition, residues 49, 52, 56, 65 and 90 have shifted to an even greater extent due to their chemical shift perturbation value lying more than two standard deviations away from the mean (red bars). These red-shifted residues are of particular interest, as these shifts may indicate the digoxin binding site with a stronger

degree of confidence compared to those which are orange-shifted. Hence, visualisation of all shifted residues concerning CLIC4 structure is paramount to gain an understanding of where digoxin may bind to CLIC4, and their significance on both the chemical environment surrounding the protein and its secondary structure.

5.4.3 CLIC4-Digoxin binding site modelling via Pymol (Manually)

5.4.3.1 CLIC4-Digoxin suspected binding site: Back and Front Views

The significantly shifted residues calculated via chemical shift perturbation statistical analysis were mapped onto the CLIC4 model in Pymol (with the same colour scheme). The model is displayed in **Figure 33** panels A and B, with assigned residues in green, unassigned in grey and shifted residues following the same colour scheme as **Figure 32** analysis. The structure of Digoxin is shown in panel C.

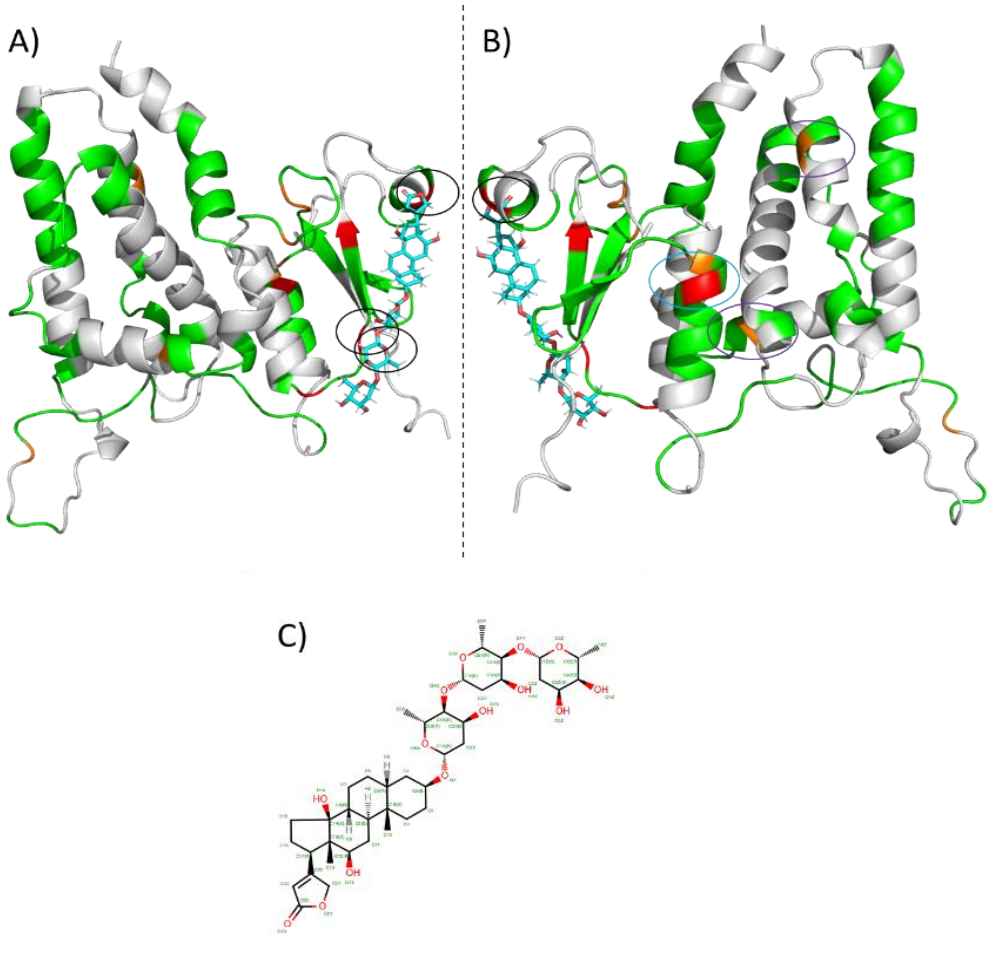

Figure 33 - Pymol model of CLIC4 manually aligned with Digoxin based on significant CSPs from 2D HSQC NMR. *A) "Backside" model of CLIC4 with a manually inserted Digoxin molecule in a region that possesses significant residue CSPs. B) "Frontside" model of CLIC4. Black circles indicated charged atoms on digoxin interacting with red-shifted residues. Blue circle = α-helix shifted residue, suggesting conformational changes in structure. Purple circle = Inner α-helices shifted residues, suggesting structural re-orientation. C) Chemical structure of Digoxin, for clarity (obtained via RCSB PDB entry DGX). Green = assigned residues. Grey = unassigned residues.*

The Digoxin ligand (shown in blue, obtained via RCSB PDB entry: DGX) was manually positioned in a region where the majority of shifted residues reside to simulate where Digoxin may bind in CLIC4. As panel A shows, the Digoxin molecule could fit into a binding cleft on the right-hand side of CLIC4, which is situated on the N-Terminus. Charged atoms such as carbonyl and hydroxyl groups present on the bottom end of the drug are lined up alongside red-shifted residues (circled in black, drug rotated 180°), which is easier to see in panel B. Here, the top of the Digoxin molecule is interacting with an α-helix (circled black) which does suggest this "binding cleft" as a region of protein-drug interaction.

Additionally, circled in blue is the top of an α-helix which is significantly shifted following Digoxin binding, which could relate to structural re-organisation as a result of the binding site interactions. This is complimented by inner helix shifts particularly seen in panel B (circled purple). Contrastingly, there is a shift noted along the "flexible foot" region of the protein, indicating some structural changes on the other side of the protein molecule.

5.4.3.2 Predicted Digoxin Binding site

Further analysis of individual residues suspected to reveal a Digoxin binding site on CLIC4 is shown in **Figure 34**. As with the other CLIC4-Digoxin Pymol models, assigned CLIC4 residues are highlighted in green, and unassigned residues are coloured in grey.

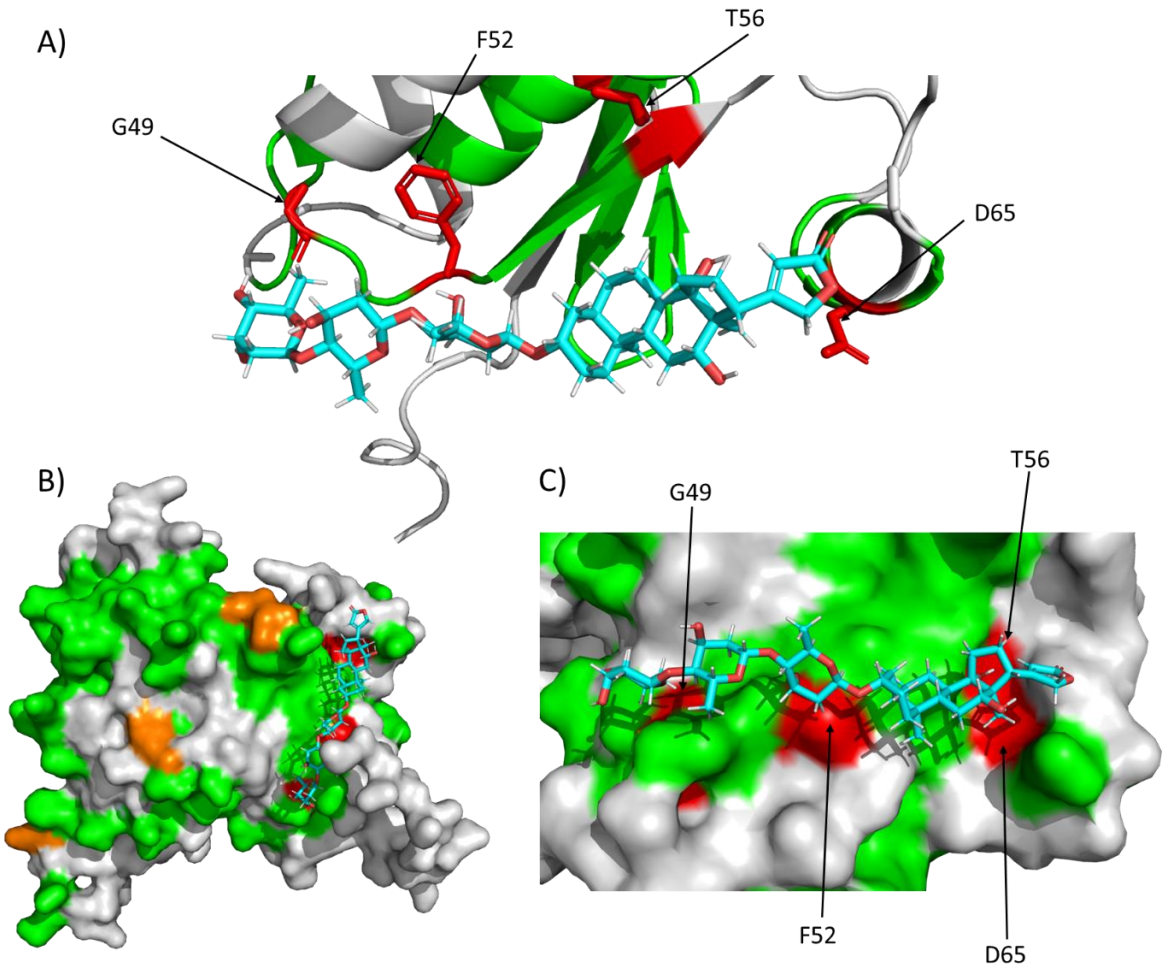

Figure 34 - Detailed CLIC4-Digoxin binding site Pymol model, including surface interactions. *A) Structural view showing Digoxin manually inserted into a potential CLIC4 binding site, with red-shifted residues highlighted to indicate potential charged atom interactions. B) Overview of predicted Digoxin binding site, with a "surface" view to indicate binding cleft. C) Surface model zoomed in, showing detailed binding site and red-shifted residues which are highlighted. Green = assigned residues. Grey = unassigned residues.*

Panel A, showing a zoomed-in inspection of this proposed binding site reveals the red-shifted residues that are first displayed in **Figure 33**. Direct interactions of the digoxin molecule to G49, F52, T56 and D65 are seen, suggesting polar interactions between the digoxin molecule and the residues. This is the case with D65 to a nearby carbonyl group on digoxin. Panels B and C highlight how the digoxin molecule can fit into a binding grove on the surface of CLIC4, allowing interactions with the protein.

Although the suggested interactions shown in figures **Figure 33** and **Figure 34** could be considered a strong suggestion towards the true location of the digoxin binding site, computational modelling via the program HADDOCK (High Ambiguity Driven protein-protein DOCKing) can accurately predict

binding site interactions between protein and ligand which can be further analysed to support or disprove manual alignment in Pymol based on NMR chemical shift perturbations.

5.4.4 HADDOCK-predicted CLIC4-Digoxin binding site in Pymol

HADDOCK (High Ambiguity Driven protein-protein DOCKing) is a programme that identifies protein-protein and protein-ligand interactions using interaction restraints placed on the protein or ligand that affect the environment around it (129). Although the binding site proposed via **Figure 33** and **Figure 34** seem to agree with the CLIC4-Digoxin chemical shift perturbations, calculated binding site interactions and modelling of interactions may prove more effective in uncovering the true interaction mechanisms between protein and ligand.

Figure 35 shows the results of HADDOCK-assisted CLIC4-Digoxin docking.

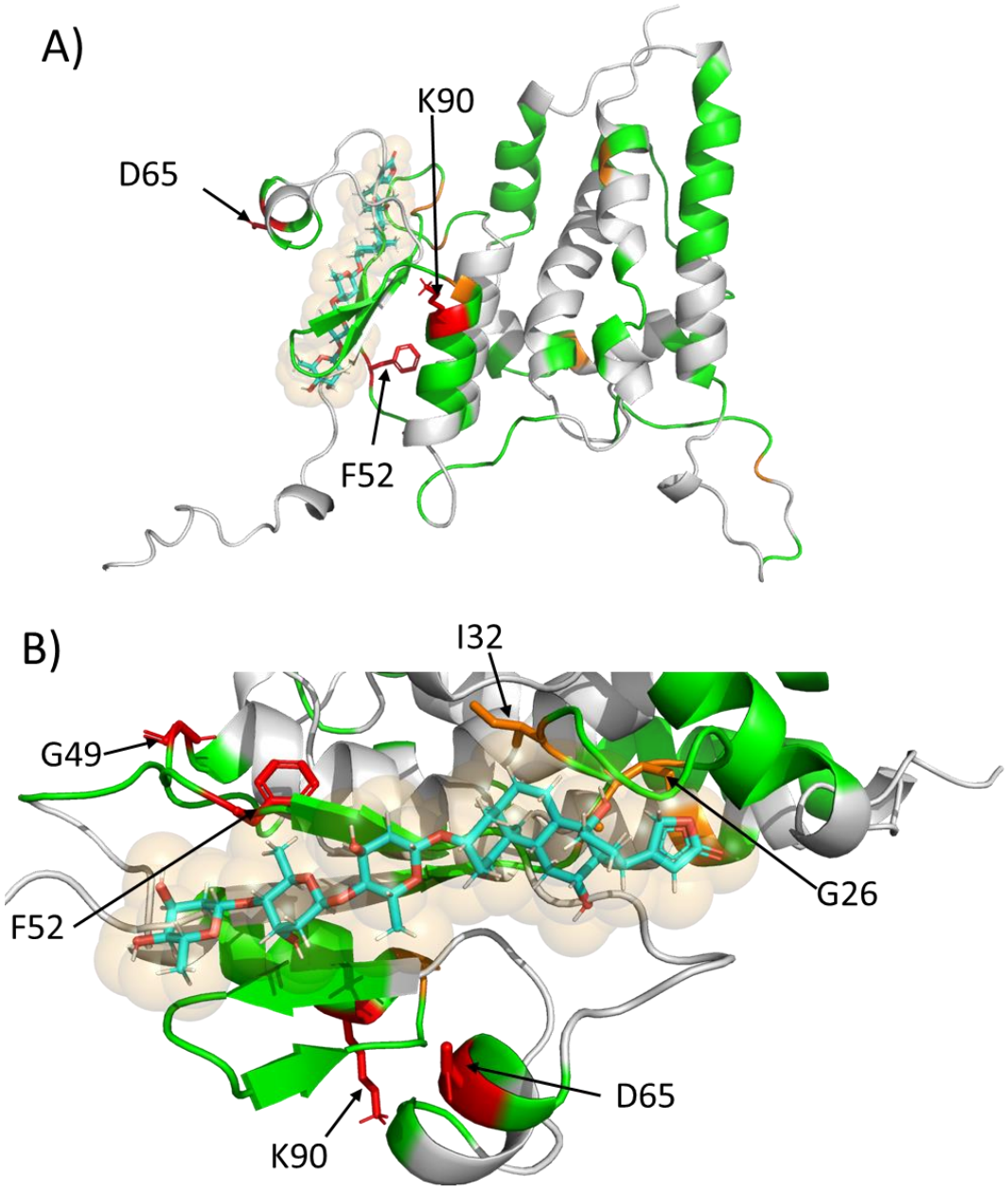

Figure 35 - HADDOCK predicted CLIC4-Digoxin binding interactions. *A) Structural overview of Digoxin placement relative to the CLIC4 structure and significantly red-shifted residues (via CSPs). Proximity calculations run by HADDOCK regarded Digoxin as a "spherical" object, hence the faint spheres around the molecule. B) A closer inspection of the predicted binding site, showing Digoxin interacting with certain Red and orange shifted residues (based on CSPs). Green = assigned residues. Grey = unassigned residues.*

The HADDOCK predictions output 3 PDB files, of which all possessed the location of the Digoxin molecule in the same place, as well as the residues involved in the digoxin interaction. **Figure 35** panel A shows an overview of CLIC4 with bound Digoxin. The Digoxin structure is shown within faint orange spheres, as HADDOCK regarded the ligand as a spherical object for its calculated interactions. Residues D65, F52 and K90 were revealed to be within close proximity to the Digoxin molecule within the predicted binding site. Zooming in on the predicted binding region (panel B), there are suggestions that more contact points between Digoxin and CLIC4 are present. In addition to D65, F52 and K90, residues G26, I32 and G49 are significantly shifted according to the chemical shift perturbations and are clearly in close proximity to the Digoxin molecule.

HADDOCK also has computationally agreed with where Digoxin would bind and its effect on the residues of CLIC4. For example, HADDOCK also indicated residues G49, F52 and D65 were involved in binding interactions as a result of the NMR chemical shift perturbations. HADDOCK also reveals these residues are in close proximity to the Digoxin which would explain the NMR chemical shift perturbations experienced. The resultant binding site of Digoxin has a clear basis for further investigation and binding assays, to improve the understanding of CLIC "druggable" sites.

5.5 GIT1 Expression: Full Length and Truncated

The suspected binding protein of CLIC4 (GIT1) which is part of the hypothesised Arf6/CLIC4 pathway, was analysed for potential interactive domains with CLIC4. This allowed the isolation of the most likely domain on GIT1 that would interact with CLIC4 (based on its interactions with GAP proteins detailed in the literature). The full-length GIT1 was also chosen for expression and binding analysis as a comparison.

5.5.1 Bioinformatics Analysis

5.5.1.1 The GIT1 Arf-GAP domain and interaction predictions

The GIT1 Arf-GAP domain was highlighted in Pymol (**Figure 36**A) and submitted to the ColabFold/Alphafold2 server for binding predictions with CLIC4. The result was modelled in Pymol,

showing both the cartoon structure of both proteins interacting (**Figure 36**B) and surface-enabled models shown in **Figure 36** C and D).

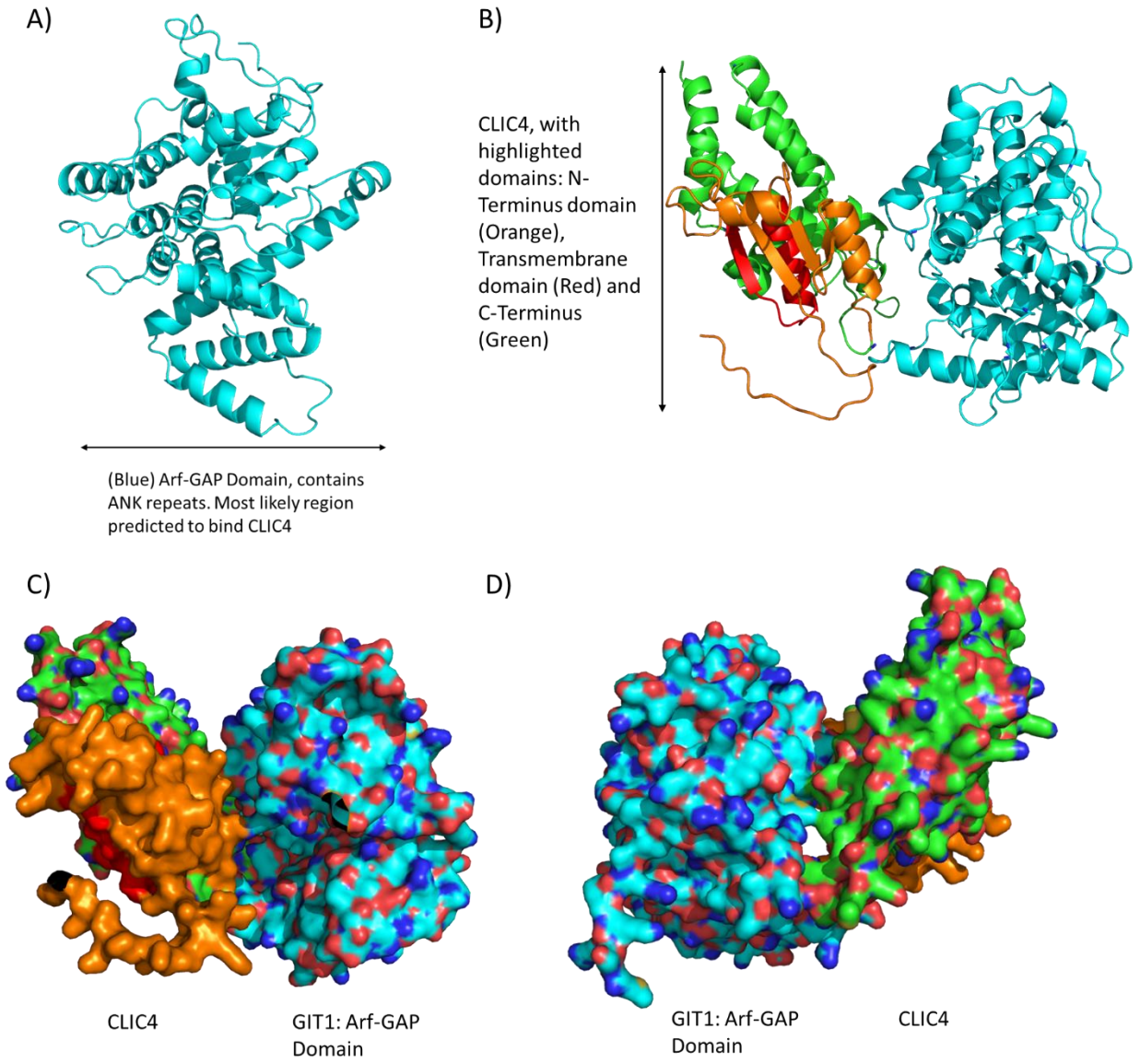

Figure 36 - Pymol models of GIT1 and its interactions with CLIC4. *A) The Arf-GAP domain, predicted to be the most likely region to successfully bind to CLIC4, based on its GAP binding properties described in the literature. B) Structural view of CLIC4 (left) binding to the Arf-GAP domain of GIT1 (right), as predicted by ColabFold/AlphaFold2 calculations. C) Surface view of interacting CLIC4 and GIT1 Arf-GAP domain. D) Alternative view of C. ANK = Ankyrin Repeats*

Based on the imagery shown in **Figure 36**, the Arf-GAP domain presents itself as a promising binding partner to CLIC4. A significant amount of the surface of the proteins are interacting with each other, which highlights the Arf-GAP domain of GIT1 as a promising binding region. Therefore, GIT1 overall is a viable protein for experimentation in CLIC4 binding assay.

5.5.1.2 GIT1 Full-length and Truncated Construct Design

The sequence of the full-length GIT1 protein, and its truncated version, was implemented into separate pET28a bacterial plasmids for the transformation of competent cells required for protein expression (T7 Express cells for the Full-length version, Rosetta 2 DE3 cells for the Truncated version). The construct design for both plasmids is shown in **Figure 37**.

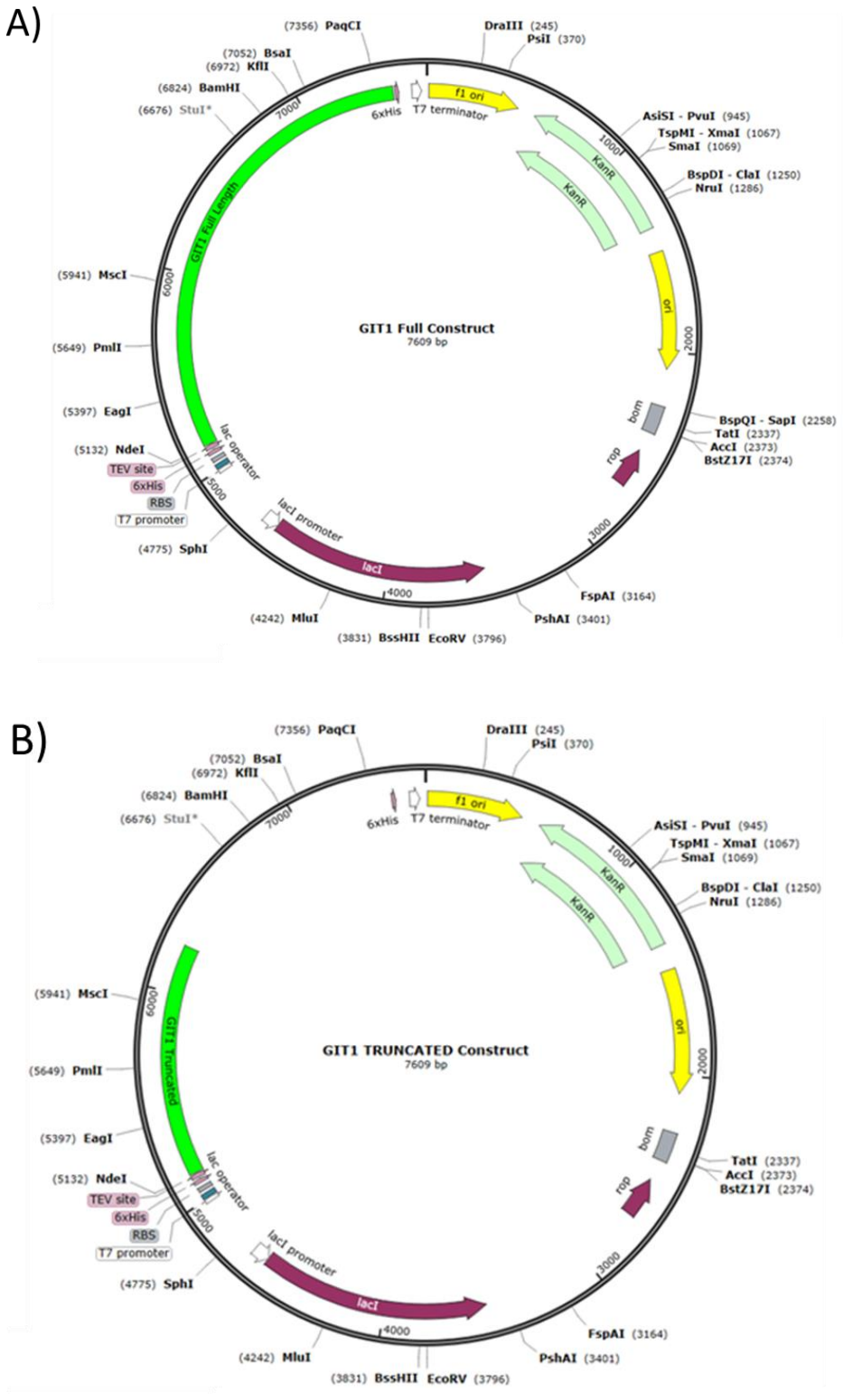

Figure 37 - Construct Design for Full-length and Truncated version of GIT1*. A) GIT1 Full-length construct. B) Key elements include Kanamycin Resistance, 6xHis-Tag and TEV cleavage site*

In **Figure 37**A showing the GIT1 Full-length vector, the construct contains common plasmid regions used for plasmid generation. The *f1 ori* region marks the start of the plasmid replication, and is derived from bacteriophages making this plasmid a "phagemid". This region allows the plasmid to be copied and reproduced inside the cell. There is the *KanR* gene, which allows selection for the transformed competent cells via enabling Kanamycin resistance. The *ori* region promotes high copy numbers of the plasmid, but when accompanied by the *rop* gene encoding a "Repressor of Primer" protein, the copy number is kept lower in *E.coli* to prevent leakage of plasmids in cells. Moving further along, the RBS site is where the ribosome will bind, which is adjacent to the *lac operator* and introduces the "lac-operon" model of gene transcription. The *lac operator* region binds the lacI protein*,* which is the natural repressor of the gene of interest (e.g. GIT1) when in an IPTG-absent environment. Therefore, the *lacI* region transcribes the lacI protein. When IPTG is introduced, lacI is inhibited which allows GIT1 to be transcribed via T7 polymerase with the *T7 Promotor* region allowing high-level protein expression, which ceases at the *T7 Terminator* region, provided T7 polymerase is present (in cells used for GIT1 expression, T7 polymerase is present). Alongside these regions, the TEV site and 6xHis-Tag are included for protein purification. Additionally, numerous restriction sites are posted along the plasmid for DNA strand ligation.

Figure 37B shows an identical pET28a vector set up, with the only difference being this vector relates to the GIT1 Truncated version.

5.5.2 Confirmation of GIT1 production using SDS-PAGE Gels

5.5.2.1 GIT1 Full-length

The GIT1 Full-length protein was purified via Ion affinity chromatography from T7 express cell harvesting, with SDS-PAGE samples taken at each purification step (see section 4.6 GIT1 (Full-length/Truncated) Expression and Purification). Additionally, samples were dialysed overnight without TEV, and an SDS-PAGE sample was taken. **Figure 38** shows the expression levels of each purification stage, with increasing purity of the sample as each stage was carried out.

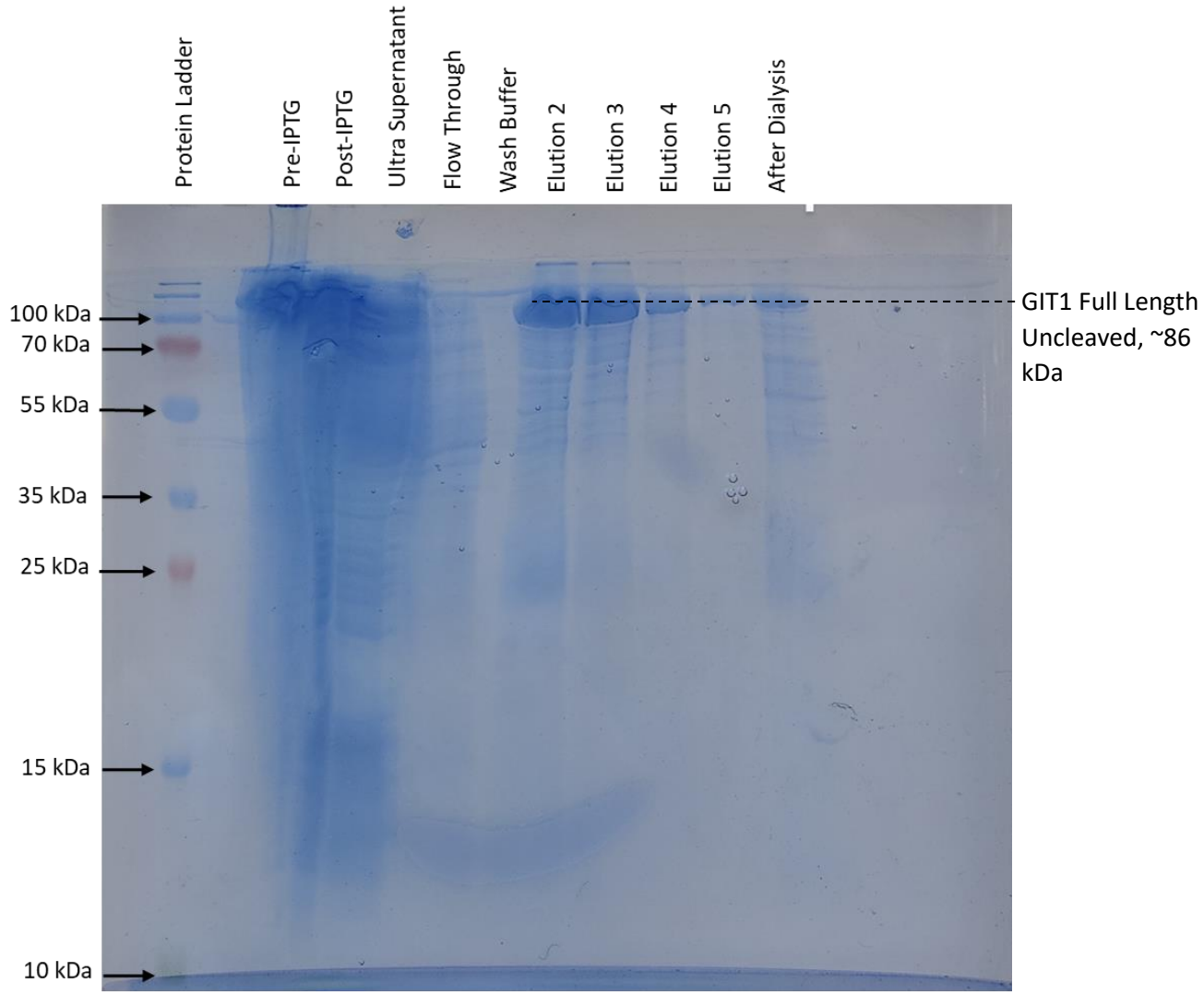

Figure 38 – SDS-PAGE gel of GIT1 Full-length (Uncleaved) using samples taken from the growth of cells and harvesting/purification of GIT1, with dialysis. *There is some expression seen in Elutions 2-5 and "After dialysis", which are approximately in the correct region for GIT1 Full length (approx. 86 kDa). However, the gel has not run correctly and there is a significant degree of smearing. The protein ladder (left) has also not run correctly, obscuring the results. Elution 1 sample was contaminated and was discarded.*

SDS-PAGE samples “Pre-ITPG” through to “Flow Through” did contain cellular proteins, however, there are no identifiable bands present due to gel running-related issues which caused the lanes to smear and appear distorted. However, there are clear expression bands located in the lanes of Elutions 2-5 (Elution 1 SDS-PAGE sample suffered contamination and was discarded as a result), decreasing in thickness of the band as elutions progress. Thus, there is an indication of protein expression. In terms of the relative size of the protein, the banding patterns are around the expected region of GIT1 expression (approx. 86kDa), but the protein ladder displayed in **Figure 38** has not run optimally. As mentioned previously, the gel has not run correctly which has led to the band for GIT1 Full length to appear to run higher than 100kDa. Also, the ladder protein bands are crowded at the top which does not allow accurate determination of the elution expression bands’ molecular weight. Given the expression of the bands located in Elution 2-5, it is clear a protein that is suspected to be GIT1 full-length was expressed although cannot be confirmed via this gel.

5.5.2.2 GIT1 Truncated

Alongside the GIT1 Full-length expression and purification, the same sample preparation for the truncated version of GIT1 was carried out, but using Rosetta 2 DE3 cells. The result of this is shown in **Figure 39**.

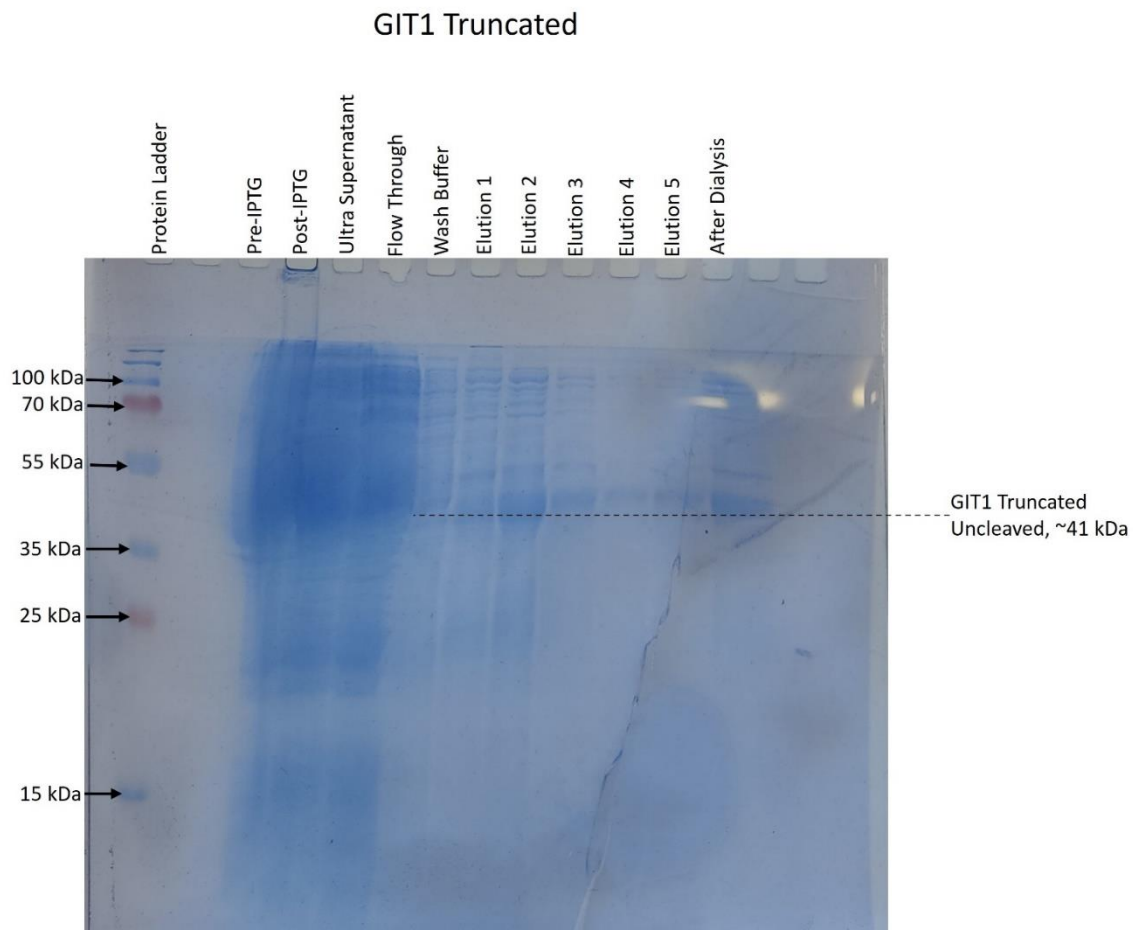

Figure 39 - SDS-PAGE gel of GIT1 Truncated (Uncleaved) using samples taken from the growth of cells and harvesting/purification of GIT1, with dialysis. *There are clear expression bands in samples Elutions 1-5 and "after dialysis", which correlate to approx. 41 kDa, the expected size of GIT1 Truncated. This is indicated by the protein ladder graduations. However, there is a lot of smearing in the "Pre-IPTG" through to "Flow Through".*

This gel also suffered smearing and distortion in "Pre-IPTG" to "Flow Through" SDS-PAGE samples. However, Elutions 1-5 and the after-dialysis samples show a clear expression band that resides between the 35kDa and 55 kDa when compared to the protein ladder. Although the protein ladder has not run particularly well, similar to the GIT Full-length gel, the banding does seem to indicate that GIT1 Truncated has been expressed as it is situated in the expected region and the molecular weight of the truncated version is 41kDa.

The expression of both versions of GIT1 is presumed to be successful, however further purification via SEC chromatography was required to evidence correct expression in addition to the elimination of contaminants from the harvesting process (e.g. DNA fragments).

5.5.3 Purification of GIT1 using Size-Exclusion Chromatography (SEC)

Both GIT1 Full-length and Truncated samples were run through the SEC for further purification, as well as an indication of successful monomer formation/removal of oligomeric states. The resultant concentration of GIT1 Full-length at this stage was 53µM, and GIT1 Truncated at 260 µM. The resulting SEC chromatogram is shown in **Figure 40**.

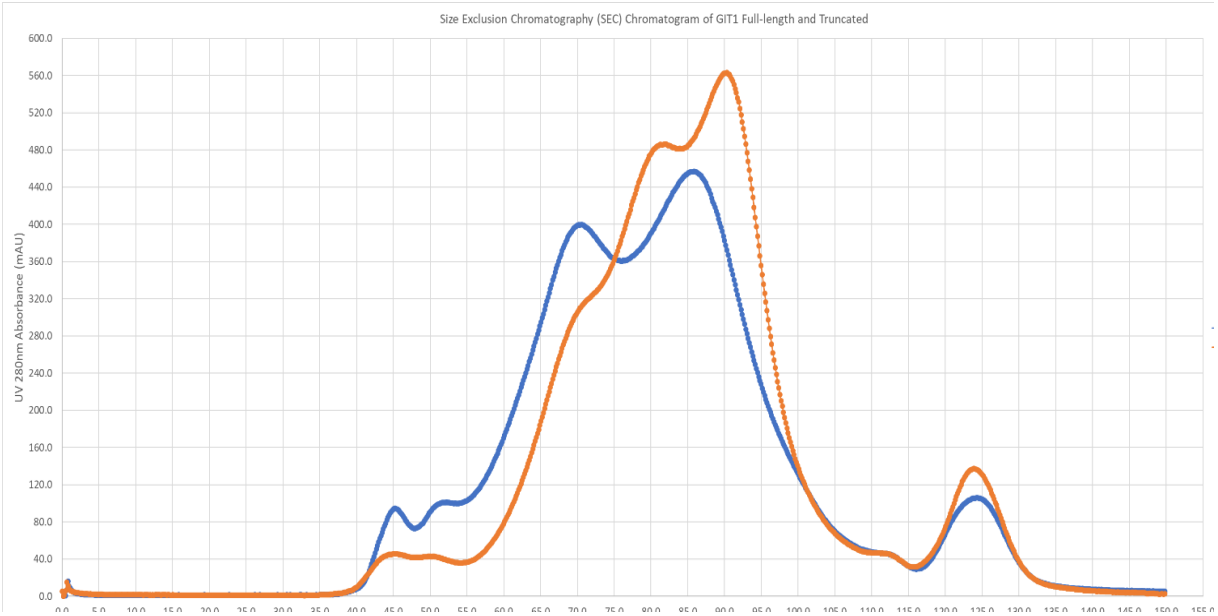

Figure 40 - Size Exclusion Chromatography (SEC) Chromatogram of Full-length (blue line) and Truncated GIT1 (orange line). *SEC column has a column volume of 120ml, with the intensity of the 280nm UV absorbance correlating to the concentration of GIT1 present. Monomeric GIT1 eluted at around 55-105ml (for both protein versions), with the intensity of the Full-length peak being 460 mAU and Truncated peak being 560 mAU.*

The monomeric full-length GIT1 has eluted between 55 ml-110 ml, with the UV 280nm intensity peaking at 460 mAU which is significantly less than CLIC4's elution intensities peaks across all sample types (Non-labelled, Triple and Single labelled). Compared to the monomeric truncated version which is eluted at a similar volume of 60 ml – 105 ml and the peak is shifted to the right, the truncated version has a higher intensity than the full-length (560 mAU compared to the full-length's 460 mAU). This suggests a higher concentration of GIT1 truncated has been expressed than GIT1 Full-length.

Although the elutions of both proteins are slightly different, the intensity of the monomeric peaks indicates overexpression of both proteins in the transformed bacterial cells. This means that the

proteins have been confidently overexpressed and that the samples prepared are of high-quality for experimental assays.

5.6 Microscale Thermophoresis (MST) to determine GIT1:CLIC4 binding

5.6.1 CLIC4-GIT1 Full-Length Binding

A Non-labelled CLIC4 sample, starting at 150 µM was serially diluted before being titrated against GIT1 Full-length (50 µM) to determine binding affinity via MST. The results are shown in **Figure 41**.

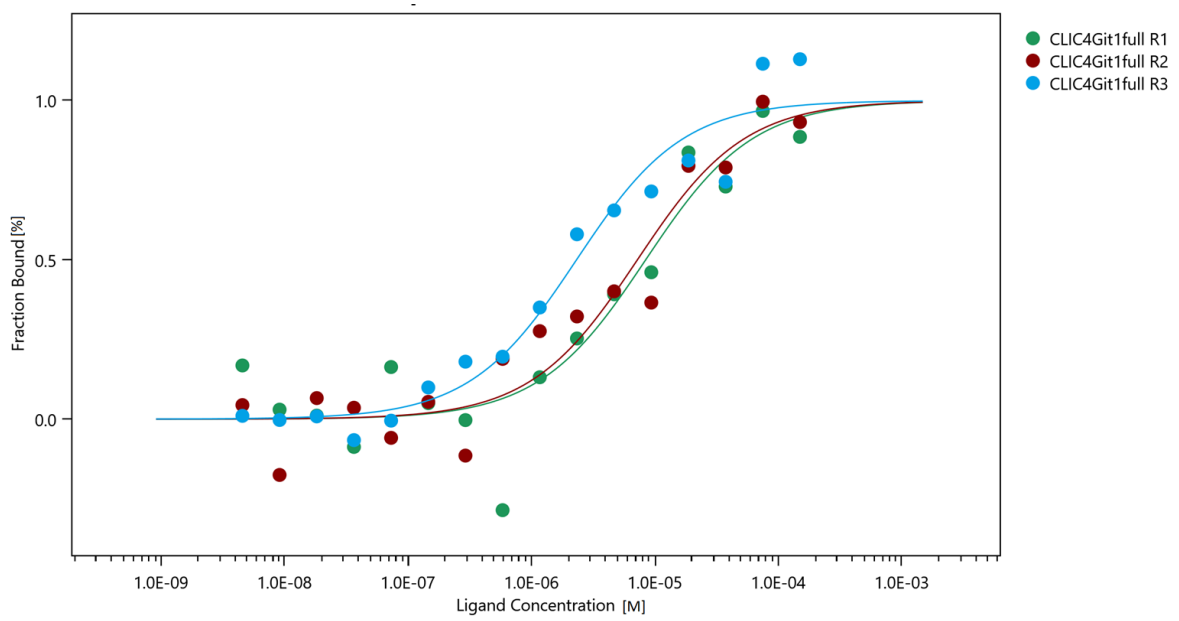

Figure 41 - Microscale Thermophoresis (MST) binding curves for Full-length GIT1. *GIT1 was serial diluted with CLIC4 at a starting concentration of 50 µM and 150 µM respectively. The binding curves for each repeat (n=3) are shown, with colouration correlating to the key (right). K_D values for each repeat: R1 = 8.4µM, R2 = 7.2 µM, R3 = 2.3 µM. Mean = 6.0 µM ±1.52 µM.*

The figure shows binding affinity curves for the binding of GIT1 Full length to CLIC4. The data points plotted across all repeats (n =3) are fairly accurate to the predicted binding curve, but there are some notable outliers particularly relating to the first repeat (R1, green). However, R2 (red) and R3 (blue) also show some variable data points. The extraction of the K_D values calculated by the MST software (M0 Affinity Analysis) for repeats are as follows: R1 = 8.4µM, R2 = 7.2 µM, R3 = 2.3 µM, with the mean being 6.0 µM ±1.52 µM (Standard error of the mean) However, the average considers the lower K_D calculated from R1 which, as **Figure 41** displays, contains notable outliers. R1 and R2 are very close in

their estimations, suggesting the true K_D value lies somewhere between the two. However, the R3 binding curve is left-shifted in comparison to R1 and R2, indicating an overall tighter binding curve with a much lower K_D value. Overall, despite the R1 and R2 K_D values being within a small deviation of each other, repeating the binding experiment further would be useful to fully determine the most accurate K_D value.

5.6.2 CLIC4-GIT1 Truncated Binding

Non-labelled CLIC4 sample was titrated with the GIT1 Truncated protein, with the same concentrations used as with GIT1 Full-length. The results are shown in **Figure 42**.

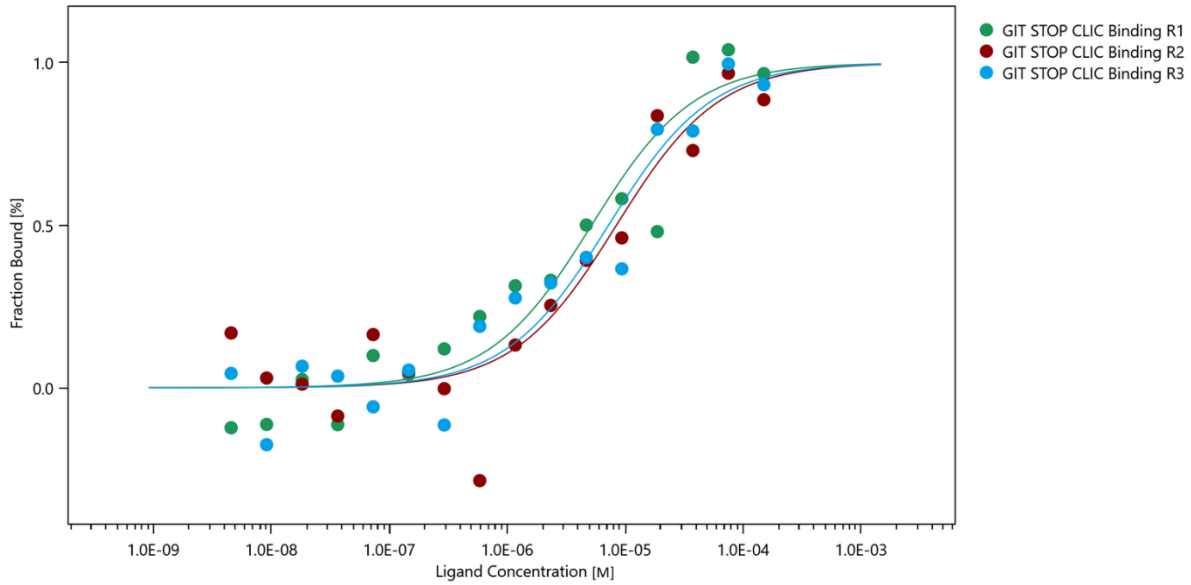

Figure 42 - Microscale Thermophoresis (MST) binding curves for Truncated GIT1. *GIT1 was serial diluted with CLIC4 at a starting concentration of 50 µM and 150 µM respectively. The binding curves for each repeat (n=3) are shown, with colouration correlating to the key (right). K_D values for each repeat: R1 = 5.2µM, R2 = 8.4 µM, R3 = 7.2 µM. Mean = 6.9 µM ±0.76 µM.*

In comparison to the GIT1 Full-length MST affinity curves, R1-R3 GIT1 Truncated appear to have less deviation in their binding affinity curves, The mean K_D value is 6.9 µM ±0.76 µM (Standard error of the mean)., with individual values being R1 = 5.2µM, R2 = 8.4 µM, R3 = 7.2 µM. Again, there are obvious outlier data points exhibited within all test numbers which does vary the reliability of the calculated K_D value. Despite this, the comparison between the K_D value of GIT1 Full-length and GIT1 Truncated is 0.9 µM which does suggest the true binding affinity of GIT1 to CLIC4 is approximately around the

values given by the MST experiments. Ideally, both GIT1 Full-length and GIT1 Truncated proteins would be repeated in full on the MST to obtain a more accurate representation of the true K_D value.

The MST experiments indicated positive binding between GIT1 and CLIC4, which was investigated further via titrations monitored via NMR.

5.7 Using Nuclear Magnetic Resonance (NMR) to identify GIT1:CLIC4 Interaction sites

5.7.1 Titrations of CLIC4 with GIT1

5.7.1.1 CLIC4 Control - 216µM

Following the successful binding interactions of both GIT1 proteins to CLIC4, a 2D ^{1}H - ^{15}N HSQC spectra was collected on ^{15}N CLIC4 at 216µM. The CLIC4 assigned residues have been overlayed on top of the spectra, as **Figure 43** displays.

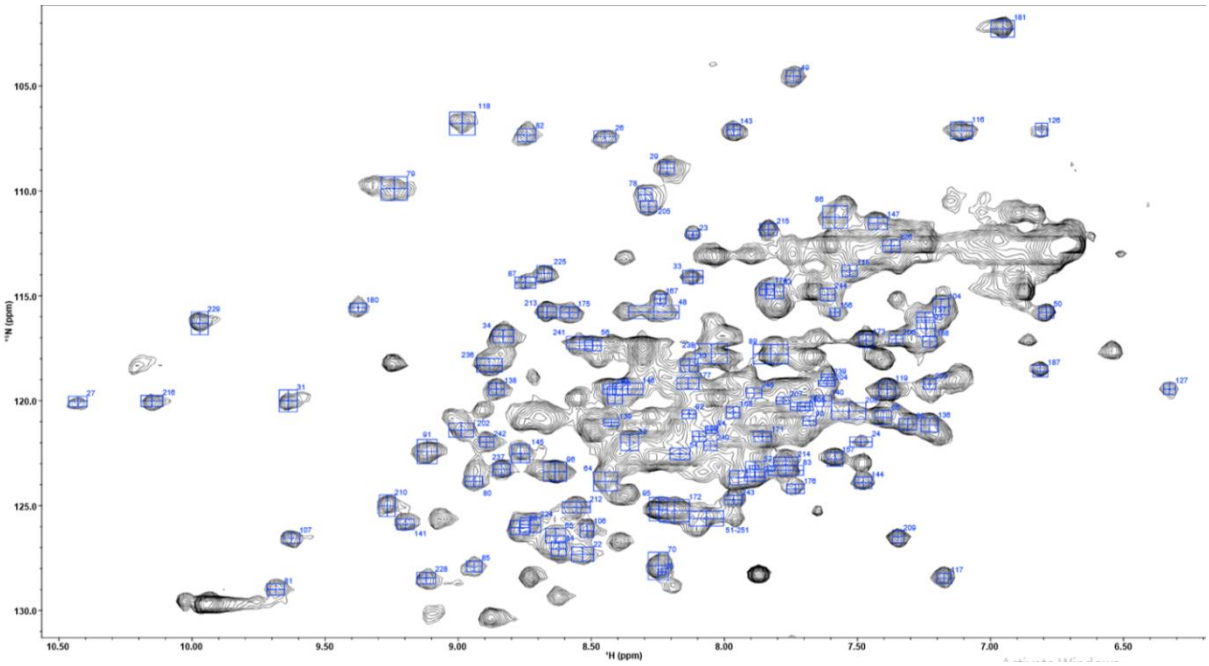

Figure 43 - 2D ^{1}H - ^{15}N HSQC Spectrum of ^{15}N Single-labelled CLIC4 with backbone assignments. *Concentration of CLIC4 is 216µM, run at 600 MHz. Blue boxes = peaks assigned to a specific residue of the CLIC4 protein sequence.*

The spectrum shows well-defined peaks that are assigned based on the triple-labelled CLIC4 sample. Despite some peaks having their assigned residue missing, there should be sufficient peaks assigned

to determine intensity changes and chemical shift perturbations upon GIT1 binding, both full-length and truncated.

5.7.1.2 GIT1 Full-length – MR 1.8:1

A 2D ^{1}H - ^{15}N HSQC of ^{15}N CLIC4 was collected upon the addition of GIT1 Full-length in concentrations of 120 µM: 68 µM or a molar ratio of 1.8: 1. The resulting spectra are displayed below:

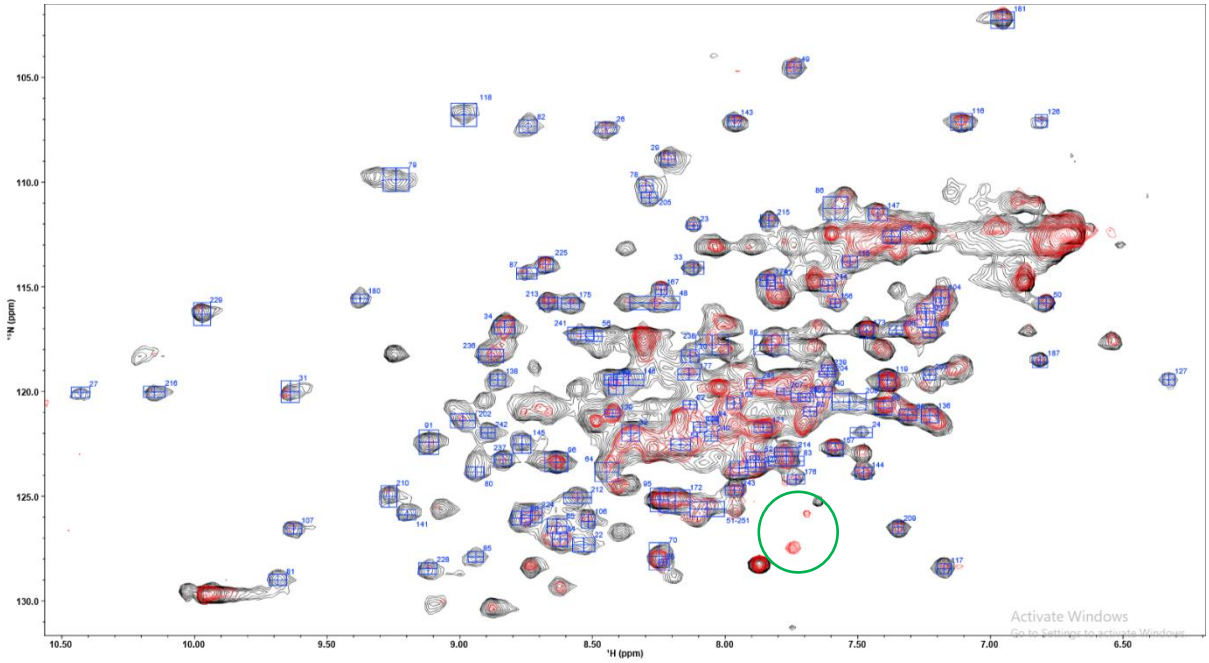

Figure 44 - Overlay of two 2D ^{1}H - ^{15}N HSQC Spectra: One of CLIC4, and one of CLIC4 bound to Full-length GIT1. *Spectra collected at 600 MHz with CLIC4 control sample at 216 µM. Black peaks = CLIC4 Control sample. Red peaks = CLIC4-GIT1 at 120 µM:68 µM (MR 1.8:1). Appearing peaks upon GIT1 binding circled in green. Blue boxes = CLIC4 Assigned residues.*

The black peaks indicate the CLIC4 control (see **Figure 43**), with the red peaks showing the CLIC4-GIT1 Full-length spectra which are overlayed. Additionally, the assigned residues of CLIC4 are shown as blue boxes with the residue numbers. As **Figure 44** shows, the CLIC4-GIT1 Full-length spectra is quite poor, with a significant amount of peaks missing or not well defined. This is primarily down to a concentration difference between the control CLIC4 at 216 µM and CLIC4-GIT1, with the GIT1 specifically being at 68 µM. The recommended protein concentration for NMR is approx. 150 µM, so GIT1 is well below the ideal concentration for a clear indication of binding and the residues of CLIC4

that are affected as a result. There may be some suggestion of interaction, given two new peaks appeared on the CLIC4-GIT1 Full-length spectra, indicated by the green circle

The concentration issue of GIT1 Full-length resulted in the inability to calculate chemical shift perturbations. Instead, the indication of binding of CLIC4 to GIT1-Full length was determined via Intensity differences between the peaks that are visible on this spectrum in comparison to the CLIC4 control.

5.7.1.3 GIT1 Truncated

Similar to the CLIC4:GIT1 Full-length NMR spectra, the 2D ^{1}H - ^{15}N HSQC of ^{15}N CLIC4 control sample was overlayed with a 2D ^{1}H - ^{15}N HSQC of CLIC4-GIT1 Truncated at concentrations of 130µM or molar ratio of 1:1. The more promising resultant spectra is shown in **Figure 45**.

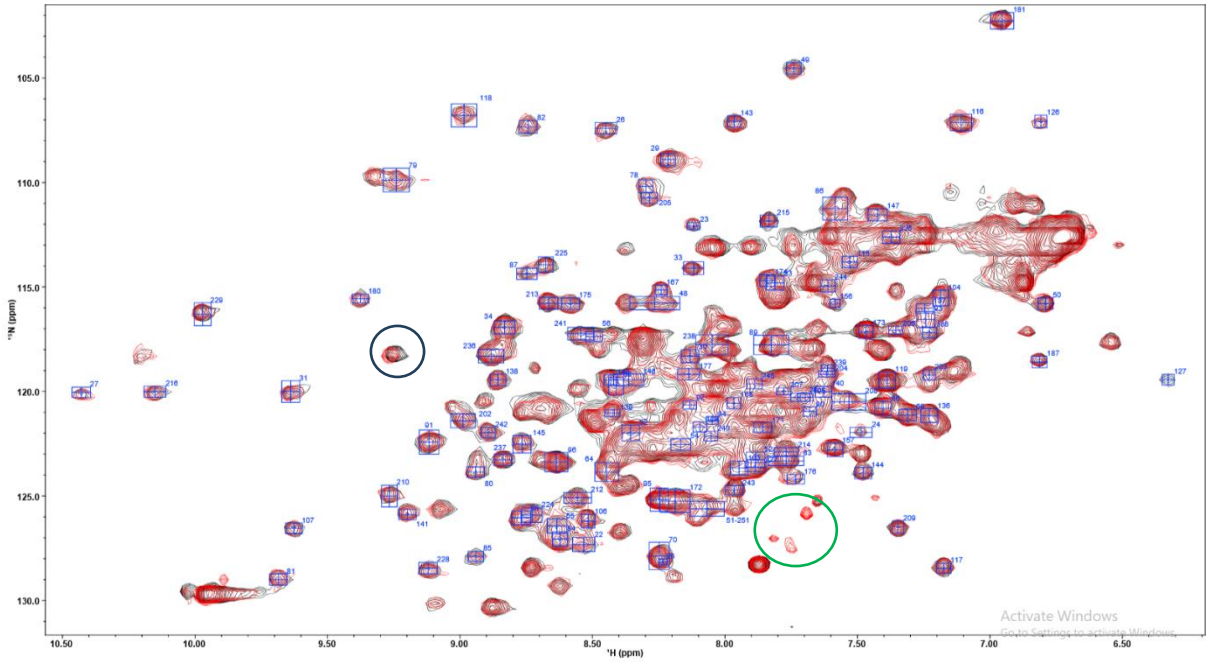

Figure 45 - Overlay of two 2D 1H - 15N HSQC Spectra: One of CLIC4, and one of CLIC4 bound to Truncated GIT1. *Spectra collected at 600 MHz with CLIC4 control sample at 216 µM. Black peaks = CLIC4 Control sample. Red peaks = CLIC4-GIT1 at 130 µM:130 µM (MR 1:1). Appearing peaks upon GIT1 binding circled in green. Shifted peaks that are not assigned are circled in Black. Blue boxes = CLIC4 Assigned residues.*

The overlay shows that the CLIC4-GIT1 Truncated spectra (red peaks) is of much better quality and gives a better perspective on peak shifts that occur due to chemical environment changes as a result of binding events. From the spectra alone, it does not immediately appear that many peaks have

shifted in comparison to the control sample (black peaks). A lot of the red peaks overlapped with the black peaks, and the ones that have shifted belong to residues that are currently not assigned (black circle). Some peaks have appeared in response to the GIT1 Truncated protein addition, noted with the green circle. Hence, the chemical environment around the GIT1 Truncated protein has changed, suggesting some element of interaction between CLIC4 and GIT1.

To further investigate the extent of any potential binding interactions between CLIC4 and GIT1, chemical shift perturbations between the control and titrated spectra were analysed for statistically significant peak shifts and residue chemical environment changes.

5.7.2 Intensity Shift Perturbations of assigned CLIC4 Peaks upon binding to GIT1 – Full-length

Due to the poor quality of the CLIC4-GIT1 Full-length spectra, the intensity differences between the control sample and the CLIC4-GIT1 Full-length binding spectra were used to detect significant residue environment changes. This is reflected in **Figure 46** below.

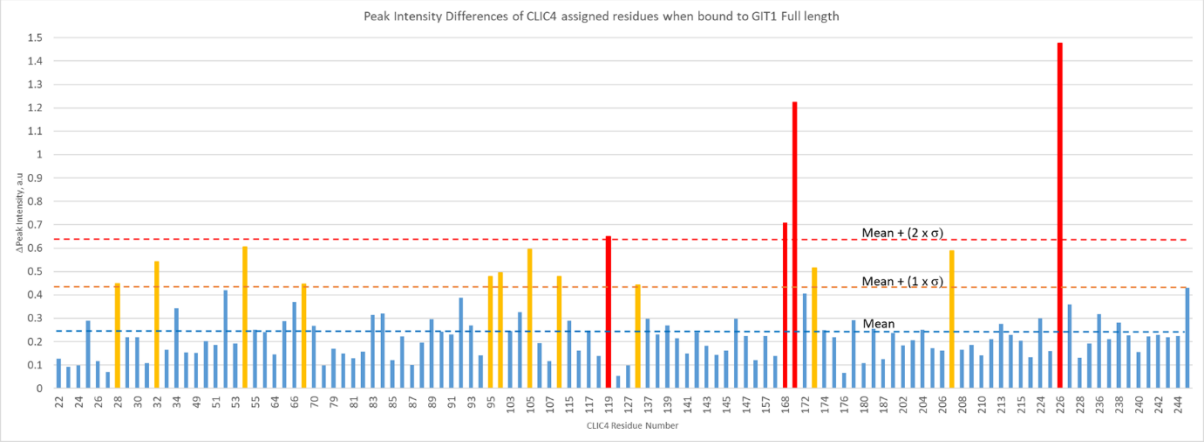

Figure 46 – Peak Intensity Differences of CLIC4 assigned residues, upon Full-length GIT1 binding*. Residues that have a peak intensity difference value around the mean, and are not statistically significant, are highlighted in blue. Those that are statistically significant by possessing a difference of more than one standard deviation (σ) from the mean are in yellow. Peaks that have differences more than two standard deviations from the mean are highlighted in red. Boundaries of mean, mean + 1 σ and mean + 2 σ are colour coded identically to the bars they represent.*

Residues 28, 32, 54, 69, 95, 96, 105, 108, 136, 173 and 207 possessed intensity difference values that were calculated to be more than one standard deviation away from the mean, proving statistical significance in their intensity difference between control and GIT1 Full-length binding. This is indicated

in **Figure 46** with these residues having orange bars. Residues 119, 168, 171 and 226 experienced an intensity difference that was calculated to be two or more standard deviations away from the mean (shown as red bars). These residues are of key importance, as they are more likely to be in direct contact with GIT1 through potential surface interactions.

Similar to the chemical shifts seen via digoxin binding (see section 5.4.2 Chemical shift Perturbations of shifted assigned CLIC4 peaks upon Digoxin Binding), the GIT1 Full-length intensity differences of key residues were mapped onto a Pymol model to analyse interaction areas of CLIC4 with GIT1.

5.7.3 Chemical Shift Perturbations of assigned CLIC4 Peaks upon binding to GIT1 – Truncated

The CLIC4:GIT1 Truncated spectra shown in **Figure 45** did show peak shifts and appearing peaks as a result of binding events occurring. Therefore, chemical shift perturbations for the CLIC4:GIT1 Truncated spectra were calculated and statistically evaluated as shown in **Figure 47** below.

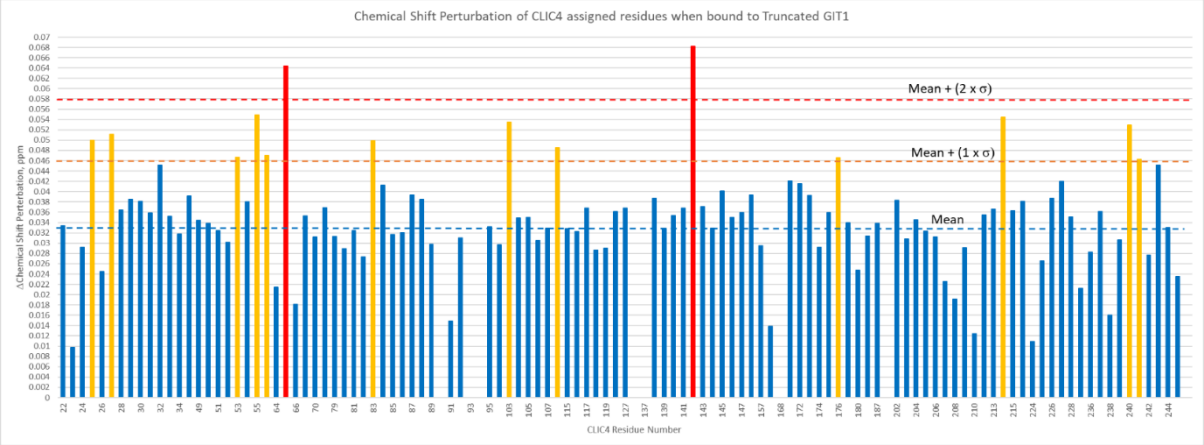

Figure 47 - Chemical Shift Perturbations (CSPs) of CLIC4 assigned residues, upon Truncated GIT1 binding. *Residues that have a chemical shift perturbation value around the mean, and are not statistically significant, are highlighted in blue. Those that are statistically significant by shifting more than one standard deviation (σ) from the mean are in yellow. Peaks that have shifted by more than two standard deviations from the mean are highlighted in red. Boundaries of mean, mean + 1 σ and mean + 2 σ are colour coded identically to the bars they represent.*

Residues 25, 27, 53, 55, 56, 83, 103, 108, 176, 214, 240 and 241 have been calculated to have a chemical shift perturbation value of more than one standard deviation away from the mean indicating significant binding (orange bars). This is in contrast to the residues revealed to be shifted significantly in the CLIC4:GIT1 Full-length spectra, suggesting the truncated version could interact with more

residues and hence tighter binding. Two residues, 65 and 142, have perturbation values of more than two standard deviations away from the mean. Thus, these residues may reveal more about the nature of the binding between CLIC4 and the Arf-GAP domain of GIT1.

The different residues shown to have shifted between the GIT1 spectra, when mapped on Pymol, reveal how the interactions may change due to the variation of the GIT1 domains interacting with CLIC4 and their relative size (i.e. the Arf-GAP domain will bind with fewer CLIC4 residues affected than the Full-length GIT1 due to less space required for binding).

5.7.4 CLIC4:GIT1 Binding visualised via Pymol

5.7.4.1 GIT1 Full-length

Taking the peak intensity differences from the CLIC4:GIT1 Full-length, particularly the significant residues outlined in **Figure 48**, a visual representation of the binding interactions on CLIC4 was created in Pymol. Assigned CLIC4 residues are highlighted in green, unassigned residues are coloured in grey.

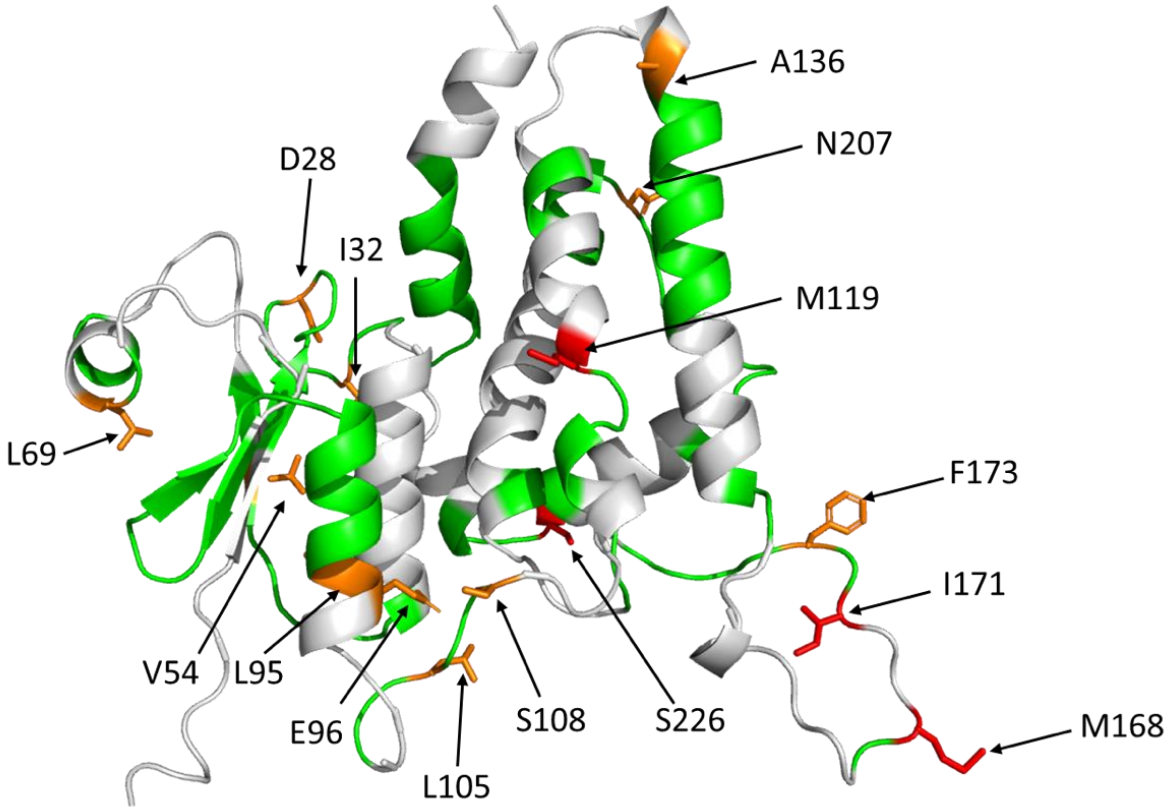

Figure 48 – Pymol model of CLIC4, with assigned residues and peak intensity difference significant residues from CLIC4-GIT1 Full length 2D HSQC NMR*. Green = assigned residues. Grey = unassigned residues. Intensity differences that statistically significant are coloured via the same scheme as the CLIC4:GIT1 Full length CSP graph. Residues of significant peak intensity differences have been highlighted with their position in the CLIC4 sequence.*

As shown in **Figure 48**, significantly shifted residues that have values more than one standard deviation away from the mean (orange residues) and those with more than two standard deviations away from the mean are distributed across the entire CLIC4 protein. Residues such as D28, V54, L69, and L95 are situated in the region where Digoxin is suspected to bind (see section 5.4.3.2 Predicted Digoxin Binding site). However, some of the more significant residues such as M168 and I171 are located in the "flexible foot loop" region which suggests this characteristic region of CLIC proteins may be key for interactions with GIT1. Therefore, it seems the binding of GIT1 Ful-length to CLIC4 induces intensity differences, and hence chemical environment changes, across the entire protein.

Due to the interactions of GIT1 Full-length to CLIC4 not being localised to specific regions, the extent of the Arf-GAP domain specifically binding to CLIC4 must be mapped onto a similar Pymol model to gauge region-specific interactions.

5.7.4.2 GIT1 Truncated

The interactions of CLIC4 to the Arf-GAP domain of GIT1 specifically were observed via the NMR 2D ^{1}H - ^{15}N HSQC spectra and chemical shift perturbations of CLIC4 were modelled on Pymol as shown in **Figure 49** Assigned CLIC4 residues are highlighted in green, unassigned residues are coloured in grey.

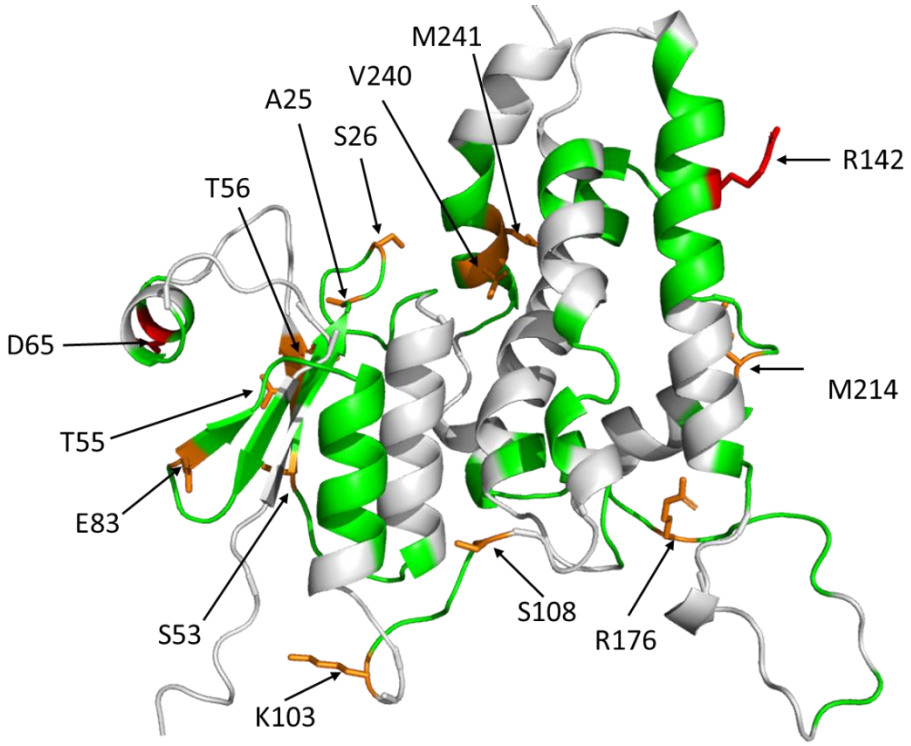

Figure 49 - Pymol model of CLIC4, with assigned residues and CSPs of significant residues from CLIC4-GIT1 Truncated 2D HSQC NMR. *Green = assigned residues. Grey = unassigned residues. Significantly shifted residues are coloured via the same scheme as the CLIC4:GIT1 Truncated CSP graph. Residues of significant shift have been highlighted with their position in the CLIC4 sequence.*

The residues statistically determined to possess a significant change in their chemical environment upon the Arf-GAP domain binding are highlighted orange (more than 1 standard deviation away from the mean) and red (more than 2 standard deviations away from the mean). There is a similarity between the GIT1 Truncated and GIT1 Full-length distribution of significant residues, however, GIT1 truncated seems to have a greater number of significant residues situated around the predicted digoxin site. Residues D65 and T56 are the same residues shifted in the CLIC4:Digoxin Pymol model, indicating the Arf-GAP domain may bind with more interactions involved at this region. However,

there are some significant shifts away from this binding site, such as R142, which could be involved in structural remodelling once the Arf-GAP domain has bound. R176 is a border residue of the “flexible foot region”, which contained residues that were implied to be involved in binding with the GIT1 Full-length, so there is evidence to suggest that this “flexible foot” could aid binding.

Overall, the shifts seen in **Figure 48** and **Figure 49** give an insight into the binding and interaction locations of CLIC4 to GIT1 but still requires further experiments and analysis to reliably confirm specific residue involvement and binding kinetics.

6. Discussion

CLIC4 is a metamorphic chloride ion channel protein that has been hypothesised to be involved with endothelial remodelling in the pathogenesis of pulmonary arterial hypertension (93,104,110). CLIC4 may be a key therapeutic target, and as such a potential ligand (Digoxin) may prevent the progression of PAH. In addition, CLIC4 is suspected to play a role in the Arf6 pathway via its supposed interactions with GIT1 (110,111). Here, this thesis investigates the interactions of CLIC4 with Digoxin and GIT1 by analysis of interacting residues, pinpointed via CSPs determined via CLIC4 assignment, between protein-ligand and protein-protein in solution.

6.1 Assignment of CLIC4 and Secondary Structure Predictions

Assigning the Cα, Cβ and C=O peaks to each residue of CLIC4 was crucial for investigating influences on CLIC4's structural dynamics when interacting with other molecules. **Figure 28** (see section: 5.2.5 Pymol representation of Assigned Residues) displays the coverage of assigned residues vs. those that are not assigned. The results of the assignment of CLIC4 led to 117 of all CLIC4 residues being assigned, which is 46% of the total amount of residues present in the sequence of CLIC4. Although this is just under half of the protein, a significant amount of residues involved in key secondary structure elements such as the β-strands and α-helices of the N-terminal thioredoxin fold (95,96). In terms of the C-Terminus, identified residues include areas of the "flexible foot loop" region which, as the literature would suggest, potentially binds inhibitors designed for CLICs (98). The assignments presented in this thesis therefore aid the discovery and design of CLIC-specific inhibitors, as this "flexible foot loop" region is CLIC-specific (95). This also provides some crucial information when investigating any CLIC4 binding interactions, be it inhibitors or protein-protein contact, to accurately determine residue interactions and whole protein dynamics.

Processing the assigned residues via TALOS to compare secondary structure elements based on NMR assigned residues vs. sequence from PDB yielded promising conclusions. 43% of CLIC4 residues (PDB) are α-helices, but TALOS predicted 44% of CLIC4 residues (NMR assignment predictions + sequence

predictions) to be α-helices. β-Strands predicted by TALOS constitute 8% of CLIC4, similar to the 10% displayed in the PDB known structure. Therefore, TALOS predicted secondary structure elements that were overall quite akin in both amount and location within the protein in comparison to the PDB file. Due to TALOS being supplied with assignment data, the results of the CLIC4 assignment can be viewed successfully, as the residues assigned contribute to correct structure predictions. If TALOS had more assigned residues to work with, resultant structural predictions would become more aligned with the reality of the PDB crystal structure.

6.2 CLIC4-Digoxin Binding and Interaction Sites

The proposed CLIC4 binding site, based on CSPs and both manual and HADDOCK Digoxin interaction alignments with CLIC4, indicated a binding site around the N-terminal thioredoxin domain (95,96). When relating to the literature, this site was predicted to be a high-interaction site for potential drug compounds and was termed "Site 1" from residues M1-K90 (98). An additional site was located around the "flexible foot loop region" (see section 2.1.7.1 CLIC 4: Overview, Structure and Function, **Figure 9**) with border residues P158-R176 (98). **Figure 50**, taken from the paper *"Structure-based discovery and in vitro validation of inhibitors of chloride intracellular channel 4 protein"* shows these two potential interaction sites that *Olotu F, et al.* identified, along with a third site (Site 3) (98). Digoxin was suggested to predominantly bind to Site 2, but this thesis shows that based on CSPs and computational docking predictions, Digoxin may bind to Site 1 instead. Results show one residue in particular, F52, is shown to be significant in the binding of Digoxin which correlates to the literature on this residue being involved in hydrophobic interactions experienced at Site 1 (98). Literature did predict Site 1 to bind the non-selective CLIC inhibitor IAA94, so Digoxin and IAA94 may bind at the same site (92,98).

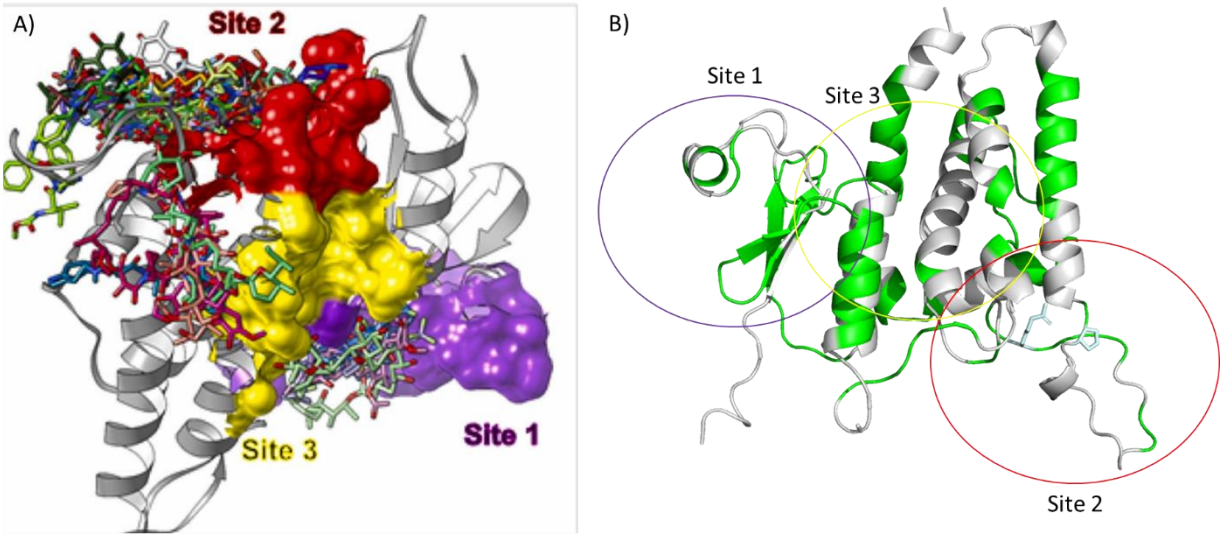

Figure 50 - Predicted CLIC4 Inhibitor binding sites based on the literature, compared to Pymol representation with CLIC4 NMR-assigned residues coloured. *A) Predicted CLIC4 inhibitor binding sites; Site 1 (Purple), Site 2 (Red), Site 3 (Yellow). Adapted from: Olotu, F et al. (2023). B) Th same sites given in panel A highlighted on the CLIC4 Alphafold model, with NMR-assigned residues highlighted. Green = assigned residues. Grey = unassigned residues.*

The binding of Digoxin to CLIC4 does suggest further analysis of the "flexible foot loop region" as residues located in this region did experience significant CSPs. The change in the chemical environment responsible for the significant CSPs could be due to conformational change due to this region's structure (a loop). Despite this, this region would be recommended to study further binding site potential with other inhibitors, as the "flexible foot loop" is responsible for translocation of the cell and progression of disease via CLIC4 involvement in signalling cascades such as RhoA and TGF-β pathways (99,110,111).

6.3 CLIC4-GIT1 Binding and Interaction Sites

The Alphafold prediction of CLIC4 binding to GIT1 was initially used to base MST experiments using CLIC4 and GIT1 Full-length / Truncated. The MST data obtained on both the Full-length and Arf-GAP domain of GIT1 resulted in a mean K_D value of 6.0µM and 6.9 µM for each protein version respectively. These low micromolar values are comparable to the K_D values of ArfGAP-Arf as explained in the literature (110,130). Thus, The NMR binding assay then shows significant intensity differences and CSPs for Full-length GIT1 and Truncated GIT1 respectively, leading to the mapping of residues

suggested to be involved in CLIC4-GIT1 binding. In both GIT1 Full-length and Truncated versions of the protein, some similarities in the distribution of the shifted residues are seen, but the full-length protein has more significantly shifted residues that are situated in the "flexible foot loop" region. The absence of significantly shifted residues on the model of CLIC4 interacting with the truncated version of GIT1 could be due to the absence of one of the GIT1 domains that could be responsible for the stabilisation of the interaction. For example, the Paxillin and TGF-β interacting domain on GIT1 (see section 2.1.10 GTPase Activating Protein (GIT) 1 and CLIC4, **Figure 11**) could interact with the "flexible foot loop" region of which the latter could stabilise binding. Combined with suggestions in the literature that CLIC4 can bind to GIT1 in the same way as GIT1 to Arf6, the findings presented here suggest strong evidence for CLIC4-GIT1 binding being involved in the proposed CLIC4:Arf6 pathway (110,111). Although the binding needs to be investigated further, the initial indications of the CLIC4:Arf6 Pathway via interactions detailed in this thesis could somewhat elucidate the role of CLIC4 in the signalling cascades that propagate vascular remodelling leading to poor PAH prognosis (99,107,108,110,111).

7. Limitations and Future Work

Although this thesis has successfully predicted both CLIC4-Digoxin Binding and CLIC4-GIT1 binding, to develop an insight into CLIC4 as being a therapeutic target in the prevention of the pathogenesis of PAH, there were several challenges and points of improvement that could be rectified. This would enable a more accurate prediction of CLIC4 interactions and would provide increased precision on the effects of ligand/protein interactions on protein dynamics

The assignment of CLIC4 featured in this thesis was limited to 47% of CLIC4 residues being assigned. In part, this was down to regions of the 2D HSQC and 3D spectra containing lower-resolution peaks with overlapping areas. To remedy this, future improvements would see a triple-labelled CLIC4 sample run at higher field strengths for longer periods. This would obtain more scans and increments necessary for sharp individual peaks, allowing enhanced assignment ability. In addition, TALOS could be run with more NMR-provided CSPs leading to a more accurate comparison of PDB CLIC4 secondary structure to TALOS predictions.

Secondly, the predictions of the Digoxin binding site used CSPs obtained from a control 2D HSQC of CLIC4, against a HSCQ of CLIC4-Digoxin at a MR of 1:1. However, to optimise CSP generation future experiments would utilise multiple titration points of increased inhibitor concentration up to saturation of a binding site is desired. Hence, exchange rates accuracy is increased and CSPs can be more precise in the tracking of chemical environment change and residue shift.

Finally, the GIT1 Full-length concentration was not at an ideal level for suitable CSP calculations using a 2D HSQC. The spectrum was very weak, hence the use of intensity differences. In future experiments, the GIT1-Full length expression protocol would be optimised to ensure high GIT1 full-length concentrations of which viable CSPs would be obtained for increased accuracy of CLIC4-GIT1 interactions. Additionally, both GIT1 protein types would be isotopically labelled for triple-resonance assignment. By assigning the protein, protein-protein interactions would be identified on a residue

scale, aiding potential inhibition, and preventing CLIC4/Arf6 pathway propagation and PAH progression.

8. Conclusion

In this thesis, the membrane protein CLIC4 has been partially assigned using 2D and 3D NMR spectra in order to identify residues with the capacity to undergo chemical shift upon protein-ligand and protein-protein interactions. CLIC4 residues of significant chemical shift perturbation as a result of digoxin binding were modelled to identify a potential binding site and structural conformational changes. This was re-enforced by computational HADDOCK protein-ligand docking predictions

The protein GIT1 in its entirety, and just the Arf-GAP domain, was expressed and tested for CLIC4 binding interactions, with binding affinity also calculated via MST. Similar to CLIC4-Digoxin, residues of significant chemical shift perturbations were modelled to understand interaction sites and residue involvement.

In conclusion, this thesis provides an insight into CLIC4's involvement in the progression of PAH, via its upregulation leading to the progression of said disease. On a molecular level, this thesis provides some identification of inhibitor binding sites on CLIC4 to aid future therapeutic strategies combatting CLIC dysregulation and downstream negative effects on PAH prognosis in patients.

9. References

1. Sysol JR, Machado RF, F Machado CR. Classification and pathophysiology of pulmonary hypertension. Continuing Cardiology Education. 2018;4(1).

2. Pulmonary Hypertension - St Vincent's Heart Health [Internet]. [cited 2023 Aug 2]. Available from: https://www.svhhearthealth.com.au/conditions/pulmonary-hypertension

3. Widrich J, Shetty M. Physiology, Pulmonary Vascular Resistance. StatPearls [Internet]. 2022 Aug 15 [cited 2023 Aug 3]; Available from: https://www.ncbi.nlm.nih.gov/books/NBK554380/

4. Widrich J, Shetty M. Physiology, Pulmonary Vascular Resistance. StatPearls [Internet]. 2022 Aug 15 [cited 2023 Aug 3]; Available from: https://www.ncbi.nlm.nih.gov/books/NBK554380/

5. Mandras SA, Mehta HS, Vaidya A. Pulmonary Hypertension: A Brief Guide for Clinicians. Mayo Clin Proc. 2020 Sep 1;95(9):1978–88.

6. Types of Pulmonary Hypertension: The WHO Groups - Pulmonary Hypertension Association [Internet]. [cited 2023 Aug 4]. Available from: https://phassociation.org/types-pulmonary-hypertension-groups/

7. Pahal P, Sharma S. Idiopathic Pulmonary Artery Hypertension. Encyclopedia of Trauma Care [Internet]. 2023 Apr 10 [cited 2023 Aug 3];799–799. Available from: https://www.ncbi.nlm.nih.gov/books/NBK482251/

8. Mclaughlin V V, Mcgoon MD. Pulmonary Arterial Hypertension. 2006 [cited 2023 Aug 3]; Available from: http://www.circulationaha.org

9. Lindegaard Pedersen M, Krüger M, Grimm D, Infanger M, Wehland M. The prostacyclin analogue treprostinil in the treatment of pulmonary arterial hypertension. Basic Clin Pharmacol Toxicol [Internet]. 2020 Jan 1 [cited 2023 Aug 10];126(1):32–42. Available from: https://onlinelibrary.wiley.com/doi/full/10.1111/bcpt.13305

10. Ibrahim B. Right Ventricular Failure. E-Journal of Cardiology Practice. 2016 Dec 12;14.

11. Stewart C. Statista. 2022 [cited 2023 Aug 3]. Pulmonary hypertension: patients in the UK 2004-2021. Available from: https://www.statista.com/statistics/571912/patients-with-pulmonary-hypertension-in-the-united-kingdom-uk/

12. Casano HAM, Anjum F. Six-Minute Walk Test. Kinesitherapie [Internet]. 2023 Apr 27 [cited 2023 Aug 3];7(68–69):68. Available from: https://www.ncbi.nlm.nih.gov/books/NBK576420/

13. Pulmonary Arterial Hypertension Symptoms and Diagnosis | American Lung Association [Internet]. [cited 2023 Aug 9]. Available from: https://www.lung.org/lung-health-diseases/lung-disease-lookup/pulmonary-arterial-hypertension/symptoms-diagnosis

14. Hoeper MM, Ghofrani HA, Grünig E, Klose H, Olschewski H, Rosenkranz S. Pulmonary Hypertension. Dtsch Arztebl Int [Internet]. 2017 Feb 3 [cited 2023 Aug 9];114(5):73. Available from: /pmc/articles/PMC5331483/

15. Thenappan T, Ormiston ML, Ryan JJ, Archer SL. Pulmonary arterial hypertension: pathogenesis and clinical management. BMJ [Internet]. 2018 Mar 14 [cited 2023 Aug 4];360. Available from: https://www.bmj.com/content/360/bmj.j5492

16. Evans JDW, Girerd B, Montani D, Wang XJ, Galiè N, Austin ED, et al. BMPR2 mutations and survival in pulmonary arterial hypertension: an individual participant data meta-analysis. Lancet Respir Med [Internet]. 2016 Feb 1 [cited 2023 Aug 4];4(2):129. Available from: /pmc/articles/PMC4737700/

17. Lan NSH, Massam BD, Kulkarni SS, Lang CC. Pulmonary Arterial Hypertension: Pathophysiology and Treatment. Diseases [Internet]. 2018 May 16 [cited 2023 Aug 18];6(2):38. Available from: /pmc/articles/PMC6023499/

18. Orriols M, Gomez-Puerto MC, ten Dijke P. BMP type II receptor as a therapeutic target in pulmonary arterial hypertension. Cellular and Molecular Life Sciences [Internet]. 2017 Aug 1 [cited 2023 Aug 29];74(16):2979. Available from: /pmc/articles/PMC5501910/

19. Simonneau G, Montani D, Celermajer DS, Denton CP, Gatzoulis MA, Krowka M, et al. Haemodynamic definitions and updated clinical classification of pulmonary hypertension. European Respiratory Journal [Internet]. 2019 Jan 1 [cited 2023 Aug 7];53(1). Available from: https://erj.ersjournals.com/content/53/1/1801913

20. Montani D, Girerd B. Orphanet. 2015 [cited 2023 Aug 4]. Orphanet: Drug or toxin induced pulmonary arterial hypertension. Available from: https://www.orpha.net/consor/cgi-bin/OC_Exp.php?Lng=GB&Expert=275786

21. Orcholski ME, Yuan K, Rajasingh C, Tsai H, Shamskhou EA, Dhillon NK, et al. Drug-induced pulmonary arterial hypertension: a primer for clinicians and scientists. Am J Physiol Lung Cell Mol Physiol [Internet]. 2018 Jun 6 [cited 2023 Aug 4];314(6):L967. Available from: /pmc/articles/PMC6032070/

22. Ucien L, Benhaim A, Oride OM, Rançois F, Renot B, Tuart S, et al. APPETITE-SUPPRESSANT DRUGS AND THE RISK OF PRIMARY PULMONARY HYPERTENSION. The New England Journal o f Medicine © Copyr ight. 1996;335.

23. Rich S, Rubin L, Walker AM, Schneeweiss S, Abenhaim L. Anorexigens and Pulmonary Hypertension in the United States. Chest. 2000 Mar 1;117(3):870–4.

24. Souza R, Humbert M, Sztrymf B, Jaïs X, Yaïci A, Le Pavec J, et al. Pulmonary arterial hypertension associated with fenfluramine exposure: report of 109 cases. European Respiratory Journal [Internet]. 2008 Feb 1 [cited 2023 Aug 4];31(2):343–8. Available from: https://erj.ersjournals.com/content/31/2/343

25. Schiess R, Senn O, Fischler M, Huber LC, Vatandaslar S, Speich R, et al. Tobacco Smoke: A Risk Factor for Pulmonary Arterial Hypertension?: A Case-Control Study. Chest. 2010 Nov 1;138(5):1086–92.

26. NORD, Hemnes A. Rare Diseases. 2021 [cited 2023 Aug 7]. Pulmonary Arterial Hypertension - Symptoms, Causes, Treatment | NORD. Available from: https://rarediseases.org/rare-diseases/pulmonary-arterial-hypertension/

27. Mayo Clinic. Scleroderma - Symptoms and causes - Mayo Clinic [Internet]. [cited 2023 Aug 7]. Available from: https://www.mayoclinic.org/diseases-conditions/scleroderma/symptoms-causes/syc-20351952

28. Schneider LK, Ali YS, Agnew JD. Scleroderma-Associated Pulmonary Arterial Hypertension: Early Detection for Better Outcomes. StatPearls [Internet]. 2023 May 1 [cited 2023 Aug 7]; Available from: https://www.ncbi.nlm.nih.gov/books/NBK576387/

29. Moglad EHO, Ahmed DAO, Awad AL-Kareem SMM, Elgoraish AG, Ali HTO, Altayb HN. Prevalence of human immunodeficiency virus among pulmonary tuberculosis patients: A cross-sectional study. Microbiol Immunol [Internet]. 2020 Dec 1 [cited 2023 Aug 7];64(12):810–4. Available from: https://onlinelibrary.wiley.com/doi/full/10.1111/1348-0421.12856

30. Almodovar S, Hsue PY, Morelli J, Huang L, Flores SC. Pathogenesis of HIV-Associated Pulmonary Hypertension: Potential Role of HIV-1 nef. Proc Am Thorac Soc [Internet]. 2011 Jun 6 [cited 2023 Aug 7];8(3):308. Available from: /pmc/articles/PMC3132790/

31. Mehta NJ, Khan IA, Mehta RN, Sepkowitz DA. HIV-Related Pulmonary Hypertension: Analytic Review of 131 Cases. Chest. 2000 Oct 1;118(4):1133–41.

32. Basyal B, Jarrett H, Barnett CF. Pulmonary Hypertension in HIV. Canadian Journal of Cardiology. 2019 Mar 1;35(3):288–98.

33. Hirakawa K, Aoki T, Tsuji A, Ogo T. Pulmonary arterial hypertension sensitive to calcium channel blocker, but not advanced pulmonary hypertension treatment:

a case report. Eur Heart J Case Rep [Internet]. 2022 Sep 5 [cited 2023 Aug 7];6(9):1–4. Available from: https://dx.doi.org/10.1093/ehjcr/ytac351

34. Rich S, Kaufmann E, Levy PS. The Effect of High Doses of Calcium-Channel Blockers on Survival in Primary Pulmonary Hypertension. http://dx.doi.org/101056/NEJM199207093270203 [Internet]. 2010 Jan 19 [cited 2023 Aug 7];327(2):76–81. Available from: https://www.nejm.org/doi/full/10.1056/nejm199207093270203

35. Sayin T, Erol C. Identify and treat pulmonary arterial hypertension. E-Journal of Cardiology Practice. 2015 Jan 20;13(10).

36. Medarov BI, Judson MA. The role of calcium channel blockers for the treatment of pulmonary arterial hypertension: How much do we actually know and how could they be positioned today? Respir Med. 2015 May 1;109(5):557–64.

37. Piloto B, Fernandes CJCDS, Jardim C, Castro M, Alves-Jr JL, Souza R. Loss of response to calcium channel blockers after long-term follow-up treatment in patients with idiopathic pulmonary arterial hypertension. Jornal Brasileiro de Pneumologia. 2023;49(3).

38. Nandula PS, Shah SD. Persistent Pulmonary Hypertension of the Newborn. StatPearls [Internet]. 2022 Aug 5 [cited 2023 Aug 8]; Available from: https://www.ncbi.nlm.nih.gov/books/NBK585100/

39. Donn SM. Persistent pulmonary hypertension of the newborn: Historical perspectives. Semin Fetal Neonatal Med. 2022 Aug 1;27(4):101323.

40. Martinho S, Adão R, Leite-Moreira AF, Brás-Silva C. Persistent Pulmonary Hypertension of the Newborn: Pathophysiological Mechanisms and Novel Therapeutic Approaches. Front Pediatr [Internet]. 2020 Jul 24 [cited 2023 Aug 8];8:342. Available from: /pmc/articles/PMC7396717/

41. Gibbs JSR. Making a diagnosis in PAH. European Respiratory Review . 2007;16(102):8–12.

42. Cleveland Clinic. Transthoracic Echocardiogram (TTE) [Internet]. 2022 [cited 2023 Aug 8]. Available from: https://my.clevelandclinic.org/health/diagnostics/13477-echocardiogram-transthoracic-tte

43. Pulmonary Hypertension Associatiion. Diagnosis - Pulmonary Hypertension [Internet]. 2020 [cited 2023 Aug 9]. Available from: https://phassociation.org/patients/diagnosis/

44. Correale M, Ferraretti A, Monaco I, Grazioli D, Di Biase M, Brunetti ND. Endothelin-receptor antagonists in the management of pulmonary arterial hypertension: where do we stand? Vasc Health Risk Manag [Internet]. 2018 [cited 2023 Aug 11];14:253. Available from: /pmc/articles/PMC6174907/

45. Shao D, Park JES, Wort SJ. The role of endothelin-1 in the pathogenesis of pulmonary arterial hypertension. Pharmacol Res. 2011 Jun 1;63(6):504–11.

46. Dupuis J. Endothelin-receptor antagonists in pulmonary hypertension. Lancet [Internet]. 2001 Oct 6 [cited 2023 Aug 11];358(9288):1113–4. Available from: http://www.thelancet.com/article/S0140673601062985/fulltext

47. Opitz CF, Ewert R. Dual ETA/ETB vs. selective ETA endothelin receptor antagonism in patients with pulmonary hypertension. Eur J Clin Invest [Internet]. 2006 Sep [cited 2023 Aug 11];36(SUPPL. 3):1–9. Available from: https://onlinelibrary.wiley.com/doi/full/10.1111/j.1365-2362.2006.01691.x

48. Sitbon O, Morrell NW. Pathways in pulmonary arterial hypertension: the future is here. European Respiratory Review [Internet]. 2012 Dec 1 [cited 2023 Aug 18];21(126):321–7. Available from: https://err.ersjournals.com/content/21/126/321

49. Boniface S, Reynaud-Gaubert M. Endothelin receptor antagonists – their role in pulmonary medicine. Rev Mal Respir. 2011 Oct 1;28(8):e94–107.

50. Houde M, Desbiens L, D'Orléans-Juste P. Endothelin-1: Biosynthesis, Signaling and Vasoreactivity. Adv Pharmacol. 2016;77:143–75.

51. Iglarz M, Steiner P, Wanner D, Rey M, Hess P, Clozel M. Vascular Effects of Endothelin Receptor Antagonists Depends on Their Selectivity for ETA Versus ETB Receptors and on the Functionality of Endothelial ETB Receptors. J Cardiovasc Pharmacol [Internet]. 2015 Oct 1 [cited 2023 Aug 11];66(4):332. Available from: /pmc/articles/PMC4598072/

52. Tonelli AR, Haserodt S, Aytekin M, Dweik RA. Nitric Oxide Deficiency in Pulmonary Hypertension: Pathobiology and Implications for Therapy. Pulm Circ [Internet]. 2013 Jan 1 [cited 2023 Aug 18];3(1):20–30. Available from: https://onlinelibrary.wiley.com/doi/full/10.4103/2045-8932.109911

53. Montani D, Chaumais MC, Savale L, Natali D, Price LC, Jaïs X, et al. Phosphodiesterase type 5 inhibitors in pulmonary arterial hypertension. Adv Ther [Internet]. 2009 Sep 19 [cited 2023 Aug 12];26(9):813–25. Available from: https://link.springer.com/article/10.1007/s12325-009-0064-z

54. Lan NSH, Massam BD, Kulkarni SS, Lang CC. Pulmonary Arterial Hypertension: Pathophysiology and Treatment. Diseases [Internet]. 2018 May 16 [cited 2023 Aug 18];6(2):38. Available from: /pmc/articles/PMC6023499/

55. Ricciotti E, Fitzgerald GA. Prostaglandins and Inflammation. Arterioscler Thromb Vasc Biol [Internet]. 2011 May [cited 2023 Aug 19];31(5):986. Available from: /pmc/articles/PMC3081099/

56. Olschewski H, Rose F, Schermuly R, Ghofrani HA, Enke B, Olschewski A, et al. Prostacyclin and its analogues in the treatment of pulmonary hypertension. Pharmacol Ther. 2004 May 1;102(2):139–53.

57. Sommer N, Ghofrani HA, Pak O, Bonnet S, Provencher S, Sitbon O, et al. Current and future treatments of pulmonary arterial hypertension. Br J Pharmacol [Internet]. 2021 Jan 1 [cited 2023 Aug 10];178(1):6–30. Available from: https://onlinelibrary.wiley.com/doi/full/10.1111/bph.15016

58. Fuso L, Baldi F, Di Perna A. Therapeutic Strategies in Pulmonary Hypertension. Front Pharmacol [Internet]. 2011 [cited 2023 Aug 10];2. Available from: /pmc/articles/PMC3108478/

59. Mayo Clinic. Pulmonary hypertension - Diagnosis and treatment - Mayo Clinic [Internet]. [cited 2023 Aug 10]. Available from:

https://www.mayoclinic.org/diseases-conditions/pulmonary-hypertension/diagnosis-treatment/drc-20350702

60. Hansen L, Burks M, Kingman M, Stewart T. Volume Management in Pulmonary Arterial Hypertension Patients: An Expert Pulmonary Hypertension Clinician Perspective. Pulm Ther [Internet]. 2018 Jun 1 [cited 2023 Aug 10];4(1):13. Available from: /pmc/articles/PMC6966996/

61. Pulmonary Arterial Hypertension Diuretics - Rare Disease Advisor [Internet]. [cited 2023 Aug 10]. Available from: https://www.rarediseaseadvisor.com/therapies/pulmonary-arterial-hypertension-diuretics/

62. Stickel S, Gin-Sing W, Wagenaar M, Gibbs JSR. The practical management of fluid retention in adults with right heart failure due to pulmonary arterial hypertension. European Heart Journal, Supplement. 2019 Dec 1;21:K46–53.

63. Green S, Stuart D. Oxygen and pulmonary arterial hypertension: effects, mechanisms, and therapeutic benefits. Eur J Prev Cardiol [Internet]. 2021 Jan 1 [cited 2023 Aug 10];28(1):127–36. Available from: https://pubmed.ncbi.nlm.nih.gov/33623970/

64. Zare P, Heller D. Treprostinil. Reactions Weekly [Internet]. 2023 May 8 [cited 2023 Aug 10];NA;(1418):44. Available from: https://www.ncbi.nlm.nih.gov/books/NBK545152/

65. McDonough A, Matura LA. Treatment update: pulmonary arterial hypertension. http://dx.doi.org/1012968/bjca20161111536 [Internet]. 2016 Nov 4 [cited 2023

Aug 10];11(11):536–42. Available from: https://www.magonlinelibrary.com/doi/10.12968/bjca.2016.11.11.536

66. Scott LJ. Sitaxentan: In pulmonary arterial hypertension. Drugs [Internet]. 2007 Sep 18 [cited 2023 Aug 11];67(5):761–70. Available from: https://link.springer.com/article/10.2165/00003495-200767050-00007

67. Pulmonary Hypertension Association. Ambrisentan - Pulmonary Hypertension Association [Internet]. 2023 [cited 2023 Aug 15]. Available from: https://phassociation.org/patients/treatments/ambrisentan/

68. Ewis L, Ubin JR, Adesch ABB, Obyn R, Arst JB, Azzareno N, et al. Bosentan Therapy for Pulmonary Arterial Hypertension. https://doi.org/101056/NEJMoa012212 [Internet]. 2002 Mar 21 [cited 2023 Aug 11];346(12):896–903. Available from: https://www.nejm.org/doi/full/10.1056/NEJMoa012212

69. Zhao Q, Guo N, Chen J, Parks D, Tian Z. Comparative assessment of efficacy and safety of ambrisentan and bosentan in patients with pulmonary arterial hypertension: A meta-analysis. J Clin Pharm Ther [Internet]. 2022 Feb 1 [cited 2023 Aug 11];47(2):146–56. Available from: https://onlinelibrary.wiley.com/doi/full/10.1111/jcpt.13481

70. Cruz-Burgos M, Losada-Garcia A, Cruz-Hernández CD, Cortés-Ramírez SA, Camacho-Arroyo I, Gonzalez-Covarrubias V, et al. New Approaches in Oncology for Repositioning Drugs: The Case of PDE5 Inhibitor Sildenafil. Front Oncol. 2021 Feb 26;11:627229.

71. Tadalafil (CIALIS) vs Sildenafil (Viagra) – Is One Better? [Internet]. [cited 2023 Aug 14]. Available from: https://www.dcurology.net/2023/06/07/comparing-tadalafil-generic-cialis-and-sildenafil-generic-viagra/

72. Doggrell SA. Comparison of clinical trials with sildenafil, vardenafil and tadalafil in erectile dysfunction. Expert Opin Pharmacother. 2005 Jan;6(1):75–84.

73. Abu Lila AS, Gomaa E, Ghazy FES, Hasan AA. Treatment of pulmonary arterial hypertension by vardenafil-solid dispersion lozenges as a potential alternative drug delivery system. J Drug Deliv Sci Technol. 2020 Feb 1;55:101444.

74. Sandner P. From molecules to patients: Exploring the therapeutic role of soluble guanylate cyclase stimulators. Biol Chem [Internet]. 2018 Jun 27 [cited 2023 Aug 14];399(7):679–90. Available from: https://www.degruyter.com/document/doi/10.1515/hsz-2018-0155/html

75. Stasch JP, Evgenov O V. Soluble Guanylate Cyclase Stimulators in Pulmonary Hypertension. 2013 [cited 2023 Aug 14];279–313. Available from: https://link.springer.com/chapter/10.1007/978-3-642-38664-0_12

76. Khaybullina D, Patel A, Zerilli T. Riociguat (Adempas): a Novel Agent For the Treatment of Pulmonary Arterial Hypertension and Chronic Thromboembolic Pulmonary Hypertension. Pharmacy and Therapeutics [Internet]. 2014 Nov 1 [cited 2023 Aug 14];39(11):749. Available from: /pmc/articles/PMC4218670/

77. Becker-Pelster EM, Hahn MG, Delbeck M, Dietz L, Hüser J, Kopf J, et al. Inhaled mosliciguat (BAY 1237592): targeting pulmonary vasculature via activating apo-sGC. Respir Res [Internet]. 2022 Dec 1 [cited 2023 Aug 14];23(1):1–15. Available

from: https://respiratory-research.biomedcentral.com/articles/10.1186/s12931-022-02189-1

78. Pluchart H, Khouri C, Blaise S, Roustit M, Cracowski JL. Targeting the Prostacyclin Pathway: Beyond Pulmonary Arterial Hypertension. Trends Pharmacol Sci [Internet]. 2017 Jun 1 [cited 2023 Aug 16];38(6):512–23. Available from: http://www.cell.com/article/S0165614717300482/fulltext

79. Lang IM, Gaine SP. Recent advances in targeting the prostacyclin pathway in pulmonary arterial hypertension. European Respiratory Review [Internet]. 2015 Dec 1 [cited 2023 Aug 16];24(138):630–41. Available from: https://err.ersjournals.com/content/24/138/630

80. Humbert M, Lau EMT, Montani D, Jaïs X, Sitbon O, Simonneau G. Advances in Therapeutic Interventions for Patients With Pulmonary Arterial Hypertension. Circulation [Internet]. 2014 Dec 9 [cited 2023 Aug 15];130(24):2189–208. Available from: https://www.ahajournals.org/doi/abs/10.1161/circulationaha.114.006974

81. Krug S, Sablotzki A, Hammerschmidt S, Wirtz H, Seyfarth HJ. Inhaled iloprost for the control of pulmonary hypertension. Vasc Health Risk Manag [Internet]. 2009 [cited 2023 Aug 16];5:465. Available from: /pmc/articles/PMC2686263/

82. Barst RJ, Galie N, Naeije R, Simonneau G, Jeffs R, Arneson C, et al. Long-term outcome in pulmonary arterial hypertension patients treated with subcutaneous treprostinil. European Respiratory Journal. 2006 Dec;28(6):1195–203.

83. Jean-Luc V. Treprostinil in Pulmonary Arterial Hypertension. European Cardiology Review. 2006;0(2):31.

84. Simonneau G, Torbicki A, Hoeper MM, Delcroix M, Karlócai K, Galiège N, et al. Selexipag: An oral, selective prostacyclin receptor agonist for the treatment of pulmonary arterial hypertension. European Respiratory Journal. 2012 Oct 1;40(4):874–80.

85. Gatfield J, Menyhart K, Wanner D, Gnerre C, Monnier L, Morrison K, et al. Selexipag Active Metabolite ACT-333679 Displays Strong Anticontractile and Antiremodeling Effects but Low β-Arrestin Recruitment and Desensitization Potential. J Pharmacol Exp Ther [Internet]. 2017 Jul 1 [cited 2023 Aug 15];362(1):186–99. Available from: https://pubmed.ncbi.nlm.nih.gov/28476928/

86. Duggan ST, Keam SJ, Burness CB. Selexipag: A Review in Pulmonary Arterial Hypertension. American Journal of Cardiovascular Drugs [Internet]. 2017 Feb 1 [cited 2023 Aug 15];17(1):73–80. Available from: https://link.springer.com/article/10.1007/s40256-016-0209-9

87. Sitbon O, Channick R, Chin KM, Frey A, Gaine S, Galiè N, et al. Selexipag for the Treatment of Pulmonary Arterial Hypertension. New England Journal of Medicine [Internet]. 2015 Dec 24 [cited 2023 Aug 15];373(26):2522–33. Available from: https://www.nejm.org/doi/full/10.1056/NEJMoa1503184

88. Guth S, Mayer E, Prüfer D, Wiedenroth CB. Pulmonary endarterectomy: technique and pitfalls. Ann Cardiothorac Surg [Internet]. 2022 [cited 2023 Aug 22];11(2):180. Available from: /pmc/articles/PMC9012198/

89. Al Maluli H, DeStephan CM, Alvarez RJ, Sandoval J. Atrial Septostomy: A Contemporary Review. Clin Cardiol [Internet]. 2015 Jun 1 [cited 2023 Aug 22];38(6):395. Available from: /pmc/articles/PMC6711087/

90. Mahmud E, Patel M, Ang L, Poch D. Advances in balloon pulmonary angioplasty for chronic thromboembolic pulmonary hypertension. Pulm Circ [Internet]. 2021 May 24 [cited 2023 Aug 22];11(2). Available from: https://journals.sagepub.com/doi/full/10.1177/20458940211007385

91. NHS. Pulmonary hypertension - Treatment - NHS [Internet]. [cited 2023 Aug 22]. Available from: https://www.nhs.uk/conditions/pulmonary-hypertension/treatment/

92. Chang KY, Duval S, Badesch DB, Bull TM, Chakinala MM, De Marco T, et al. Mortality in Pulmonary Arterial Hypertension in the Modern Era: Early Insights From the Pulmonary Hypertension Association Registry. J Am Heart Assoc [Internet]. 2022 May 3 [cited 2023 Aug 22];11(9):24969. Available from: https://www.ahajournals.org/doi/abs/10.1161/JAHA.121.024969

93. Abdul-Salam VB, Wharton J, Cupitt J, Berryman M, Edwards RJ, Wilkins MR. Proteomic analysis of lung tissues from patients with pulmonary arterial hypertension. Circulation [Internet]. 2010 Nov 16 [cited 2023 Aug

22];122(20):2058–67. Available from: https://www.ahajournals.org/doi/abs/10.1161/CIRCULATIONAHA.110.972745

94. Wojciak-Stothard B, Abdul-Salam VB, Lao KH, Tsang H, Irwin DC, Lisk C, et al. Aberrant chloride intracellular channel 4 expression contributes to endothelial dysfunction in pulmonary arterial hypertension. Circulation [Internet]. 2014 Apr 29 [cited 2023 Aug 22];129(17):1770–80. Available from: https://pubmed.ncbi.nlm.nih.gov/24503951/

95. Kim Y, Cha SJ, Choi HJ, Kim K. Omega Class Glutathione S-Transferase: Antioxidant Enzyme in Pathogenesis of Neurodegenerative Diseases. Oxid Med Cell Longev [Internet]. 2017 [cited 2023 Aug 23];2017. Available from: /pmc/articles/PMC5757135/

96. Littler DR, Harrop SJ, Goodchild SC, Phang JM, Mynott A V., Jiang L, et al. The enigma of the CLIC proteins: Ion channels, redox proteins, enzymes, scaffolding proteins? FEBS Lett [Internet]. 2010 May 17 [cited 2023 Aug 23];584(10):2093–101. Available from: https://onlinelibrary.wiley.com/doi/full/10.1016/j.febslet.2010.01.027

97. Argenzio E, Moolenaar WH. Emerging biological roles of Cl− intracellular channel proteins. J Cell Sci [Internet]. 2016 Nov 15 [cited 2023 Aug 27];129(22):4165–74. Available from: https://dx.doi.org/10.1242/jcs.189795

98. Gururaja Rao S, Ponnalagu D, Patel NJ, Singh H. Three Decades of Chloride Intracellular Channel Proteins: from organelle to organ physiology. Curr Protoc

Pharmacol [Internet]. 2018 Mar 1 [cited 2023 Aug 24];80(1):11.21.1. Available from: /pmc/articles/PMC6060641/

99. Littler DR, Assaad NN, Harrop SJ, Brown LJ, Pankhurst GJ, Luciani P, et al. Crystal structure of the soluble form of the redox-regulated chloride ion channel protein CLIC4. FEBS J [Internet]. 2005 Oct 1 [cited 2023 Aug 24];272(19):4996–5007. Available from: https://onlinelibrary.wiley.com/doi/full/10.1111/j.1742-4658.2005.04909.x

100. Li YF, Li DF, Zeng ZH, Wang DC. Trimeric structure of the wild soluble chloride intracellular ion channel CLIC4 observed in crystals. Biochem Biophys Res Commun. 2006 May 19;343(4):1272–8.

101. Suh KS, Mutoh M, Nagashima K, Fernandez-Salas E, Edwards LE, Hayes DD, et al. The Organellular Chloride Channel Protein CLIC4/mtCLIC Translocates to the Nucleus in Response to Cellular Stress and Accelerates Apoptosis. Journal of Biological Chemistry. 2004 Feb 6;279(6):4632–41.

102. Olotu F, Medina-Carmona E, Serrano-Sanchez A, Ossa F, El-Hamdaoui A, Bishop ÖT, et al. Structure-based discovery and in vitro validation of inhibitors of chloride intracellular channel 4 protein. Comput Struct Biotechnol J. 2023 Jan 1;21:688–701.

103. Shukla A, Edwards R, Yang Y, Hahn A, Folkers K, Ding J, et al. CLIC4 regulates TGF-β dependent myofibroblast differentiation to produce a cancer stroma. Oncogene [Internet]. 2014 Feb 2 [cited 2023 Aug 27];33(7):842. Available from: /pmc/articles/PMC3912213/

104. Varela L, Hendry AC, Cassar J, Martin-Escolano R, Cantoni D, Ossa F, et al. A Zn2+-triggered two-step mechanism of CLIC1 membrane insertion and activation into chloride channels. J Cell Sci [Internet]. 2022 Aug 8 [cited 2023 Aug 28];135(15). Available from: /pmc/articles/PMC9511705/

105. Singh H, Ashley RH. Redox regulation of CLIC1 by cysteine residues associated with the putative channel pore. Biophys J [Internet]. 2006 Mar 1 [cited 2023 Aug 28];90(5):1628–38. Available from: http://www.cell.com/article/S0006349506723529/fulltext

106. Suh KS, Mutoh M, Gerdes M, Yuspa SH. CLIC4, an Intracellular Chloride Channel Protein, Is a Novel Molecular Target for Cancer Therapy. Journal of Investigative Dermatology Symposium Proceedings. 2005 Nov 1;10(2):105–9.

107. Ponsioen B, Van Zeijl L, Langeslag M, Berryman M, Littler D, Jalink K, et al. Spatiotemporal Regulation of Chloride Intracellular Channel Protein CLIC4 by RhoA. Mol Biol Cell [Internet]. 2009 Nov 11 [cited 2023 Aug 27];20(22):4664. Available from: /pmc/articles/PMC2777097/

108. Gururaja Rao S, Patel NJ, Singh H. Intracellular Chloride Channels: Novel Biomarkers in Diseases. Front Physiol. 2020 Feb 14;11:502425.

109. Suh KS, Malik M, Shukla A, Ryscavage A, Wright L, Jividen K, et al. CLIC4 is a tumor suppressor for cutaneous squamous cell cancer. Carcinogenesis [Internet]. 2012 [cited 2023 Aug 28];33(5):986–95. Available from: https://academic.oup.com/carcin/article/33/5/986/2463663

110. Yang P, Yu PB. In Search of the Second Hit in Pulmonary Arterial Hypertension. Circ Res [Internet]. 2019 Jan 4 [cited 2023 Aug 29];124(1):6–8. Available from: https://www.ahajournals.org/doi/abs/10.1161/CIRCRESAHA.118.314270

111. Singh H. Two decades with dimorphic Chloride Intracellular Channels (CLICs). FEBS Lett. 2010 May 17;584(10):2112–21.

112. Mao DY, Kleinjan ML, Jilishitz I, Swaminathan B, Obinata H, Komarova YA, et al. CLIC1 and CLIC4 mediate endothelial S1P receptor signaling to facilitate Rac1 and RhoA activity and function. Sci Signal [Internet]. 2021 Apr 20 [cited 2023 Aug 27];14(679):425. Available from: https://www.science.org/doi/10.1126/scisignal.abc0425

113. He S, Zhu T, Fang Z. The Role and Regulation of Pulmonary Artery Smooth Muscle Cells in Pulmonary Hypertension. Int J Hypertens [Internet]. 2020 [cited 2023 Aug 29];2020. Available from: /pmc/articles/PMC7441461/

114. Abdul-Salam VB, Russomanno G, Chien-Nien C, Mahomed AS, Yates LA, Wilkins MR, et al. CLIC4/Arf6 Pathway: A New Lead in BMPRII Inhibition in Pulmonary Hypertension. Circ Res [Internet]. 2019 Jan 1 [cited 2023 Aug 30];124(1):52. Available from: /pmc/articles/PMC6325770/

115. Sun D, Guo Y, Tang P, Li H, Chen L. Arf6 as a therapeutic target: Structure, mechanism, and inhibitors. Acta Pharm Sin B. 2023 Jun 14;

116. Liu B, Billington CK, Henry AP, Bhaker SK, Kheirallah AK, Swan C, et al. Chloride intracellular channel 1 (CLIC1) contributes to modulation of cyclic AMP-activated whole-cell chloride currents in human bronchial epithelial cells. Physiol Rep

[Internet]. 2018 Jan 1 [cited 2023 Sep 2];6(2):e13508. Available from: https://onlinelibrary.wiley.com/doi/full/10.14814/phy2.13508

117. Mirdita M, Schütze K, Moriwaki Y, Heo L, Ovchinnikov S, Steinegger M. ColabFold: making protein folding accessible to all. Nature Methods 2022 19:6 [Internet]. 2022 May 30 [cited 2023 Aug 21];19(6):679–82. Available from: https://www.nature.com/articles/s41592-022-01488-1

118. Pang J, Hoefen R, Pryhuber GS, Wang J, Yin G, White RJ, et al. G-protein-coupled receptor kinase interacting protein-1 is required for pulmonary vascular development. Circulation [Internet]. 2009 Mar 24 [cited 2023 Sep 4];119(11):1524–32. Available from: https://www.ahajournals.org/doi/abs/10.1161/CIRCULATIONAHA.108.823997

119. Marion D. An introduction to biological NMR spectroscopy. Molecular and Cellular Proteomics [Internet]. 2013 Nov 1 [cited 2023 Sep 22];12(11):3006–25. Available from: http://www.mcponline.org/article/S1535947620345850/fulltext

120. Bothwell JHF, Griffin JL. An introduction to biological nuclear magnetic resonance spectroscopy. Biological Reviews [Internet]. 2011 May 1 [cited 2023 Sep 22];86(2):493–510. Available from: https://onlinelibrary.wiley.com/doi/full/10.1111/j.1469-185X.2010.00157.x

121. Sprawls P. Magnetic Resonance Imaging Principles, Methods, and Techniques. 2000 [cited 2023 Sep 22];25–6. Available from: http://www.sprawls.org

122. Zuiderweg ERP. Mapping protein-protein interactions in solution by NMR spectroscopy. Biochemistry [Internet]. 2002 Jan 8 [cited 2023 Sep 22];41(1):1–7. Available from: https://pubs.acs.org/doi/full/10.1021/bi011870b

123. Higman V. Protein NMR | A Practical Guide [Internet]. 2019 [cited 2023 Sep 23]. Available from: https://protein-nmr.org.uk/

124. Maity S, Gundampati RK, Kumar TKS. NMR methods to characterize protein-ligand interactions. Nat Prod Commun [Internet]. 2019 May 1 [cited 2023 Sep 24];14(5). Available from: https://journals.sagepub.com/doi/full/10.1177/1934578X19849296

125. Williamson MP. Using chemical shift perturbation to characterise ligand binding. Prog Nucl Magn Reson Spectrosc. 2013 Aug 1;73:1–16.

126. Alderson TR, Markley JL. Biophysical characterization of α-synuclein and its controversial structure. Intrinsically Disord Proteins. 2013 Jan;1(1):e26255.

127. Schrödinger LLC. The PyMOL Molecular Graphics System, Version~1.8. 2015 Nov.

128. Bruker Corporation. TopSpin Guide Book Basic NMR Experiments User Manual Innovation with Integrity • NMR [Internet]. 2017 [cited 2023 Sep 12]. Available from: www.bruker.com

129. Delaglio F, Grzesiek S, Vuister GW, Zhu G, Pfeifer J, Bax A. NMRPipe: A multidimensional spectral processing system based on UNIX pipes. J Biomol NMR [Internet]. 1995 Nov [cited 2023 Sep 12];6(3):277–93. Available from: https://link.springer.com/article/10.1007/BF00197809

130. Maciejewski MW, Schuyler AD, Gryk MR, Moraru II, Romero PR, Ulrich EL, et al. NMRbox: A Resource for Biomolecular NMR Computation. Biophys J [Internet]. 2017 Apr 25 [cited 2023 Sep 12];112(8):1529–34. Available from: https://pubmed.ncbi.nlm.nih.gov/28445744/

131. Johnson BA. From Raw Data to Protein Backbone Chemical Shifts Using NMRFx Processing and NMRViewJ Analysis. Methods Mol Biol [Internet]. 2018 [cited 2023 Sep 12];1688:257–310. Available from: https://pubmed.ncbi.nlm.nih.gov/29151214/

132. Shen Y, Delaglio F, Cornilescu G, Bax A. TALOS+: A hybrid method for predicting protein backbone torsion angles from NMR chemical shifts. J Biomol NMR [Internet]. 2009 [cited 2023 Sep 19];44(4):213. Available from: /pmc/articles/PMC2726990/

133. Van Zundert GCP, Rodrigues JPGLM, Trellet M, Schmitz C, Kastritis PL, Karaca E, et al. The HADDOCK2.2 Web Server: User-Friendly Integrative Modeling of Biomolecular Complexes. J Mol Biol. 2016 Feb 22;428(4):720–5.

134. Scheffzek K, Ahmadian MR. GTPase activating proteins: Structural and functional insights 18 years after discovery. Cellular and Molecular Life Sciences [Internet]. 2005 Dec 28 [cited 2023 Sep 26];62(24):3014–38. Available from: https://link.springer.com/article/10.1007/s00018-005-5136-x